

AEDC-TR-73-9

cy. B

SEP 14 1973

MAR 5 1974

SEP 22 1975

AUG 11 1992



A METHOD TO INCREASE THE FULL-SCALE INLET/ENGINE SYSTEM TESTING CAPABILITY OF THE AEDC 16-FT TRANSONIC WIND TUNNEL

R. L. Palko

ARO, Inc.

June 1973

TECHNICAL REPORTS
FILE COPY

Approved for public release; distribution unlimited.

Property of U. S. Air Force
AEDC LIBRARY
F40600-74-C-0001

cy-R

**PROPULSION WIND TUNNEL FACILITY
ARNOLD ENGINEERING DEVELOPMENT CENTER
AIR FORCE SYSTEMS COMMAND
ARNOLD AIR FORCE STATION, TENNESSEE**

NOTICES

When U. S. Government drawings specifications, or other data are used for any purpose other than a definitely related Government procurement operation, the Government thereby incurs no responsibility nor any obligation whatsoever, and the fact that the Government may have formulated, furnished, or in any way supplied the said drawings, specifications, or other data, is not to be regarded by implication or otherwise, or in any manner licensing the holder or any other person or corporation, or conveying any rights or permission to manufacture, use, or sell any patented invention that may in any way be related thereto.

Qualified users may obtain copies of this report from the Defense Documentation Center.

References to named commercial products in this report are not to be considered in any sense as an endorsement of the product by the United States Air Force or the Government.

**A METHOD TO INCREASE THE FULL-SCALE
INLET/ENGINE SYSTEM TESTING CAPABILITY
OF THE AEDC 16-FT TRANSONIC WIND TUNNEL**

**R. L. Palko
ARO, Inc.**

Approved for public release; distribution unlimited.

FOREWORD

The work reported herein was conducted by the Arnold Engineering Development Center (AEDC), Air Force Systems Command (AFSC), under Program Element 64719F. Technical monitoring of the effort was performed by Captain Carlos Tirres, USAF, Research and Development Division, Directorate of Technology.

The results of research presented were obtained by ARO, Inc. (a subsidiary of Sverdrup & Parcel and Associates, Inc.), contract operator of the Arnold Engineering Development Center (AEDC), Air Force Systems Command (AFSC), Arnold Air Force Station, Tennessee. The investigation was conducted under ARO Project Nos. PW5146 and PW5246 from January 1971 to July 1972, and the manuscript was submitted for publication on July 31, 1972.

Acknowledgment is made of the assistance of Mr. J. L. Jacocks of the Propulsion Wind Tunnel Facility, 16T/S Projects Branch, who was responsible for the design and calibration of the flow angularity probe, to Mr. W. P. Harmon of the Propulsion Wind Tunnel Facility, Test Operations Branch, who designed the test models, and to Mr. C. R. Fitch and Mr. D. C. Todd of the Central Computer Operations, who handled the analytical program.

This technical report has been reviewed and is approved.

CARLOS TIRRES
Captain, USAF
Research and Development Division
Directorate of Technology

ROBERT O. DIETZ
Director of Technology

ABSTRACT

A study was conducted of a new testing technique using flow shaping that together with some modifications of the AEDC 16-ft Transonic Propulsion Wind Tunnel will provide the capability to test full-scale inlet/engine configurations with forebody effects at high maneuvering angles at transonic velocities. The method used to obtain the flow simulation for high maneuvering angles utilized auxiliary flow shaping and geometric pitch. An analytical potential flow method was used to determine the configuration of devices necessary to produce the required flow fields; these devices were then checked experimentally to verify the results. The experimental results compare favorably with the predicted flow fields, and the use of flow shaping devices for simulation of the inlet flow field for certain inlet configurations is promising for angles of attack up to 20 deg with angles of yaw up to 5 deg.

CONTENTS

	<u>Page</u>
ABSTRACT	iii
NOMENCLATURE	viii
I. INTRODUCTION	1
II. OBJECTIVE	1
III. FLOW SHAPING	
3.1 Introduction	2
3.2 Computer Analysis	2
3.3 Wind Tunnel Experiments	5
3.4 Results and Discussion	7
IV. BLOCKAGE STUDY	
4.1 Introduction	13
4.2 Wind Tunnel Experiments	14
4.3 Results and Discussion	15
V. SUMMARY AND RECOMMENDATIONS	16
REFERENCES	17

APPENDIXES

I. ILLUSTRATIONS

Figure

1. Typical Performance for Highly Maneuverable Aircraft	21
2. Aircraft Study Configuration Installed in the AEDC 16-ft Transonic Wind Tunnel	22
3. Mathematical Model of the Fuselage of the Wind Tunnel Test Configuration	23
4. Comparison between Analytical and Wind Tunnel Data for Mach Number 0.9 at an Angle of Attack of 25 deg	24
5. Mathematical Model of Dual Hollow Cylinders in the Wind Tunnel	25
6. Predicted Upwash for the Dual Hollow Circular Cylinders, Mach Number 0.9	26
7. Predicted Sidewash for the Dual Hollow Circular Cylinders, Mach Number 0.9	27
8. Mathematical Model of the Dual Hollow Circular Cylinder Configuration	28
9. Typical Predicted Flow Field for the Final Dual Hollow Circular Cylinder Configuration	29
10. Mathematical Model of the Modified Hollow Cylinder Configuration	30
11. Typical Predicted Flow Field for the Modified Hollow Cylinder Configuration	31
12. Mathematical Model of the Large Turning Vanes	32

<u>Figure</u>	<u>Page</u>
13. Local Flow Angles for Large Turning Vanes in Plane of Trailing Edges	33
14. Mathematical Model of the Small Turning Vanes	34
15. Typical Predicted Flow Field for the Small Turning Vanes	35
16. General Arrangement of Tunnel 1T and Supporting Equipment	36
17. Schematic of Tunnel 1T Test Leg	37
18. Flow Angularity Probe and Support Mechanism	38
19. Schematic of the Dual Hollow Circular Cylinder Installation	39
20. Dual Hollow Cylinders Installed in the AEDC 1-ft Transonic Wind Tunnel	40
21. Probe Survey Grid for the Dual Hollow Circular Cylinder Wind Tunnel Test	41
22. Modified Hollow Cylinders Installed in the AEDC PWT-1T	42
23. Probe Survey Grid for the Modified Hollow Cylinder Wind Tunnel Test	43
24. Schematic of the Large Turning Vane Installation	44
25. Large Turning Vanes Installed in the AEDC PWT-1T	45
26. Probe Survey Grid for the Large Turning Vane Wind Tunnel Test	46
27. Schematic of the Small Turning Vane Installation	47
28. Small Turning Vanes Installed in the AEDC PWT-1T	48
29. Probe Survey Grid for the Small Turning Vane Wind Tunnel Test	49
30. Local Flow Vector Diagram	50
31. Experimental and Theoretical Comparison of Local Flow Vectors for the Dual Hollow Circular Cylinders	51
32. Experimental and Theoretical Comparison of Upwash and Sidewash Angles for the Dual Hollow Circular Cylinders	52
33. Experimental and Theoretical Comparison of Local Mach Numbers for the Dual Hollow Circular Cylinders	53
34. Experimental Pressure Coefficients around Cylinder Number 1 of the Dual Hollow Circular Cylinder Configuration	54
35. Variation in Experimental Flow Field with Free-Stream Mach Number for the Dual Hollow Circular Cylinders	55
36. Experimental and Theoretical Comparison of Local Flow Vectors for the Modified Hollow Cylinders (Cylinder No. 1, $\alpha = 30$ deg; Cylinder No. 2, $\alpha = 20$ deg)	56
37. Experimental and Theoretical Comparison of Upwash and Sidewash Angles for the Modified Hollow Cylinders (Cylinder No. 1, $\alpha = 30$ deg; Cylinder No. 2, $\alpha = 20$ deg)	57
38. Experimental and Theoretical Comparison of Local Mach Numbers for the Modified Hollow Cylinders (Cylinder No. 1, $\alpha = 30$ deg; Cylinder No. 2, $\alpha = 20$ deg)	58
39. Experimental Pressure Coefficients around Cylinder Number 1 of the Modified Hollow Cylinder Configuration	59

<u>Figure</u>	<u>Page</u>
40. Variation in Experimental Flow Field with Free-Stream Mach Number for the Modified Hollow Cylinders (Cylinder No. 1, $\alpha = 30$ deg; Cylinder No. 2, $\alpha = 20$ deg)	60
41. Experimental and Theoretical Comparison of Local Flow Vectors for the Modified Hollow Cylinders (Cylinder No. 1, $\alpha = 30$ deg; Cylinder No. 2, $\alpha = 30$ deg)	61
42. Experimental and Theoretical Comparison of Upwash and Sidewash Angles for the Modified Hollow Cylinders (Cylinder No. 1, $\alpha = 30$ deg; Cylinder No. 2, $\alpha = 30$ deg)	62
43. Experimental and Theoretical Comparison of Local Mach Numbers for the Modified Hollow Cylinders (Cylinder No. 1, $\alpha = 30$ deg; Cylinder No. 2, $\alpha = 30$ deg)	63
44. Variation in Experimental Flow Field with Free-Stream Mach Number for the Modified Hollow Cylinders (Cylinder No. 1, $\alpha = 30$ deg; Cylinder No. 2, $\alpha = 30$ deg)	64
45. Variation in Experimental Local Flow Vectors with Yaw Angles for Modified Hollow Cylinders	65
46. Experimental and Theoretical Comparison of Local Flow Vectors for Large Turning Vanes	66
47. Experimental and Theoretical Comparison of Upwash and Sidewash Angles for the Large Turning Vanes	67
48. Experimental Surface Pressure Coefficients for the Large Turning Vanes	68
49. Experimental and Theoretical Comparison of Local Flow Vectors for Small Turning Vanes	69
50. Experimental and Theoretical Comparison of Upwash and Sidewash Angles for the Small Turning Vanes	70
51. Comparison of Local Flow Vectors in the AEDC PWT-16T with the Study Configuration at an Angle of Attack of 10 deg with Simulated Local Flow Vectors Taken in the AEDC PWT-1T	71
52. Comparison of Local Flow Vectors Taken in the AEDC PWT-16T with the Study Configuration at an Angle of Attack of 19.8 deg with Simulated Local Flow Vectors Taken in the AEDC PWT-1T	72
53. Comparison of Local Flow Vectors Taken in the AEDC PWT-16T with the Study Configuration at an Angle of Attack of 10 deg and an Angle of Yaw of 4 deg with Simulated Local Flow Vectors Taken in the AEDC PWT-1T	73
54. Experimental and Theoretical Comparison of Upwash and Sidewash Angles for the Study Configuration and Modified Hollow Cylinders	74
55. Comparison of Local Flow Vectors Taken in AEDC PWT-16T with the Study Configuration at an Angle of Attack of 10 deg and an Angle of Yaw of 4 deg with Simulated Local Flow Vectors Taken in the AEDC PWT-1T	75

<u>Figure</u>	<u>Page</u>
56. Installation of the Inlet/Engine Model with the Dual Hollow Circular Cylinders in the AEDC PWT-1T	76
57. Installation of the Inlet/Engine Model with the Modified Hollow Cylinders in the AEDC PWT-1T	78
58. Increase in Upwash and Sidewash Angles due to the Installation of the Inlet/Engine with the Dual Hollow Circular Cylinders	80
59. Auxiliary Weight Flow Required to Operate the Tunnel with Flow Shaping Devices and Inlet/Engine Installed	81
II. VORTEX-LATTICE PROGRAM FOR 3-D POTENTIAL FLOW PROBLEMS . . .	82

NOMENCLATURE

C_p	Pressure coefficient, $(p_L - p_\infty)/q_\infty$
K_θ	Circumferential distortion factor
M_L	Local Mach number
ΔM_L	$M_L - M_\infty$
M_∞	Free-stream Mach number
N	Any free-stream Mach number $\neq 0.9$
p_L	Local static pressure, psfa
p_{t2}	Compressor-face local total pressure, psfa
p_∞	Free-stream static pressure, psfa
$p_{t\infty}$	Free-stream total pressure, psfa
$p_{t2}/p_{t\infty}$	Steady-state inlet total pressure recovery
q_∞	Free-stream dynamic pressure, psfa
W_A	Auxiliary weight flow, lb/sec
W_T	Theoretical tunnel weight flow, lb/sec
X	Coordinate along tunnel axis, positive downstream

Y	Horizontal coordinate, positive as indicated
Z	Vertical coordinate, positive down
α	Angle of attack, deg, positive up
β	Angle of yaw, deg, sign as indicated
ϵ	Upwash angle, deg, positive up
$\Delta\epsilon$	$(\epsilon_{M_\infty=0.9} - \epsilon_{M_\infty=N})$ or $(\epsilon_{Cyl.+Inlet/Engine} - \epsilon_{Cyl. Only})$, deg
θ	Local flow vector, $(\tan^{-1}\sqrt{\tan^2\epsilon + \tan^2\sigma})$, or angle around cylinder, deg (see Fig. 30)
θ_w	Angle of top and bottom test section walls, deg
σ	Sidewash angle, deg, positive away from Cylinder No. 1
$\Delta\sigma$	$(\sigma_{M_\infty=0.9} - \sigma_{M_\infty=N})$ or $(\sigma_{Cyl.+Inlet/Engine} - \sigma_{Cyl. Only})$, deg
ψ	Local flow orientation, deg; $\tan^{-1} (\tan \sigma)/(\tan \epsilon)$ (see Fig. 30)

SECTION I INTRODUCTION

A major problem area in the development programs of highly maneuverable aircraft is the integration of the propulsion unit and airframe into an efficient operational system. Ground test facilities provide an economical means of determining solutions to design problems, but the degree of full-scale flight simulation is generally much less than desired. The performance requirements of many of these aircraft may include considerable maneuvering at angles of attack up to 25 deg in the transonic Mach number range as shown in Fig. 1a (Appendix I). As the angle-of-attack requirement increases, the inlet recovery decreases and the engine face circumferential distortion factor increases as shown in Fig. 1b (Ref. 1). This results in a decrease in the engine performance at maneuvers where high performance is essential for an air superiority aircraft.

Existing propulsion wind tunnels are not capable of testing the full-scale inlet/engine systems at angles of attack above 10 to 12 deg simply because of physical limits of the tunnels, and, at present, there exists no capability to test at a pitch and yaw attitude simultaneously. This angle-of-attack limitation is reduced further because of the necessity of simulating the aircraft forebody. The degree of forebody simulation required depends on the aircraft configuration, but certain wind tunnel tests (Ref. 2) have shown that the forebody may produce differential flow angularity across the inlet as high as 15 deg. This leaves a considerable gap between desired and available test angle-of-attack capability. This gap is shown clearly in Fig. 1a. Placing this test limitation on Fig. 1b shows that the problems of reduced inlet recovery and increased circumferential distortion are only starting to occur at the upper limit of the testing capability leaving the real problem to be solved during flight test. Solving the inlet/engine compatibility problems during flight test can be very costly as demonstrated clearly in a recent high performance aircraft development program.

Since the full-scale engine must ultimately operate with the full-scale inlet in the presence of the airframe throughout the required operating envelope, it is highly desirable that the full-scale performance be simulated in a ground test facility before flight test. However, using present testing techniques, this simulation would require a new, very large propulsion wind tunnel.

In order to utilize existing test facilities, a study was made to determine new test techniques and tunnel modification requirements that would increase the range of flight conditions for testing full-scale inlet/engine systems in the AEDC 16-ft Transonic Wind Tunnel (PWT-16T).

SECTION II OBJECTIVE

The objective of the study was to develop a testing technique and to produce criteria for the modifications of the AEDC PWT-16T that together would provide a capability to test full-scale inlet/engine configurations for highly maneuverable aircraft at transonic velocities over an angle-of-attack range up to 25 deg and at angles of yaw up to 5 deg.

SECTION III FLOW SHAPING

3.1 INTRODUCTION

The new testing techniques investigated involved the generation of the inlet flow field corresponding to a maneuvering condition (that is, pitch and yaw) through the use of auxiliary flow shaping (or flow deflection) devices in the vicinity of the inlet. The approach taken during the investigation was to approximate the inlet flow field for the higher angles of attack through a combination of flow shaping and geometric positioning of the inlet/engine system. For moderate angles of attack and yaw, the desired yaw component of the flow field could be produced by flow shaping devices and the upwash (or downwash) could be produced by either flow shaping, geometric positioning of the model, or a combination of both.

The steps taken in developing the new test technique for testing full-scale inlet/engine systems at simulated pitch and yaw were: (1) determine for a given aircraft configuration the flow field at the inlet, (2) develop flow shaping devices which are capable of producing the desired flow, and (3) verify the ability of the device by conducting flow survey tests using subscale models of the devices in the AEDC 1-Ft Transonic Wind Tunnel (PWT-1T). The success of such an approach obviously depends on the ability to correctly determine the flow field produced by the aircraft and the flow shaping devices. To correctly determine the flow fields, both the one to be simulated and the one produced by the simulation device, requires the use of either experimental data obtained from wind tunnel tests or predictions made by analytical procedures. No doubt, using only a wind tunnel and a trial and error method, shaping devices could be designed to give the desired flow field. However, this would be both costly and time consuming because a larger number of models probably would need to be fabricated and tested. Therefore, an analytical method of determining the shaping device requirements was needed. In addition, analytical predictions of the aircraft flow field could eliminate the need for conducting a wind tunnel test to survey the aircraft flow field.

3.2 COMPUTER ANALYSIS

3.2.1 Analytical Method

The analytical method used to calculate the flow field is a three-dimensional potential flow solution which utilizes a vortex lattice to describe the model. A compressibility correction using Goethert's Rule has been incorporated into the solution for use at high subsonic Mach numbers. By using the mathematical model, the flow angularity and local Mach number are computed at the desired location for the study model. Plots of flow streamlines, constant flow angularity, and local velocity vectors are all available if desired. Most of the computer analyses were made at Mach number 0.9 since this was determined to be near the upper limit of Mach number for this analytical method. A complete description of the analytical method including the theory, a program listing, and a sample problem is given in Appendix II.

3.2.2 Study Configuration

It was not the intent during this study to determine flow simulation for a specific aircraft configuration; however, a specific configuration was analyzed in order to verify the analytical prediction method and to have an example of the type of flow simulation required.

Because of the difficulties encountered in trying to model an inlet analytically, it was assumed in this study that a given inlet would affect a given flow field in the same manner and degree regardless of how the flow field was created. Whether or not this assumption is true can only be answered by testing the complete vehicle, but the assumption is reasonable and the simplification was introduced into the analytical calculations because of the greatly reduced complexity of the analytical calculations.

The configuration shown in Fig. 2, which is a fuselage forebody of a typical high performance aircraft, was selected for the study because wind tunnel data of flow angularity surveys from previous tests in the AEDC PWT-16T (Ref. 2) were readily available for verification of the analytical method. This configuration was also a good choice because the inlets are side mounted (typical of today's high performance aircraft), and flow surveys were made far aft where the forebody effect should be larger. The mathematical model (location of vortex filaments and velocity control points) used for the study configuration is shown in Fig. 3.

The analytical data for one model position are shown in Fig. 4. These data are for an angle of attack of 25 deg with zero yaw angle and are shown as lines of constant angles of upwash and sidewash. A comparison between the analytical data and wind tunnel data taken at the model position indicated in Fig. 3 is also shown in Fig. 4 to verify the capability of predicting the desired flow field with the three-dimensional potential flow solution used. The figure shows the data to agree well within the range needed for flow simulation.

A preliminary analysis of the upwash at the inlet station due to wing lift was also made to determine if the wing effect needed to be simulated. The intersection between the leading edge of the wing and the fuselage was at Station 390 with the inlet survey location at Station 356 (see Fig. 3). The analysis showed the wing to have little effect on the flow angularity at the inlet station for Mach numbers of 0.9 and 0.75. The maximum differential flow angularity was less than two degrees in upwash and less than one-half degree in sidewash for a Mach number of 0.75 and an angle of attack of 25 deg, one degree in upwash, and one-quarter degree in sidewash for a Mach number of 0.9 and an angle of attack of 25 deg.

3.2.3 Dual Hollow Circular Cylinders

Two main criteria for the shaping devices aside from producing the flow field simulation are that they have minimum tunnel blockage and generate as little turbulence in the test region as possible. The first device analyzed that showed promise was a pair of hollow circular cylinders placed in a cross flow. During the theoretical analysis made on this device, the spacing between the cylinders and the angle of attack of each cylinder was varied until a flow field was produced which resembled the flow field produced by the study model configuration.

An analysis was made with the cylinders in a tunnel and in uniform free flow to ensure that the presence of the tunnel walls would not greatly modify the analytical results at least up to Mach numbers of 0.9. Figure 5 shows the mathematical model of the cylinders in the wind tunnel. Figures 6 and 7 show the upwash and sidewash for the cylinders in the tunnel and in uniform free flow. This comparison shows only slight changes in the data between the two conditions analyzed.

The mathematical model of the dual hollow circular cylinder configuration with the cylinder diameter and spacing that were used in the experimental study is shown in Fig. 8. The theoretical values of constant angles of upwash and sidewash are shown in Fig. 9. The analysis of this configuration predicted that increases in the angle of attack simulation of six degrees could be obtained.

3.2.4 Modified Hollow Cylinders

In an attempt to get a flow field with an upwash that was more nearly uniform in the vertical plane rather than the horizontal plane, as was the case of the dual hollow circular cylinders, and to get better yaw simulation, a pair of modified hollow cylinders was analyzed.

These devices were flattened on the side toward the tunnel centerline by the width of one radius. Figure 10 shows a computer plot of the mathematical model of this configuration (a cross-sectional view of the device is shown in Fig. 11). Theoretical calculations were made on this configuration with variations in pitch on both cylinders and in combination of pitch and yaw on one cylinder. The increase in upwash for a given set of pitch angles was less with this device than with the original dual hollow circular cylinders; however, the upwash did become more nearly uniform in the vertical plane as desired. By decreasing the spacing between the cylinder, an overall increase was shown which resulted in an increase in the predicted angle of attack simulation of seven degrees.

The results of the analysis made with combination of pitch and yaw on one of the cylinders showed that this configuration could be used to obtain the yaw simulation requirements. The computer plots with constant angles of upwash and sidewash for a typical pitch-yaw combination are shown in Fig. 11.

Although the primary objective of this study was to test shaping devices that would give a degree of simulation of the study configuration, it was felt that basic information about the flow-shaping characteristic of other devices was needed for future use on other types of aircraft configurations. As a result, two other sets of flow shaping devices were chosen and analyzed as possible candidates. The two sets were pairs of turning vanes to be placed in the flow ahead of the inlet. A description and the results of the analysis of the two sets of vanes are given in the next two sections of this report.

3.2.5 Large Turning Vanes

To obtain general information for possible future flow-shaping requirements, a set of large turning vanes which spanned the tunnel were analyzed. The end effect of the

tunnel walls was neglected, and the vanes were assumed to be two-dimensional for the analysis. To get uniform flow entering the vanes, the walls in the plane of the vanes were also assumed to be two-dimensional. The mathematical model of this pair of vanes is shown in Fig. 12, and resulting flow angles using both vanes or either vane are shown in Fig. 13. Analytically this device appeared to give very uniform flow across the trailing-edge plane.

3.2.6 Small Turning Vanes

For further information, a set of small turning vanes was analyzed. These vanes were designed to shape the tunnel flow locally. The mathematical model of these vanes is shown in Fig. 14. The vanes were assumed to be in a uniform free stream. The theoretical values of constant angles of upwash and sidewash are shown in Fig. 15. Data for only half of the survey plane are shown since the theoretical analysis was made using only half of the vanes and the symmetry capability of the computer program. These data show an inflow around the convex vane (No. 2) and an outflow around the concave vane (No. 1).

3.3 WIND TUNNEL EXPERIMENTS

After theoretically determining the shape of some devices which have predicted flow fields that can be used to simulate an inlet flow field, subscale model wind tunnel tests were conducted to verify the theoretical analysis. This experimental effort was carried out in the AEDC PWT-1T. A description of the test hardware and models is given in the following sections.

3.3.1 Wind Tunnel (AEDC PWT-1T)

The AEDC PWT-1T is a continuous-flow nonreturn, transonic wind tunnel equipped with a two-dimensional, flexible nozzle and a plenum evacuation system. The test section Mach number range can normally be varied from 0.2 to 1.50. Total pressure control is not available in the AEDC-PWT-1T, and the tunnel is operated at a stilling chamber total pressure of about 2,850 psfa with a ± 5 -percent variation depending on tunnel resistance and ambient conditions. The stagnation temperature can be varied from 80 to 120°F above ambient temperature as necessary to prevent moisture condensation in the test region.

The general arrangement of the tunnel and its associated equipment is shown in Fig. 16, and a schematic of the nozzle, test section, and wall geometry is shown in Fig. 17. A detailed description of the tunnel and its capabilities is given in Ref. 3.

3.3.2 Flow Angularity Probe

A flow angularity probe was used to survey the flow field at the engine inlet location. Details of the probe are shown in Fig. 18. This probe was 1/4 in. in diameter and was designed to survey an area two inches on either side of the center of the tunnel and approximately two inches above and four inches below the center of the tunnel. The probe was calibrated in the AEDC PWT-1T with data being obtained through a Mach

number range from 0.5 to 1.4 at probe angles up to ± 33 deg in both pitch and yaw. The flow was repeatable to ± 0.1 deg, and the measuring accuracy of the probe was within 0.5 deg in flow angularity and 0.05 in local Mach number.

The probe mechanism was mounted to the sector roll mechanism (see Fig. 17) which allowed the probe to be rolled to get up to two inches offset from either side of the tunnel centerline for positioning of the probe tip in the z-axis. The sector was then set to traverse up or down to allow positioning of the probe tip in the y-axis. Position changes in the x-axis could only be made manually with the tunnel shut down.

3.3.3 Instrumentation

The tunnel plenum chamber pressure was measured with a self-balancing precision manometer. All of the other pressures were measured with differential transducers referenced to the tunnel plenum pressure and displayed on electromanometers.

The tunnel stagnation temperature was measured with an iron-constantan thermocouple and displayed on an indicating potentiometer-type recorder.

3.3.4 Experimental Models

3.3.4.1 Dual Hollow Circular Cylinders (Dual Cylinders)

Based on the unit size, unit space between the cylinders, the size requirement and location of a typical engine inlet, which were determined from the analytical method, a pair of hollow half-circular cylinders was designed for testing in the AEDC PWT-1T. Because of the relative large cylinder radius to separation distance required, it was necessary to use half cylinders to allow space for a normal inlet/engine installation. The cylinders could be individually positioned to vary the spacing between them, and both could be pitched in 5-deg increments up to 40 deg. In addition, one of the cylinders could be yawed up to 10 deg.

Figure 19 shows a schematic of the general layout of the cylinders installed in the tunnel, and Fig. 20 shows an installation photograph. A sketch showing the position of the probe tip for the survey grid and sign convention used with the dual hollow cylinders is presented in Fig. 21. The x-axis location of the probe tip was at the middle of the cylinders for the majority of the data surveys.

Five pressure orifices were located around Cylinder No. 1 at 30-deg intervals 6 in. from the leading edge of the cylinder (see Fig. 19). Three static orifices and a total pressure probe were located inside the cylinder.

3.3.4.2 Modified Hollow Cylinders (Modified Cylinders)

Based on information determined from the analytical method, a pair of modified hollow cylinders was designed for testing in the AEDC PWT-1T. These cylinders were

the same basic size as the dual hollow-circular cylinders but were flattened on the sides by a straight segment equal in length to one cylinder radius. These modified cylinders were designed to fit on the same strut system used by the dual cylinders and could be positioned over the same pitch and yaw range.

Figure 22 shows an installation photograph of the modified cylinders. A sketch showing the position of the probe tip for the survey grid and sign convention used with the modified hollow cylinders is presented in Fig. 23. The x-axis location of the probe tip was at the middle of the cylinders for the majority of the data surveys.

Five pressure orifices were located around Cylinder No. 1. Three orifices were located on the flattened side and two on the leeward curve at 30-deg increments 6 in. from leading edge (see Fig. 23). Three static orifices and a total pressure probe were located inside the cylinder (similar to the arrangement in Fig. 19).

3.3.4.3 Large Turning Vanes

Using the contours and spacing determined by the analytical method, a set of large turning vanes was designed for testing in the AEDC PWT-1T. These vanes were strut mounted to the tunnel frame and spanned the tunnel.

Figure 24 shows a schematic of the general layout of the large turning vane installation, and Fig. 25 shows an installation photograph. The survey and sign convention used with the large turning vanes are shown in the sketch in Fig. 26. The x-axis location of the probe tip was located at the trailing edge of vane No. 2. This was the same plane for which the theoretical data were computed.

Four pressure orifices were located along the centerline of the top vane at 2-in. intervals starting 8 in. from the leading edge. Five pressure orifices were located along the centerline of the bottom vane at 2-in. intervals starting 5.5 in. from the leading edge (see Fig. 24).

3.3.4.4 Small Turning Vanes

A set of small turning vanes was designed which used the contours determined from the analytical program. These vanes were mounted to the struts used by the dual hollow cylinders.

Figure 27 shows a schematic of the location of the vanes in the tunnel, and Fig. 28 shows an installation photograph. The location of the probe tip for the survey grid and the sign convention used with the small turning vanes are shown in Fig. 29. The x-axis location for both the theoretical analysis and the experimental surveys was at the trailing edge of the vanes.

3.4 RESULTS AND DISCUSSION

Since it is difficult to present flow angularity data for three-dimensional flow with a two-dimensional plot, the majority of the data is presented two ways. First, a local

flow vector is used where the length of the vector indicates the magnitude of the angle θ , which is the resultant local flow angle relative to the free stream and is essentially proportional to the cross flow velocity, and the orientation (ψ) indicates the component of upwash and sidewash. A diagram of the local vector is shown in Fig. 30. The second way shows a graphical display of the data at constant angles of upwash and sidewash.

3.4.1 Dual Hollow Circular Cylinders

During the wind tunnel test, data were obtained at Mach numbers of 0.6, 0.9, 1.0, and 1.2. Cylinder No. 1 was positioned from 0 to 40 deg in pitch and was varied in yaw from 0 to -10 deg (nose toward tunnel centerline). Cylinder No. 2 was positioned from 0 to 30 deg in pitch and remained at 0 deg yaw for all test conditions. Data were obtained at three different x-stations in the tunnel over the y-z survey grid as shown in Fig. 21.

The local flow vectors showing the comparison between the predicted and the experimental flow field for the cylinder configuration indicated are shown in Fig. 31 for a free-stream Mach number of 0.9. These same data are shown in Fig. 32 at constant angles of upwash and sidewash. In Fig. 32, the wind tunnel survey data are presented as the solid circles showing the location of the probe with the number above the circles showing the measured upwash angle and the number below the circles showing the measured sidewash angle. A maximum deviation of one degree is noted between the predicted and measured angles at any one probe location.

Figure 33 shows a comparison between predicted and measured local Mach number for the same test condition. Here the agreement is not as good. However, the overall trends are the same.

As indicated in the model description, pressure orifices were located around Cylinder No. 1 to determine if any anomalies are present when the two cylinders are varied in the proximity of each other that would cause early separation. Figure 34 shows a plot of the pressure coefficients as determined from the static pressure measurements for pitch angles of 30 and 40 deg when the other cylinder is pitched to 20 and 30 deg, respectively.

Figure 34 indicates that the flow did not separate with 30-deg pitch up to an angle of 150 deg around the cylinder, whereas the flow separated between 120 and 150 deg around the cylinder at a pitch angle of 40 deg. By using Reynolds number based on the cross flow component of velocity for each pitch angle, these data appear to be consistent with other data taken with a cylinder in cross flow, and the presence of the other cylinder does not appear to create any premature flow separation on the cylinder.

Static and total pressure pickups were also located inside the cylinder to determine the internal flow. The data from these locations showed that the flow through the cylinders was slightly greater than free stream at Mach numbers of 0.6 and 0.9. However, at Mach numbers above 0.9, the flow through the cylinders remained constant at the Mach number 0.9 value. This indicates that the critical mass flow ratio, that is mass flow going through

the cylinder to mass flow capture area, must occur near Mach number 0.9 for this cylinder design.

Figure 35 shows the variation in local Mach number, upwash, and sidewash with free-stream Mach number at four probe locations when Cylinder No. 1 is positioned at 30-deg pitch and 0-deg yaw, and Cylinder No. 2 is positioned at 20-deg pitch and 0-deg yaw. Figure 35a shows that even though there is a variation in local Mach number from point to point of approximately Mach number 0.2 for the same free-stream Mach number, this variation is uniform over the free-stream Mach number range. Therefore, it is expected that if a particular local Mach number is needed at a certain location, then the free-stream Mach number could be set to give this local Mach number.

Figures 35b and c show the delta values of upwash and sidewash over the free-stream Mach number range as compared with the data at a free-stream Mach number of 0.9. This figure shows a maximum deviation of approximately 2 deg in upwash and 1.5 deg in sidewash over the free-stream Mach number range. This indicates that if a change is necessary in free-stream Mach number to get a correct local Mach number, the flow field simulation will still be within the desired range.

3.4.2 Modified Hollow Cylinders

During the wind tunnel experiments, data were obtained at Mach numbers of 0.6, 0.9, 1.0, and 1.1. Both cylinders were positioned from 0 to 30 deg in pitch and Cylinder No. 1 was varied in yaw from 0 to 10 deg (nose away from tunnel centerline). Data were obtained at two different x-stations in the tunnel over the y-z survey grid as shown in Fig. 23.

The local flow vectors showing the comparison between the predicted and the experimental flow fields at a free-stream Mach number of 0.9 when Cylinder No. 1 was set at 30-deg pitch and 0-deg yaw and Cylinder No. 2 was set at 20-deg pitch and 0-deg yaw are shown in Fig. 36. Figure 37 shows the data contours for the same conditions at constant angles of upwash and sidewash. The wind tunnel survey data are presented in Fig. 37 as the solid circles with the number above the circles showing the measured upwash and the number below the circles showing the measured sidewash. The maximum deviation between the predicted and measured angles is approximately 1.5 deg. It is interesting to note that the analytical method underestimated the upwash and sidewash angles for the modified hollow cylinders and overestimated them for the dual hollow cylinders.

Figure 38 shows the comparison between predicted local Mach number and measured local Mach number. Here again the agreement is not as good as the upwash and sidewash, but the trends are the same.

The pressure coefficients for the ray of pressure orifices around the cylinder are shown in Fig. 39 for the cylinder pitched 30 deg with 0-deg yaw. These data show that the flow did not separate up to an angle of 150 deg around the cylinder.

Static and total pressure pickups were also located inside these cylinders to determine the internal flow. The data from these pickups showed that the flow through the cylinders was slightly greater than Mach number 0.6 at a free-stream Mach number of 0.6 but did not increase as free-stream Mach number increased. This indicates that the critical mass flow ratio must occur near Mach number 0.6 for the cylinder design. The cylinder wall thickness was considerably greater for the modified cylinders than for the dual circular cylinders (strictly for simplicity of fabrication) which reduced the internal flow area thus lowering the Mach number at which the critical mass-flow ratio occurred. This caused the modified cylinders to block the tunnel at free-stream Mach numbers above 1.1 and at some cylinder pitch angles at Mach numbers above 1.0. Careful design of the cylinder should increase the maximum free-stream Mach number at which the cylinder shape could be used.

Figure 40 shows the variation of local Mach number, upwash, and sidewash with free-stream Mach number at four probe locations when Cylinder No. 1 was set at 30-deg pitch and 0-deg yaw, and Cylinder No. 2 was set at 20-deg pitch and 0-deg yaw. Figure 40a shows a variation in local Mach number from point to point for the same free-stream Mach number of less than 0.1 Mach number, and the variation is uniform over the free-stream Mach number range. This should allow for adjusting the free-stream Mach number to set any local Mach number within the range of the data.

Figures 40b and c show the delta values of upwash and sidewash over the free-stream Mach number range as compared with the data at a free-stream Mach number of 0.9. This figure shows that, at free-stream Mach numbers of 1.0 and below, the maximum deviation is 1.5 deg in upwash and 0.75 deg in sidewash. (From Fig. 40a, it is noted that a free-stream Mach number of 1.0 gives a maximum local Mach number of 1.15.) At a free-stream Mach number of 1.1, the data show one point to deviate up to 1.75 deg in upwash and 2.5 deg in sidewash.

Figure 41 is the flow vectors showing the comparison between the predicted and the experimental flow field at a free-stream Mach number of 0.9 with both modified cylinders set at 30-deg pitch and 0-deg yaw. The same data are shown in Fig. 42 for constant angles of upwash and sidewash. The wind tunnel data are again shown as solid circles with the number above the circle giving the measured upwash and the number below the circle giving the measured sidewash. The maximum deviation between predicted and measured values is somewhat higher for this condition resulting in a maximum upwash deviation of 2.5 deg and a maximum sidewash deviation of 2 deg. This condition gave the maximum area over which there was a uniform upwash. The approximate upwash angle over this area was 9 deg.

Figure 43 shows a comparison between predicted and measured local Mach number. Here again, the trends are similar as before, but the absolute values are still not in good agreement.

Figure 44 shows the variation of local Mach number, upwash, and sidewash with free-stream Mach number at four probe locations when both cylinders were set at 30-deg pitch and 0-deg yaw. Data were only obtained up to a free-stream Mach number of 1.0 because of tunnel blockage at these settings. The deviation in local Mach number with free-stream Mach number is shown in Fig. 44a and is in the order of 0.2 Mach number.

Figures 44b and c show the delta values of upwash and sidewash over the free-stream Mach number range as compared with the data at a free-stream Mach number of 0.9. The deviation in upwash over the free-stream Mach number range is shown to be 0.2 deg, and the deviation in sidewash over the free-stream Mach number range is shown to be 0.75 deg.

Figure 45 shows the effect of yawing Cylinder No. 1 at a constant pitch angle of 30 deg with Cylinder No. 2 set at 30-deg pitch and 0-deg yaw. Cylinder No. 1 was positioned nose away from the tunnel centerline at 0, 5, and 10 deg. Cylinder No. 1 was yawed to create the flow fields necessary for inlet/engine yaw simulation. The data show that as the yaw angle is increased, the sidewash angle increases. It should be noted that when the cylinder was yawed to 10 deg, the survey area was decreased because of interference between the survey probe and the aft end of the cylinder.

3.4.3 Large Turning Vanes

During the wind tunnel experiments, data were obtained at Mach numbers of 0.6, 0.9, and 1.0 with both vanes installed and at Mach numbers of 0.6, 0.9, 1.0, and 1.1 with vanes individually installed.

The local flow vectors showing the comparison between the predicted and measured flow fields at a free-stream Mach number of 0.9 are shown in Fig. 46. These same data are shown in Fig. 47 for constant sidewash (or upwash) angles. It is apparent from this figure that the analytical method does not work with this type of model. It should be noted that although the vanes span the tunnel, the flow field is not uniform spanwise as it would be for the truly two-dimensional case analyzed.

Analysis of the surface pressure data shown in Fig. 48 indicates that the flow choked between the vane at Mach numbers above 1.0. Data for the individual vane tests show the vanes to act similar to a wing surface with the bottom vane having a shock wave formed on the upper surface at Mach numbers above 1.0.

3.4.4 Small Turning Vanes

During the wind tunnel experiments, data were obtained at Mach numbers of 0.6, 0.9, 1.0, and 1.1 with both vanes installed and with the vanes individually installed.

Figure 49 presents the local flow vectors showing the comparison between the predicted and the experimental flow fields for a free-stream Mach number of 0.9 with

the small vanes located four inches apart. These same data are shown in Fig. 50 for constant angles of upwash and sidewash. In Fig. 50, the wind tunnel survey data are again shown as solid circles with the number above the circle indicating the upwash angle and the number below the circle indicating the sidewash angle.

It is interesting to note in this comparison that the theoretical method predicted the flow trends and the overall values quite well. The deviation between the theoretical and measured data varies, from the vane that is convex to the plane of the flow toward the vane that is concave to the plane of flow, from a maximum of 3 deg on one side to approximately 5 deg on the other side. Apparently the shorter length, outflow, and the lower pressure at the trailing edge created by the design of the convex vane tended to eliminate the viscous problems that were present with the large turning vanes. Although the flow field produced by the small vanes does not appear to represent the required flow field, the analysis does indicate that within limits the theoretical method can be used to predict the flow field for this type of model.

3.4.5 Study Configuration Flow Simulation

The final comparisons are those between the data obtained with the study aircraft configuration in the AEDC PWT-16T and the data obtained with the shaping devices in the AEDC PWT-1T.

A comparison between the local flow vectors obtained at Mach number 0.9 with the study configuration in the AEDC PWT-16T at an angle of attack of 10 deg and a yaw angle of zero and data obtained at Mach number 0.9 with the dual hollow circular cylinders in the AEDC PWT-1T is shown in Fig. 51. Cylinder No. 1 was set at 40-deg pitch and 0-deg yaw, and Cylinder No. 2 was set at 30-deg pitch and 0-deg yaw. To get the simulation shown, it was necessary to locate Cylinder No. 1 as indicated in the figure and to adjust the data for a geometric pitch of the inlet/engine to 5 deg. (To adjust the data for geometric pitch, the assumed geometric pitch angle of the inlet/engine is added to the measured upwash angle. The new upwash angle is then used in the computation of the flow vector.) Thus, the forebody effect plus a net gain of 5 deg in pitch is obtained from the cylinders. As shown in Fig. 40, if the local Mach number is not simulated, the free-stream Mach number could be adjusted to give the correct local Mach number without greatly affecting the upwash and sidewash simulation.

Figure 52 presents the local flow vectors showing the comparison between data obtained at Mach number 0.9 with the study configuration at an angle of attack of 19.8 deg and a yaw angle of zero and data obtained at Mach number 0.9 with the dual hollow cylinders. The setting of the dual hollow cylinders is the same as in Fig. 51. However, to get correct simulation as shown in Fig. 52, it was necessary to move Cylinder No. 1 nearer to the inlet and to adjust the data for a geometric pitch of the inlet/engine of 12 deg. This is the maximum geometric pitch available with the full-scale inlet/engine. Here the forebody effect plus a net gain of 7.8 deg was realized with the flow shaping.

Figures 53 and 54 present the comparison between the experimental data obtained at Mach number 0.9 with the study configuration and the theoretical results computed at Mach number 0.9 for the modified hollow cylinders. Figure 53 shows the flow vector plot for the study configuration at an angle of attack of 10 deg and a yaw angle of 4 deg (lee side). The modified hollow cylinders were set with Cylinder No. 1 at 30-deg pitch and 10-deg yaw (nose away from tunnel centerline), and Cylinder No. 2 at 20-deg pitch and 0-deg yaw. The theoretical results are adjusted for a geometric pitch of the inlet/engine of 10 deg. Thus, the forebody effect and yaw angle simulation were obtained using the flow shaping and the pitch simulation by geometric pitch.

Figure 54 shows the same data compared at constant angles of upwash and sidewash. From this figure, the actual differences in the numerical value of the angles can be seen. It is noted that a maximum of 2 deg difference is shown between the experimental data with the study configuration and the theoretical results with the modified cylinders.

Figure 55 shows the comparison between data obtained at Mach number 0.9 in the AEDC PWT-16T with the study configuration and data obtained at Mach number 0.9 in the AEDC PWT-1T with the dual modified cylinders. Here again the study configuration was at an angle of attack of 10 deg with an angle of yaw of 4 deg (lee side). However, the modified hollow cylinders are set with Cylinder No. 1 at 30-deg pitch and 10-deg yaw (nose away from tunnel centerline) and Cylinder No. 2 at 20-deg pitch. The difference between these data and the previous data is the spacing between the cylinders. The theoretical data for the cylinder are for a spacing of 154 in. full scale, and the experimental cylinder data are for a spacing of 138 in. full scale. In Fig. 55, the modified cylinder data are only adjusted for a geometric pitch of the inlet/engine of 5 deg. Thus, the forebody effect, yaw angle simulation, and a net gain in pitch angle of 5 deg are obtained from the flow shaping.

SECTION IV BLOCKAGE STUDY

4.1 INTRODUCTION

A simulation technique developed using shaping devices is of little value unless there remains sufficient space in the tunnel for the inlet/engine, and the tunnel will operate with the inlet/engine installed. Therefore, throughout the design of the shaping devices, space was always allowed for the installation of an inlet/engine. The final phase of the study was to determine the operating characteristics of the wind tunnel when both the shaping devices and equivalent full-scale inlet/engine are installed in the test section. Although the majority of effort in this phase was devoted to determining wind tunnel operating parameters, the flow angularity probe was mounted at a fixed location just above and in front of the inlet to determine, if possible, the effect of the inlet on the flow angularity.

4.2 WIND TUNNEL EXPERIMENTS

4.2.1 Wind Tunnel (AEDC PWT-1T)

The AEDC PWT-1T is described in Section 3.3.7 and Ref. 3. However, attention should be called to the plenum evacuation duct and scavenging scoop duct shown in Fig. 16 which are metered to determine the auxiliary weight flow requirement for operation of the wind tunnel. Pressure orifices were located along both test section walls and in the tunnel diffuser to determine the Mach number variations in the test section and the tunnel pressure ratio, respectively. During the blockage study, the top and bottom test section walls were diverged one deg, and the diffuser flaps were closed.

4.2.2 Instrumentation

The basic instrumentation was the same as that described in Section 3.3.3. In addition, however, the scavenging scoop and plenum airflows were measured with square-edged orifices. The general location of the metering orifices is shown in Fig. 16. The pressure upstream of the orifices and the pressure differentials across the orifice were measured with differential transducers and were displayed on electromanometers.

The orifice airflow temperatures were measured with iron constantan thermocouples and were displayed on indicating potentiometer-type recorders.

4.2.3 Models

The shaping device models used in the blockage study were the dual hollow cylinders described in Section 3.3.4.1 and the modified hollow cylinders described in Section 3.3.4.2.

The inlet/engine model used was a one-sixteenth scale, two-dimensional, supersonic inlet/engine which was available from a previous wind tunnel blockage study. The forebody was removed since the technique is to simulate forebody effects and maneuvering conditions. The inlet/engine model could be manually set in pitch from 0 to 8 deg. The flow through the inlet/engine could be varied by a control valve in the scavenging scoop line to simulate different engine power settings.

Figure 56a shows an installation photograph of the dual hollow cylinders and the inlet/engine model as viewed from the top of the inlet. Figure 56b shows the dual hollow cylinders and the inlet/engine model viewed from the wind tunnel nozzle section. In both of these photographs, Cylinder No. 1 is pitched to 30 deg with 0-deg yaw and Cylinder No. 2 is pitched to 20 deg with 0-deg yaw.

Figure 57a shows an installation photograph of the modified hollow cylinders and the inlet/engine model as viewed from the top of the inlet. Here Cylinder No. 1 is pitched 30 deg with 10-deg yaw (nose away from tunnel centerline), and Cylinder No. 2 is pitched 20 deg with 0-deg yaw. Figure 57b shows an installation photograph of the modified

hollow cylinders and the inlet/engine model as viewed from the wind tunnel nozzle section. Here both cylinders are pitched 30 deg with 0-deg yaw.

4.3 RESULTS AND DISCUSSION

4.3.1 Effect of Inlet/Engine Installation on the Flow Angularity

To determine how the installation of the inlet/engine would affect the measured flow field using only the dual hollow cylinders, the flow angularity probe was installed with the inlet/engine model during the blockage study testing. The probe was located at an x-station and y-z axis location for which data were obtained with the dual hollow cylinder flow shaping devices.

Figure 58 shows the changes in the upwash and sidewash as a function of Mach number that resulted from two settings of the dual hollow cylinders with the inlet/engine model at 0-deg pitch. In both cases, the presence of the inlet/engine increased both the upwash and the sidewash angles. With Cylinder No. 1 set at 30-deg pitch and 0-deg yaw and Cylinder No. 2 set at 20-deg pitch and 0-deg yaw, the upwash was increased approximately 1.5 deg maximum, and the sidewash was increased approximately 2.25 deg maximum. With Cylinder No. 1 set at 40-deg pitch and 0-deg yaw and Cylinder No. 2 set at 30-deg pitch and 0-deg yaw, the upwash was increased approximately 2 deg maximum, and the sidewash was increased approximately 2.5 deg maximum. These data have the expected trends in both cases showing the maximum increase of the lower Mach number with the effect decreasing as Mach number increases.

4.3.2 Tunnel Operating Characteristics

During the blockage test, tunnel runs were made for most positions of the dual hollow cylinders and modified hollow cylinders previously tested with inlet/engine model set at 0- and 8-deg angle of attack with simulated engine power settings of idle and cruise. It was found, for the most part, that the addition of the inlet/engine model with either pair of cylinders had little effect on the maximum Mach number operating capability of the tunnel for the same cylinder settings without the inlet/engine model.

During the blockage test, scavenging and auxiliary weight flows required for operating the tunnel were determined by metering the flow through the scavenging scoop and plenum evacuation ducts. Calculations of the weight flows, measured by metering orifices, were consistent with the procedures outlined in Ref. 4.

Figure 59 shows the ratio of the auxiliary weight flow to the tunnel weight flow required to operate the AEDC PWT-1T when the dual hollow cylinders or modified hollow cylinders are installed with the inlet/engine model, assuming the tunnel is started with the cylinders and inlet/engine set at zero pitch and yaw until after the engine is started. The present performance curves for the Plenum Evacuation System (PWT-PES) for operation of the AEDC PWT-16T are shown in the figure.

By assuming that the AEDC Engine Test Facility airside and exhaust plants are used for make-up air and scavenging, respectively, thus leaving the total capacity of the PWT-PES for plenum pumping, it appears that the majority of the requirement for operation with the dual hollow cylinders and inlet/engine could be met. However, the majority of the requirement for operation with the modified hollow cylinders and the inlet/engine is outside the present PWT-PES capability.

Two additional curves are shown in the figure which represent the capacity that would be available with the addition of a double compressor unit equal to the present double units or the addition of a complete third increment (five units). It can be seen that the addition of a double unit would satisfy the requirements for operation with either pair of cylinders with the inlet/engine and allow some leeway for flow shaping devices on inlet/engines with greater tunnel blockage.

SECTION V

SUMMARY AND RECOMMENDATIONS

The analytical and experimental data obtained during the flow shaping study with the dual hollow circular cylinders and modified hollow cylinders show excellent agreement. The analytical and experimental data obtained with the small turning vanes gave fair agreement, but the agreement between analytical and experimental data with the large turning vanes was poor.

Of the devices tested, the modified hollow cylinders appeared to give the best overall increases in both pitch and yaw simulation. An increase of approximately 9 deg in upwash was obtained and was fairly uniform over a region typical of an inlet capture area. By using a combination of flow shaping and geometric pitch, the capability of simulating 20-deg angle of attack for the study configuration was demonstrated. The yaw simulation capability was also demonstrated with the modified hollow cylinders by using a combination of flow shaping and geometric pitch.

Although the pitch simulation obtained was 5 deg short of the objective, the data obtained show that this testing technique can significantly increase the present testing capability of the AEDC PWT-16T for testing of inlet/engine systems, particularly those that are fuselage side mounted and are located forward of the wing. Further study is needed before it can be assumed that the technique will work for all inlet/engine locations. In terms of modifications or additions that need to be added to PWT-16T to utilize this technique, the following recommendations are made:

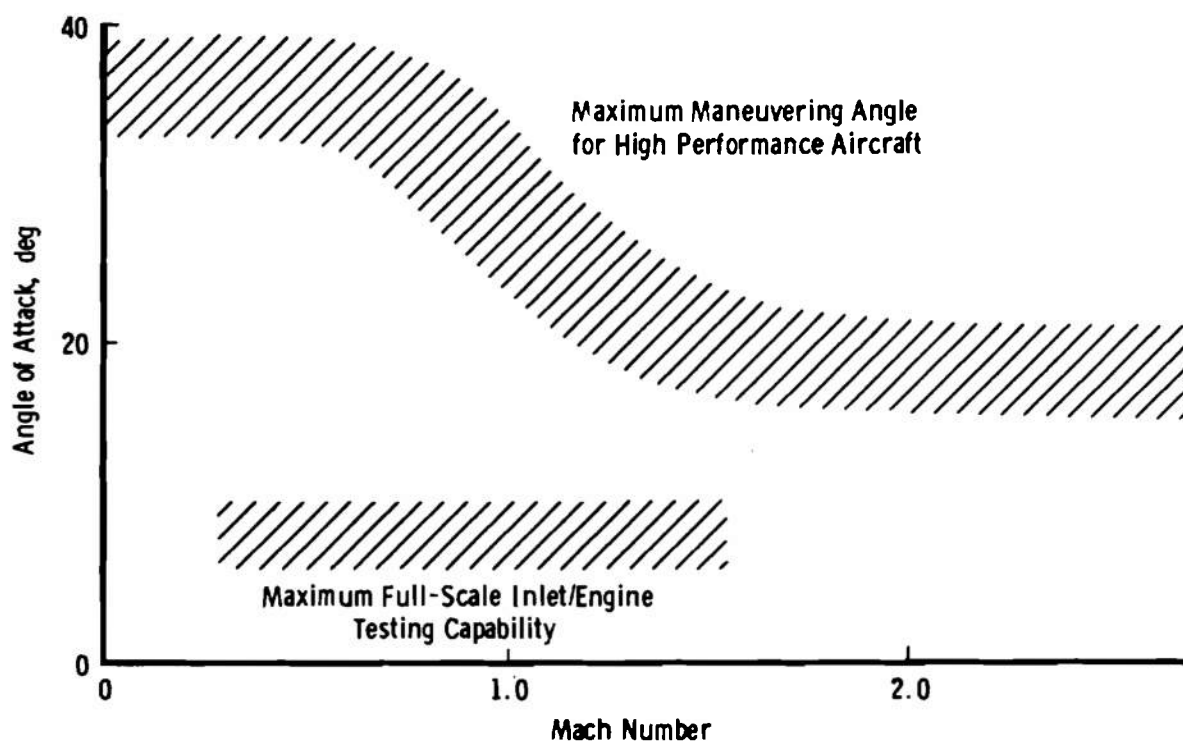
1. A double compressor unit equal to the present double units needs to be added to the PWT-PES. This unit is required to cover the added auxiliary flow with the flow shaping devices and a full-scale inlet/engine model.
2. A test cart needs to be modified in order to have remote control of the flow shaping devices in pitch, yaw, and vertical position in the tunnel.

REFERENCES

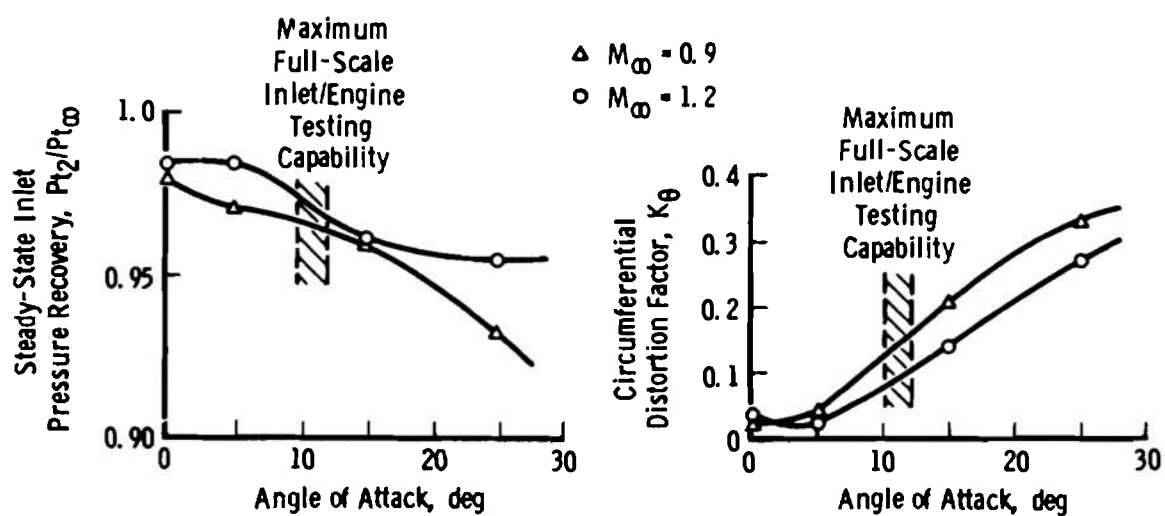
1. Lauer, R. F., Jr. "Inlet Performance Characteristics of Generalized 1/4-Scale Tactical Aircraft Models at Transonic and Supersonic Mach Numbers". AEDC-TR-71-87 (AD515022L), May 1971.
2. Lauer, R. F., Jr. "Inlet Flow-Field Surveys of Generalized 1/4-Scale Tactical Aircraft Models at Transonic and Supersonic Mach Numbers." AEDC-TR-70-189 (AD872696), August 1970.
3. Test Facility Handbook (Ninth Edition). "Propulsion Wind Tunnel Facility, Vol. 4." Arnold Engineering Development Center, July 1971.
4. Fluid Meters; Their Theory and Application. The American Society of Mechanical Engineers, New York, 1959.
5. Rubbert, P. E. "Theoretical Characteristics of Arbitrary Wings by a Non-Planar Vortex-Lattice Method." Boeing Company Document D6-9244, The Boeing Company, Seattle, Washington, August 1962.
6. Fitch, Clark R. "Three-Dimensional Aerodynamic Representation of V/STOL Wings by the Vortex-Lattice Method." AEDC-TR-68-6 (AD826007), January 1968.
7. Shapiro, Ascher H. The Dynamic and Thermodynamics of Compressible Fluid Flow. Vol. 1, The Ronald Press Company, New York, 1953.
8. Ames Research Staff. "Equations, Tables, and Charts for Compressible Flow." NACA Report 1135, 1953.

APPENDIXES

- I. ILLUSTRATIONS**
- II. VORTEX-LATTICE PROGRAM
FOR 3-D POTENTIAL FLOW
PROBLEMS**



a. Predicted Maximum Angles of Attack



b. Inlet Performance for a 1/4-Scale Model (Ref. 1)

Fig. 1 Typical Performance for Highly Maneuverable Aircraft

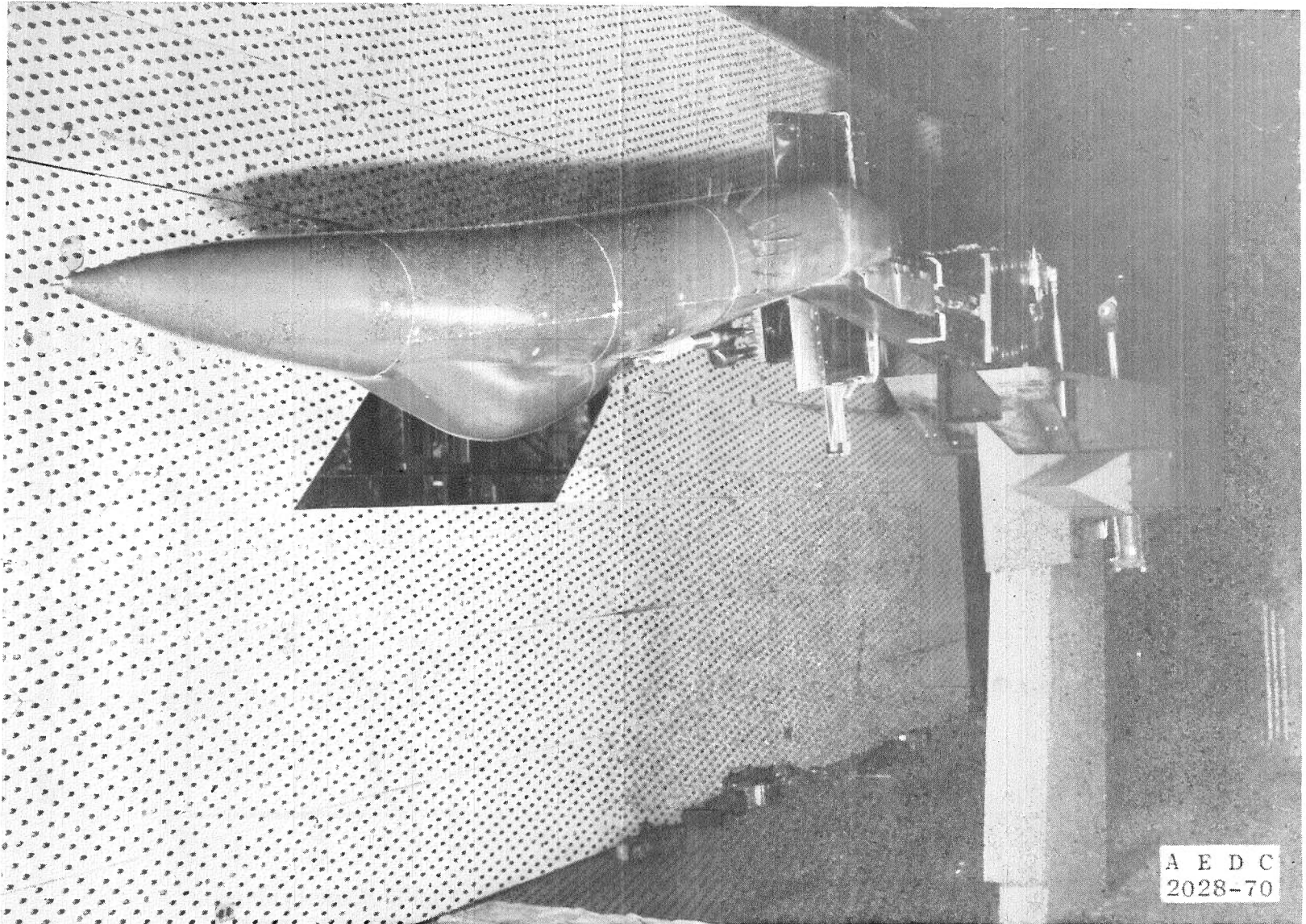


Fig. 2 Aircraft Study Configuration Installed in the AEDC 16-ft Transonic Wind Tunnel

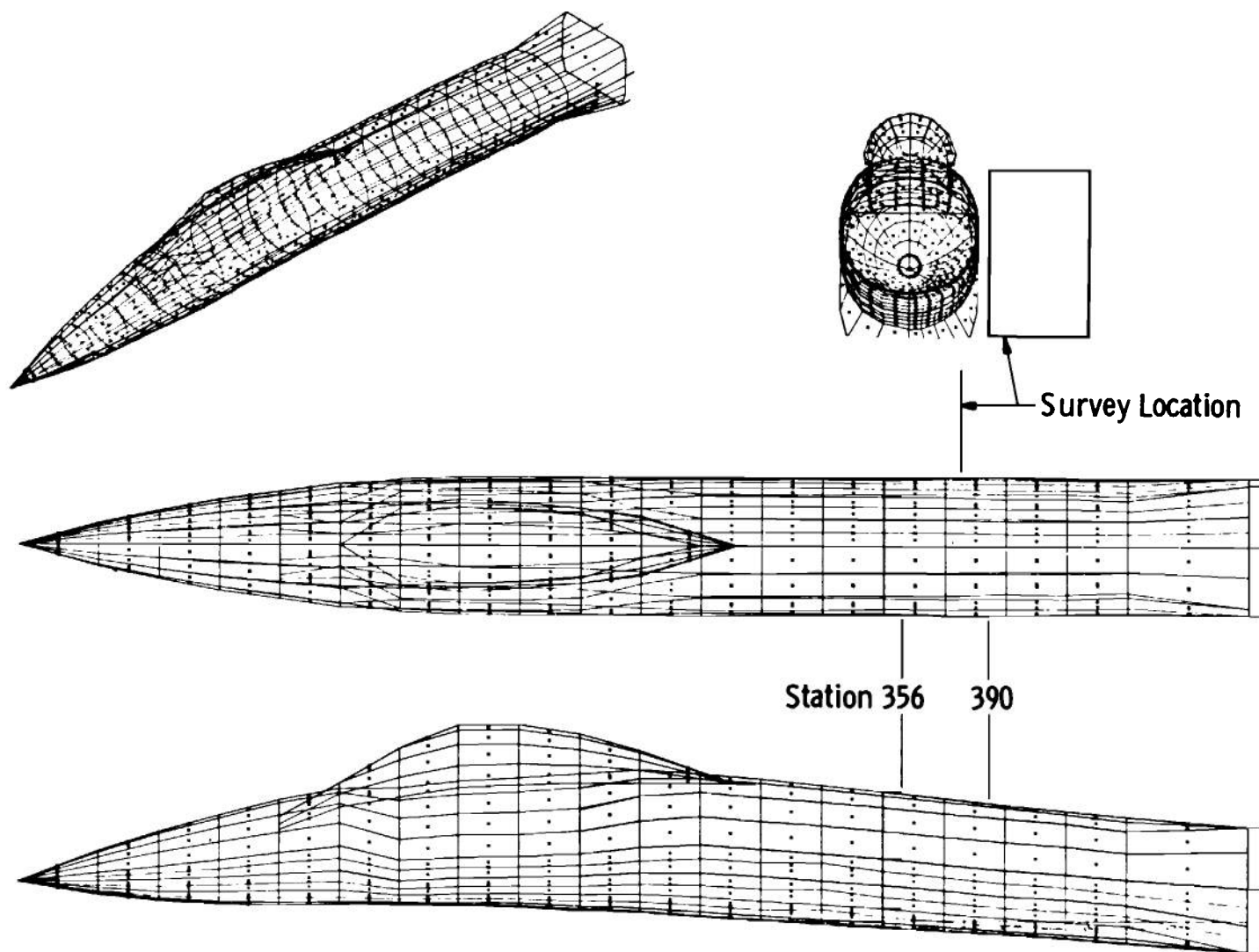


Fig. 3 Mathematical Model of the Fuselage of the Wind Tunnel Test Configuration

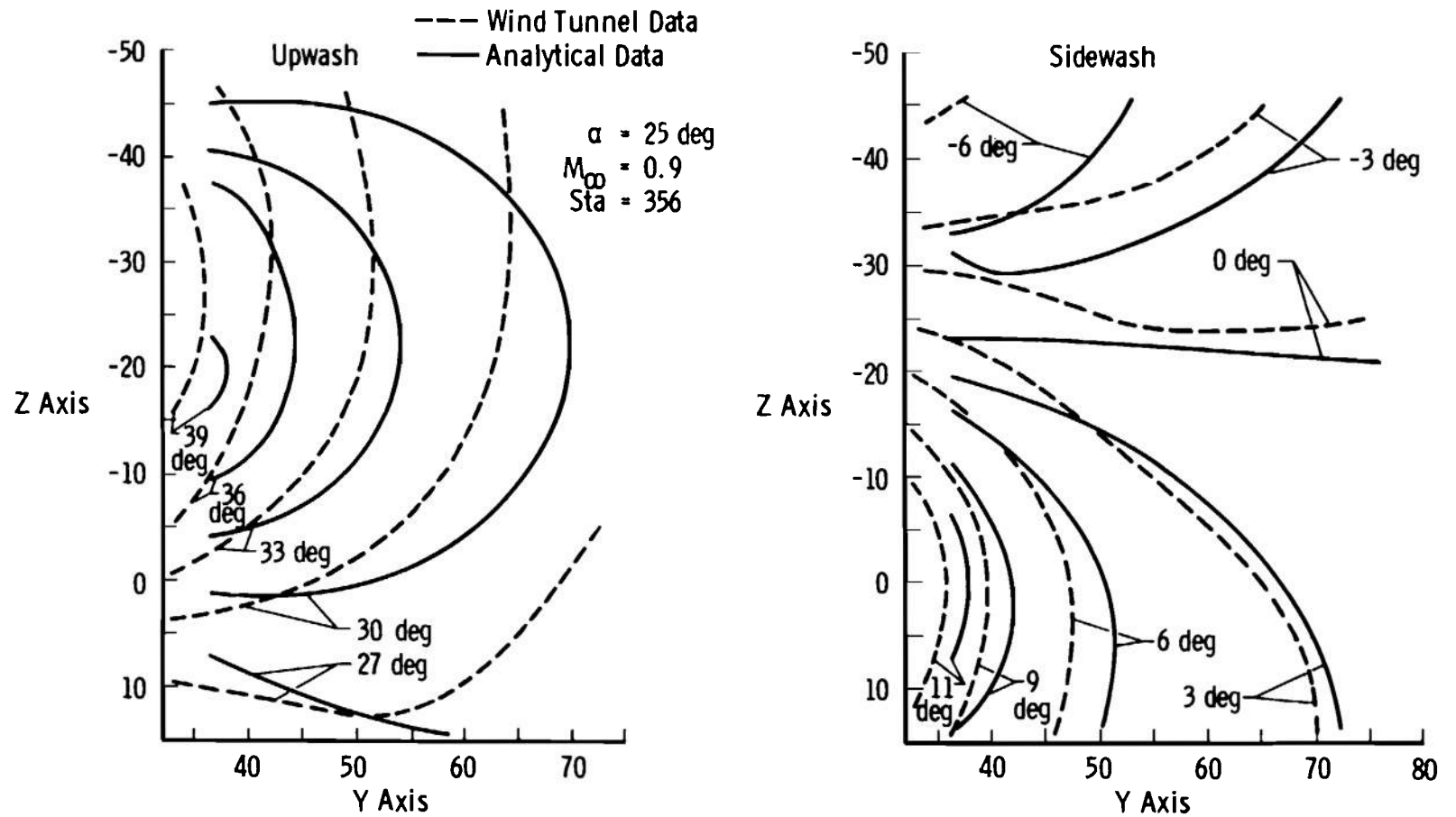


Fig. 4 Comparison between Analytical and Wind Tunnel Data for Mach Number 0.9 at an Angle of Attack of 25 deg

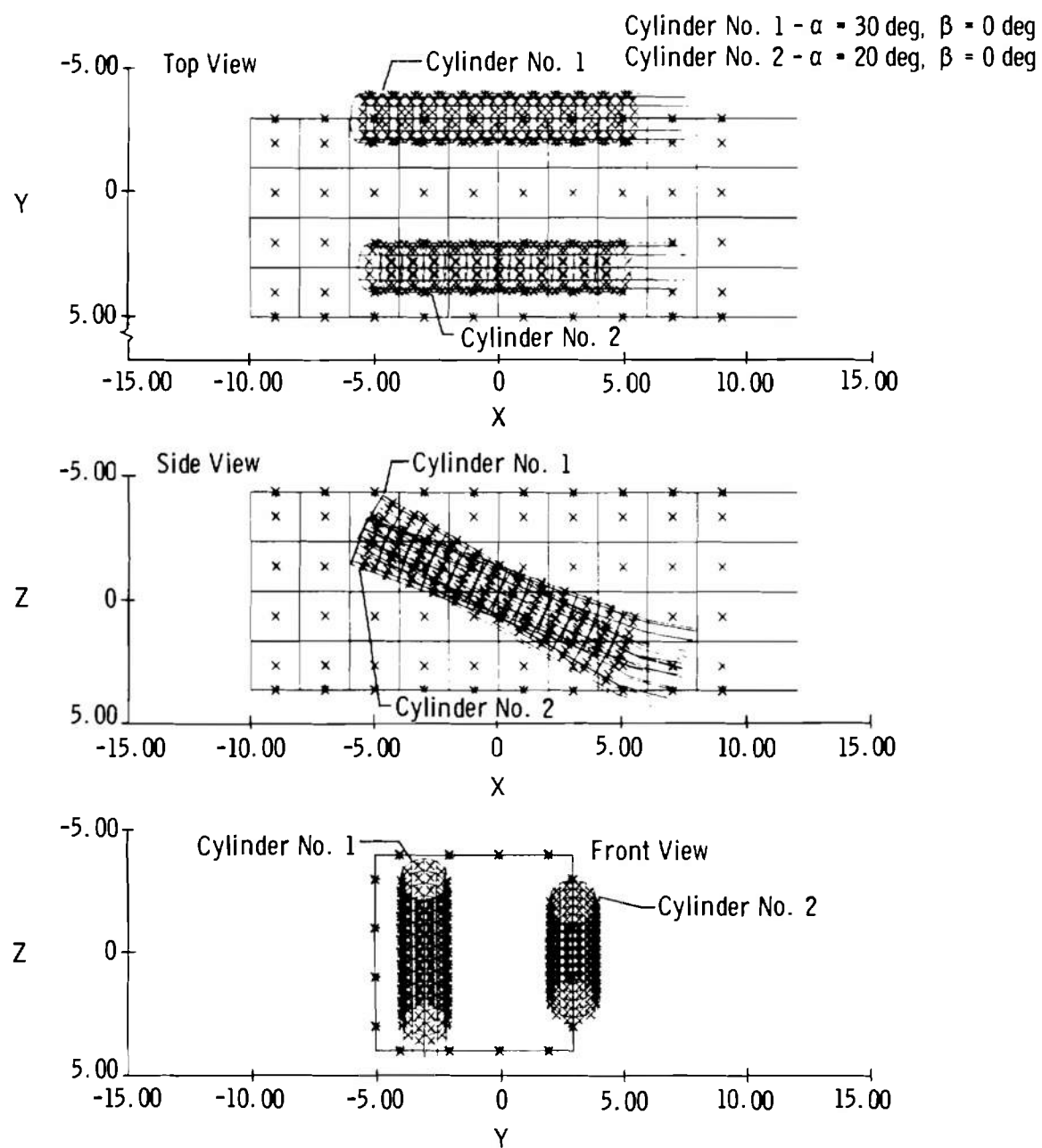
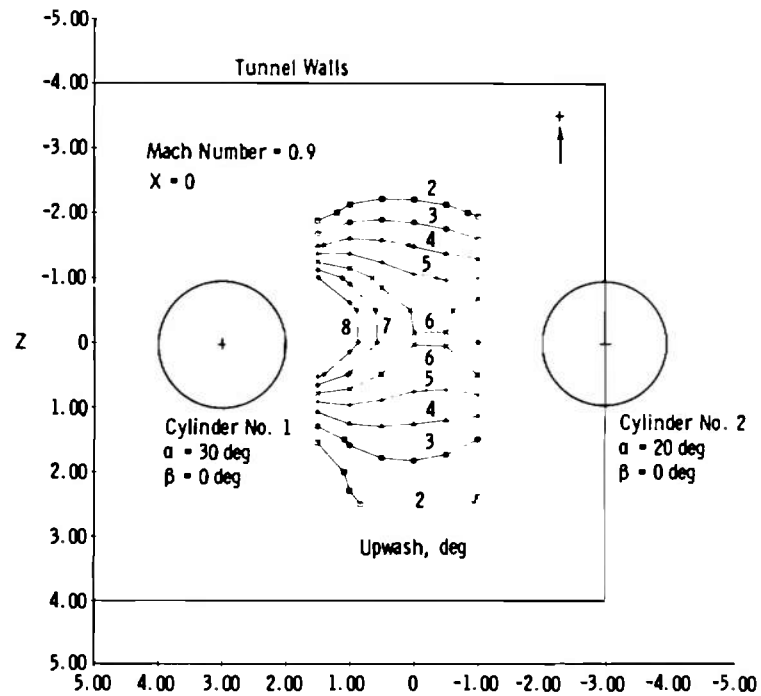
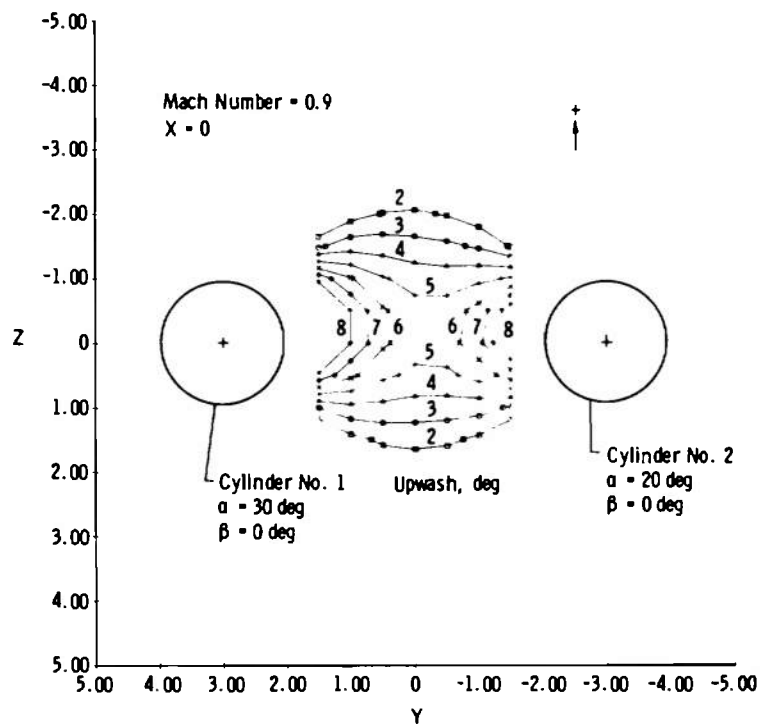


Fig. 5 Mathematical Model of Dual Hollow Cylinders in the Wind Tunnel

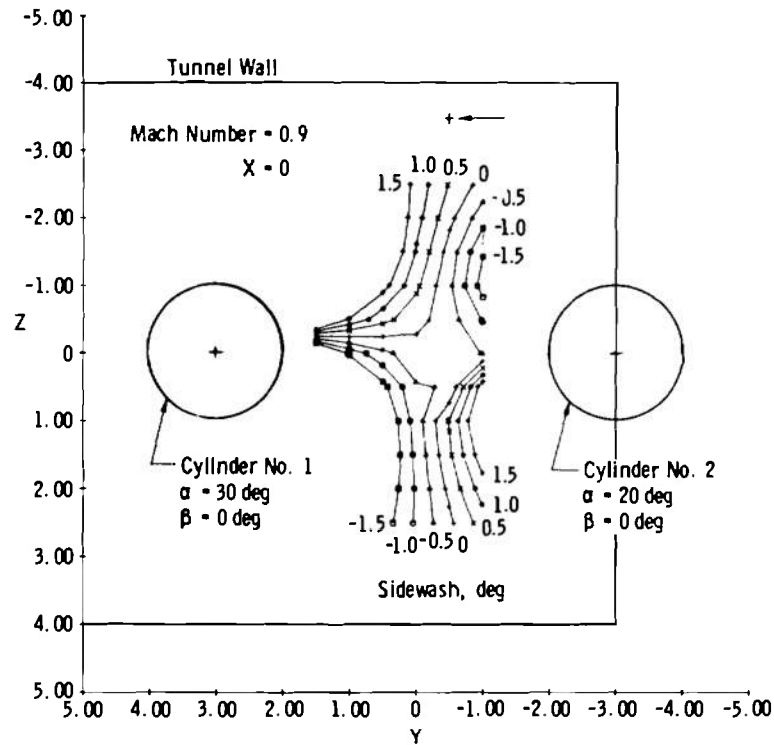


a. In the Wind Tunnel

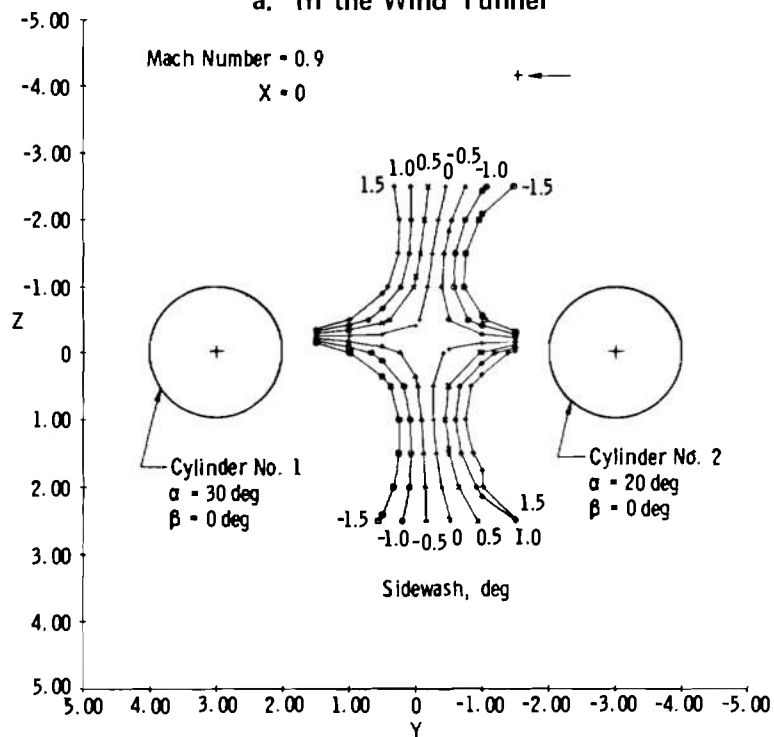


b. In Uniform Free Flow

Fig. 6 Predicted Upwash for the Dual Hollow Circular Cylinders, Mach Number 0.9



a. In the Wind Tunnel



b. In Uniform Free Flow

Fig. 7 Predicted Sidewash for the Dual Hollow Circular Cylinders, Mach Number 0.9

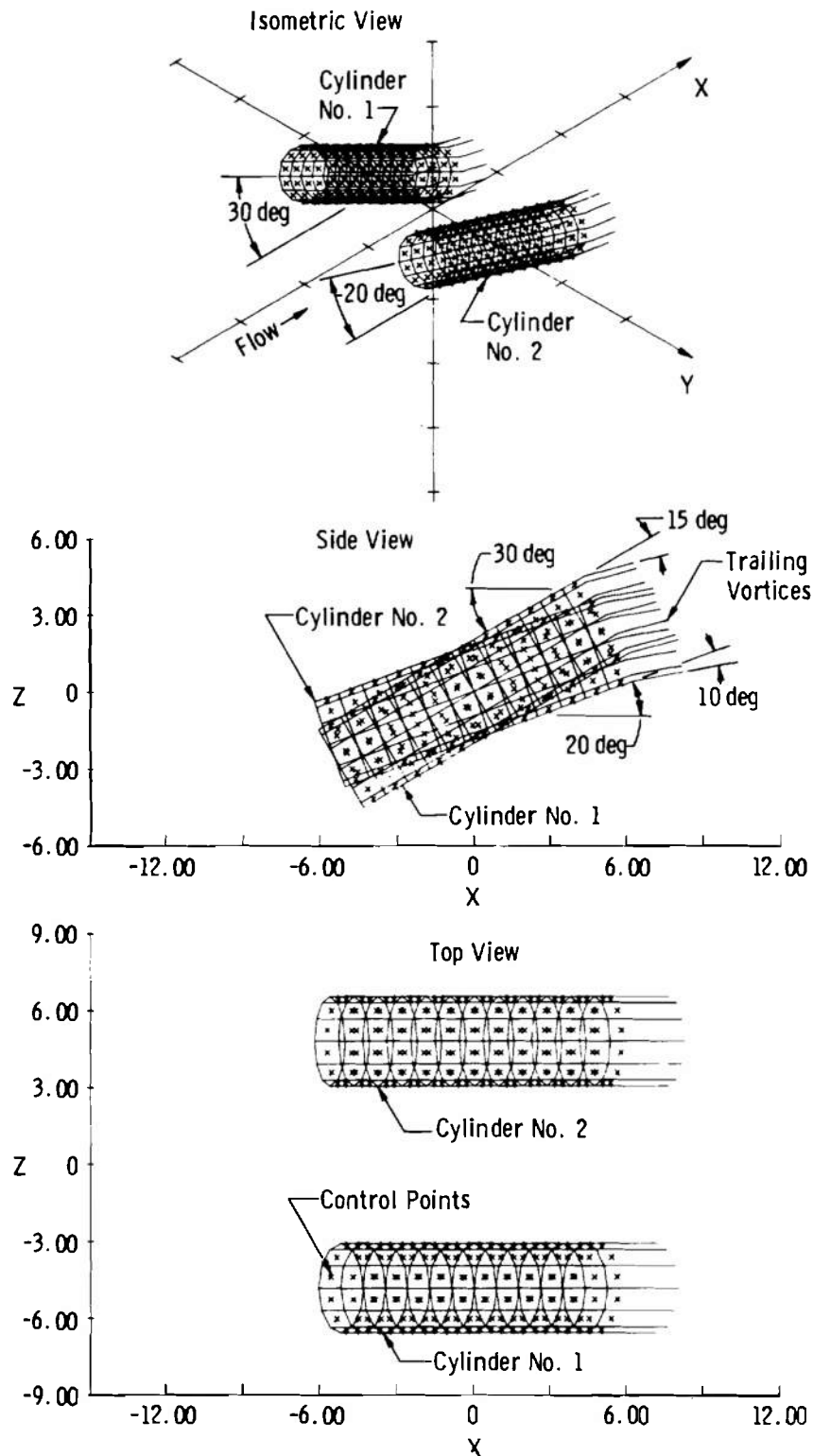


Fig. 8 Mathematical Model of the Dual Hollow Circular Cylinder Configuration

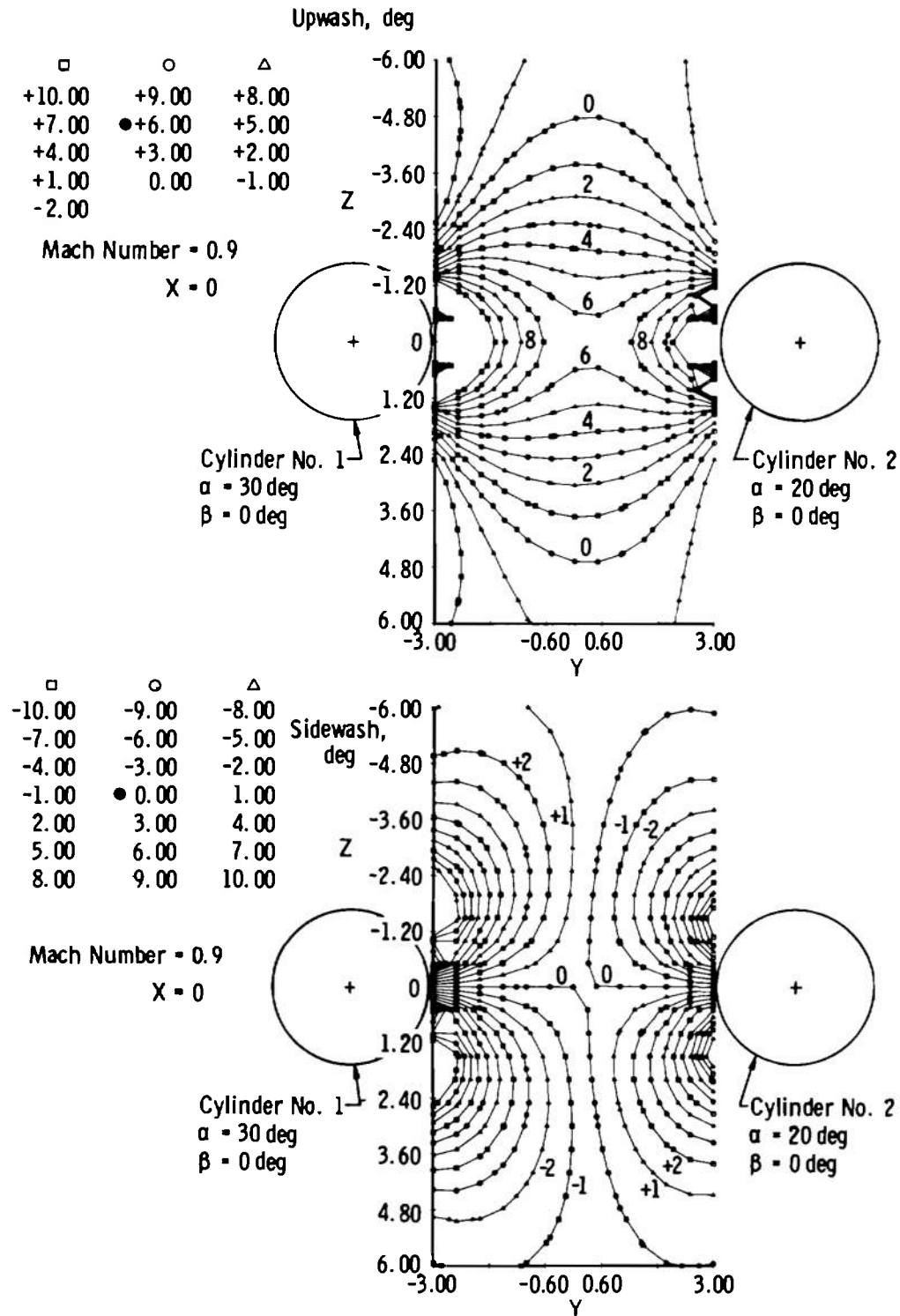


Fig. 9 Typical Predicted Flow Field for the Final Dual Hollow Circular Cylinder Configuration

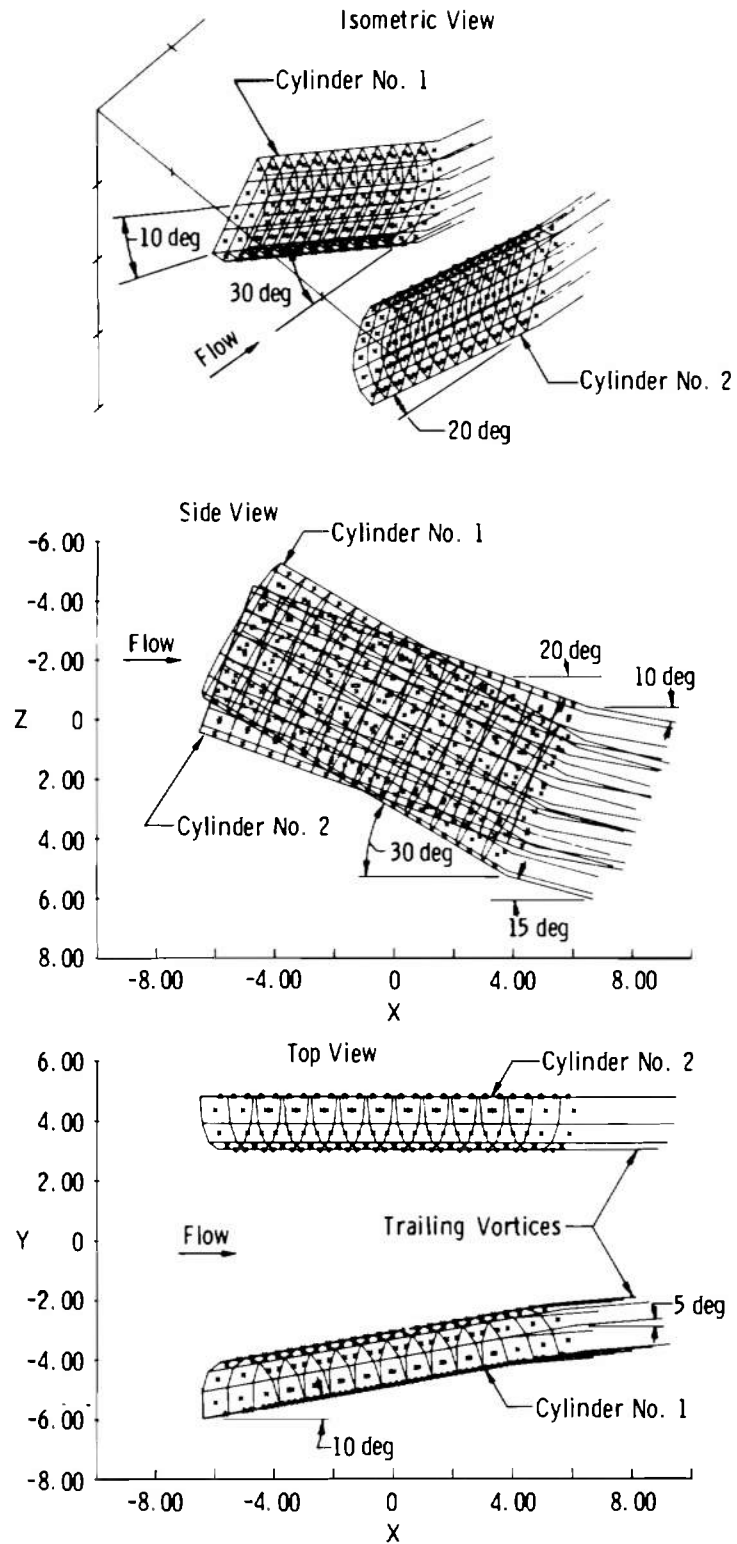


Fig. 10 Mathematical Model of the Modified Hollow Cylinder Configuration

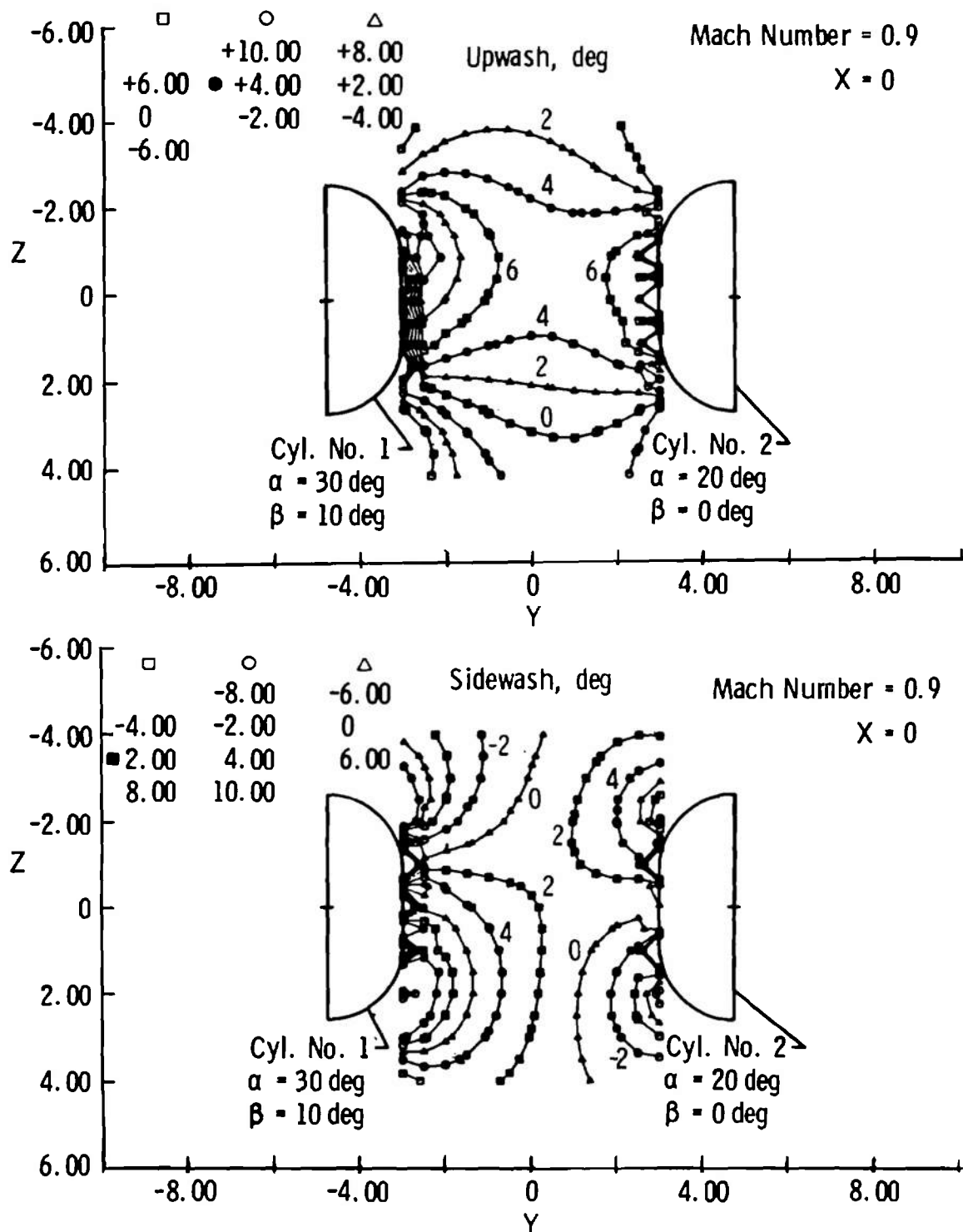


Fig. 11 Typical Predicted Flow Field for the Modified Hollow Cylinder Configuration

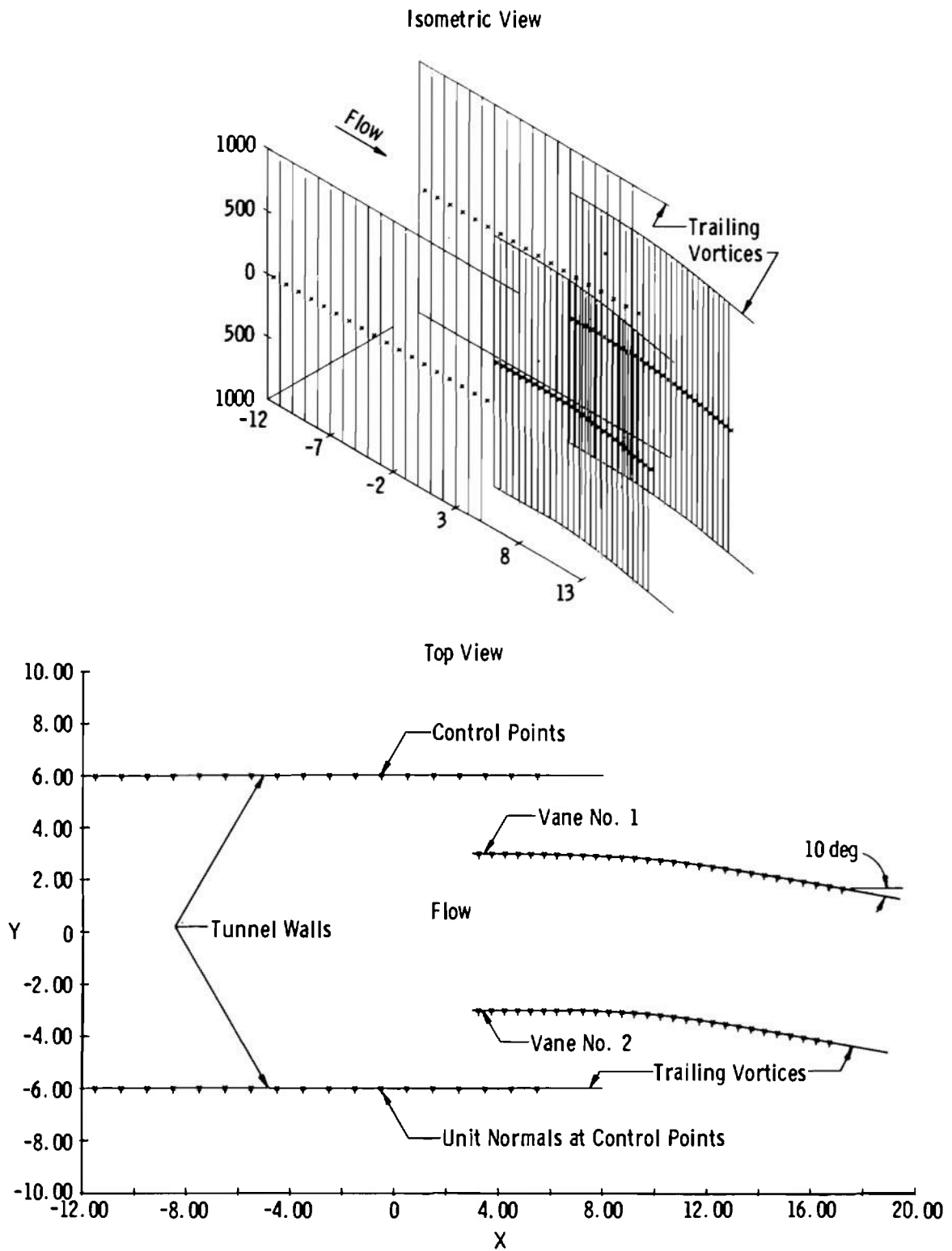


Fig. 12 Mathematical Model of the Large Turning Vanes

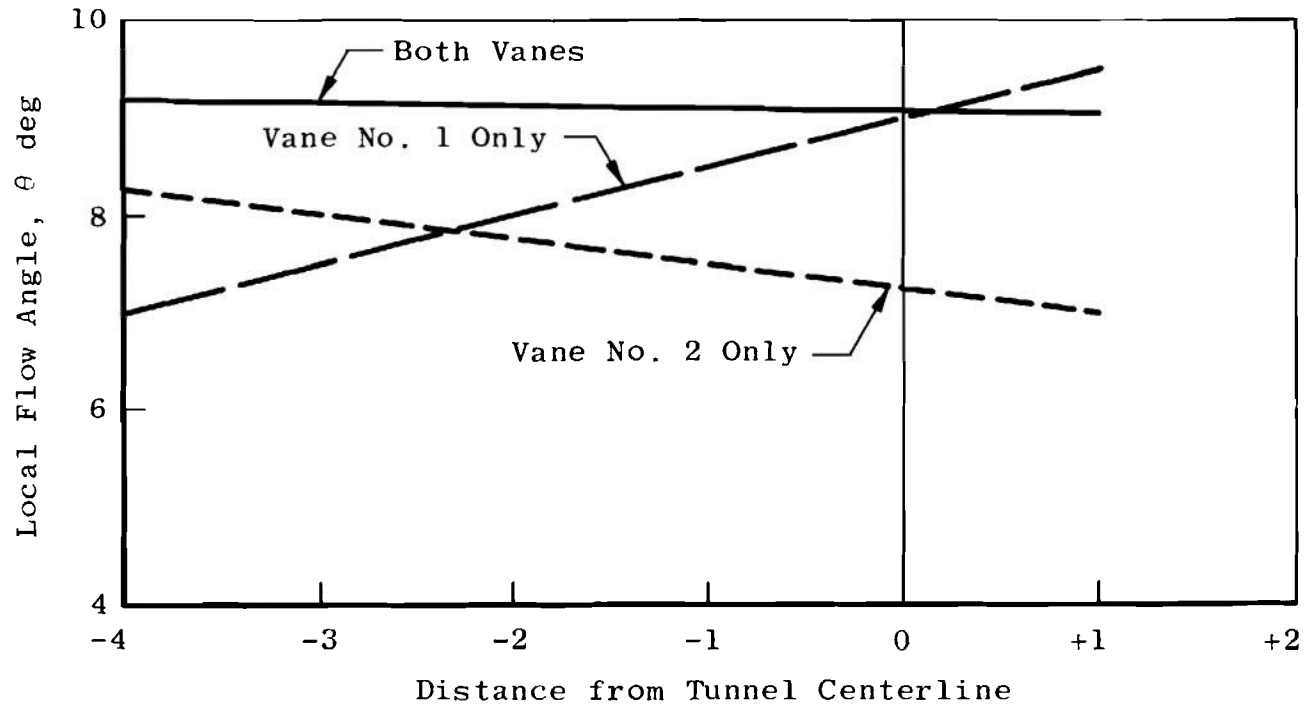


Fig. 13 Local Flow Angles for Large Turning Vanes in Plane of Trailing Edge

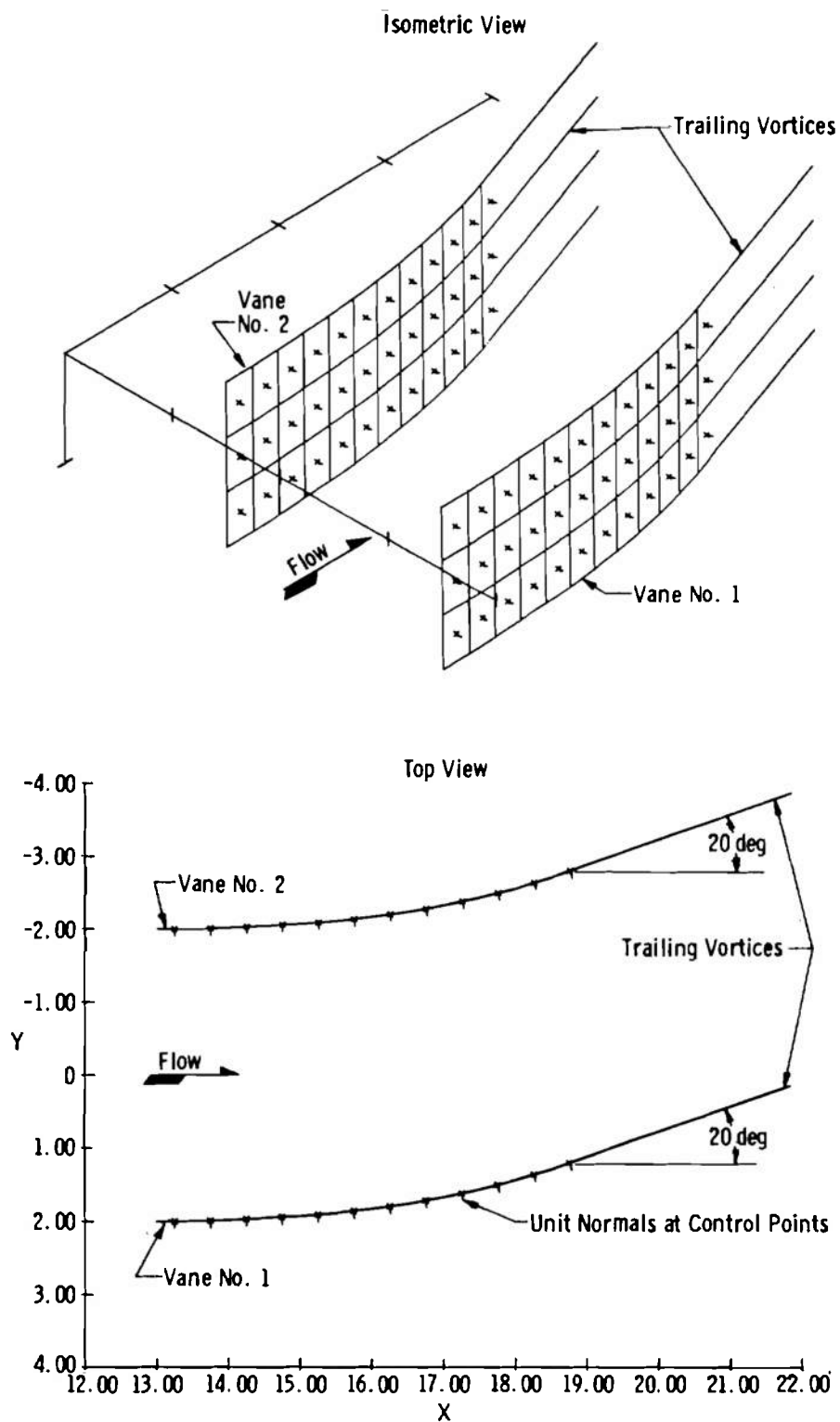


Fig. 14 Mathematical Model of the Small Turning Vanes

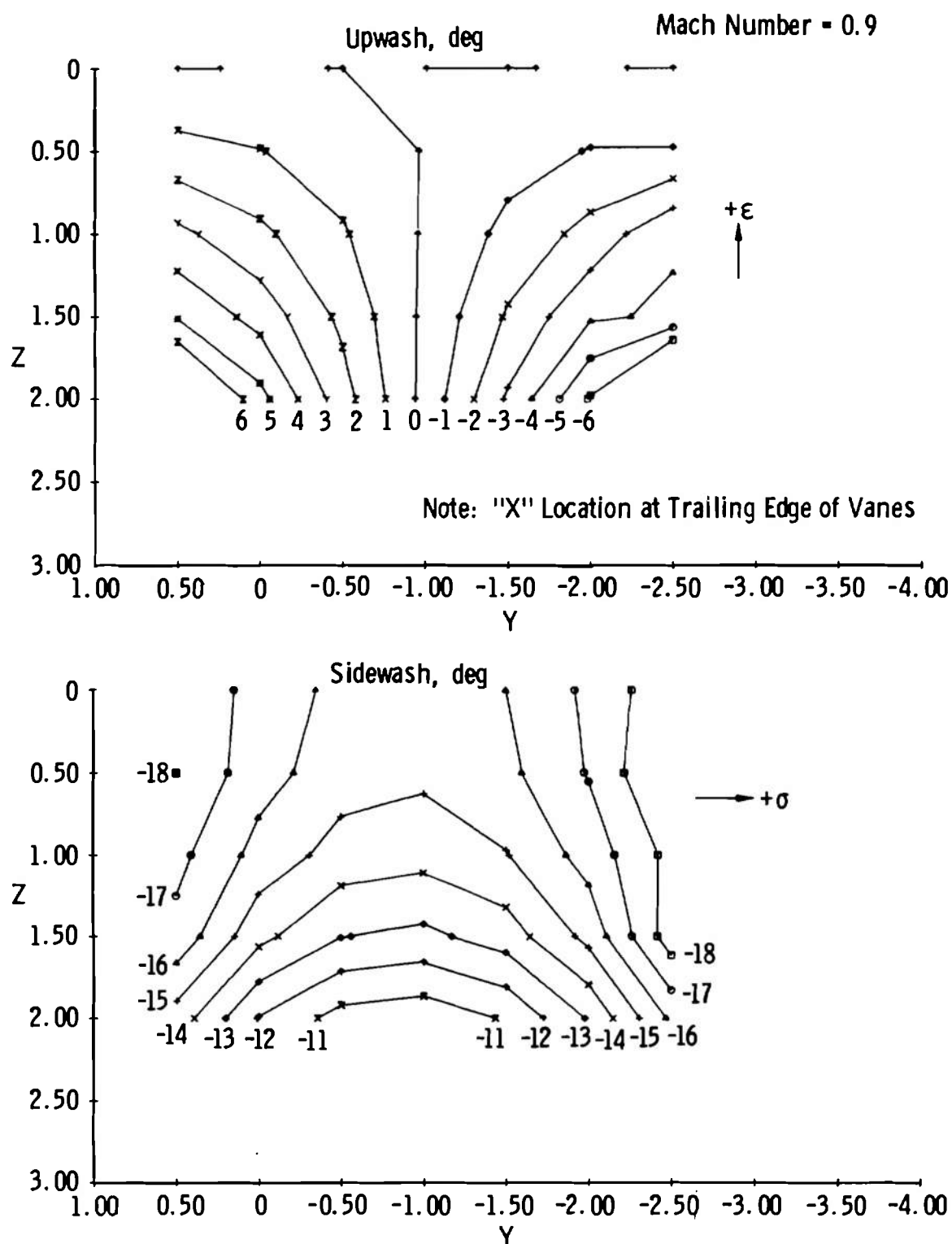


Fig. 15 Typical Predicted Flow Field for the Small Turing Vanes

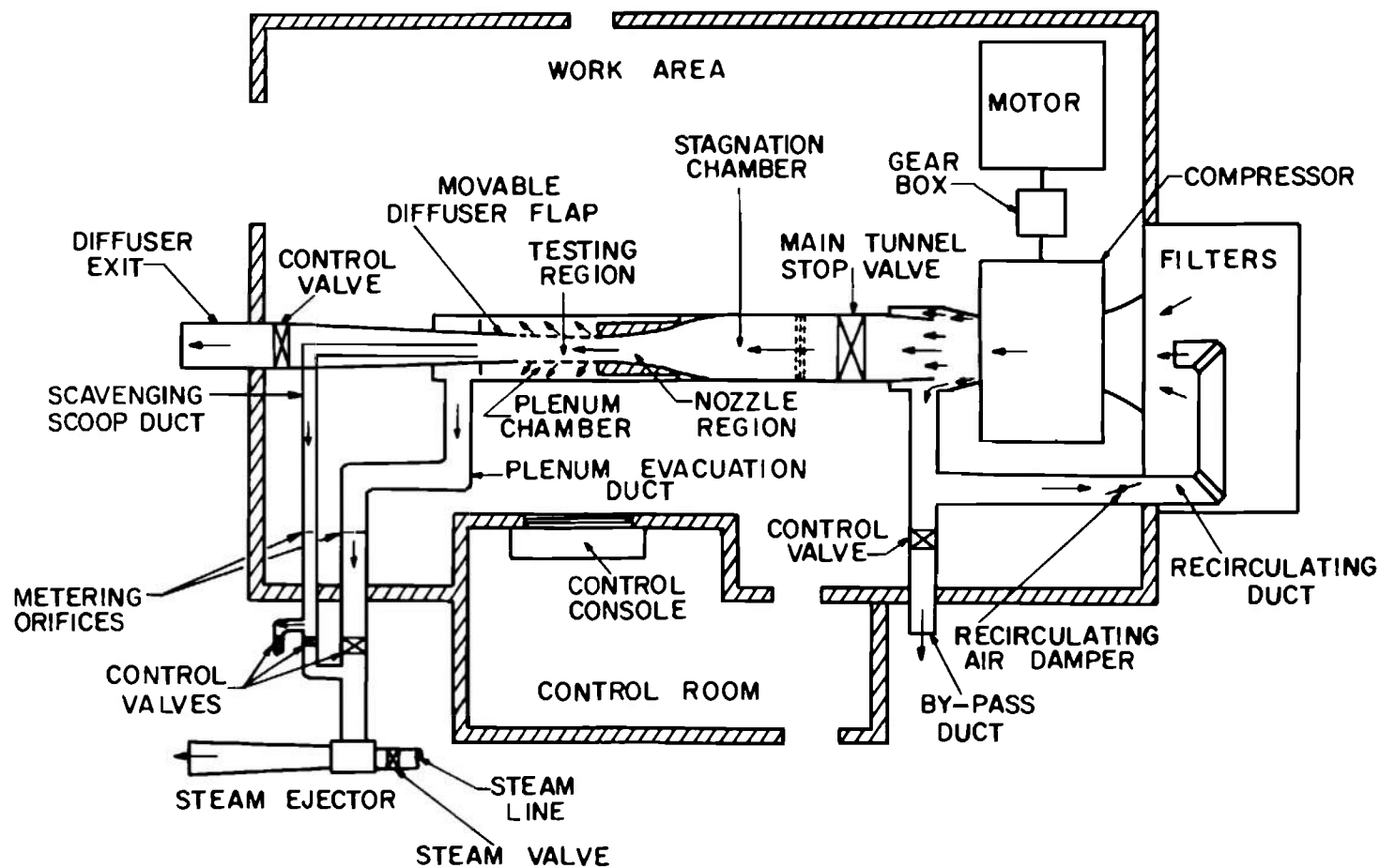


Fig. 16 General Arrangement of Tunnel 1T and Supporting Equipment

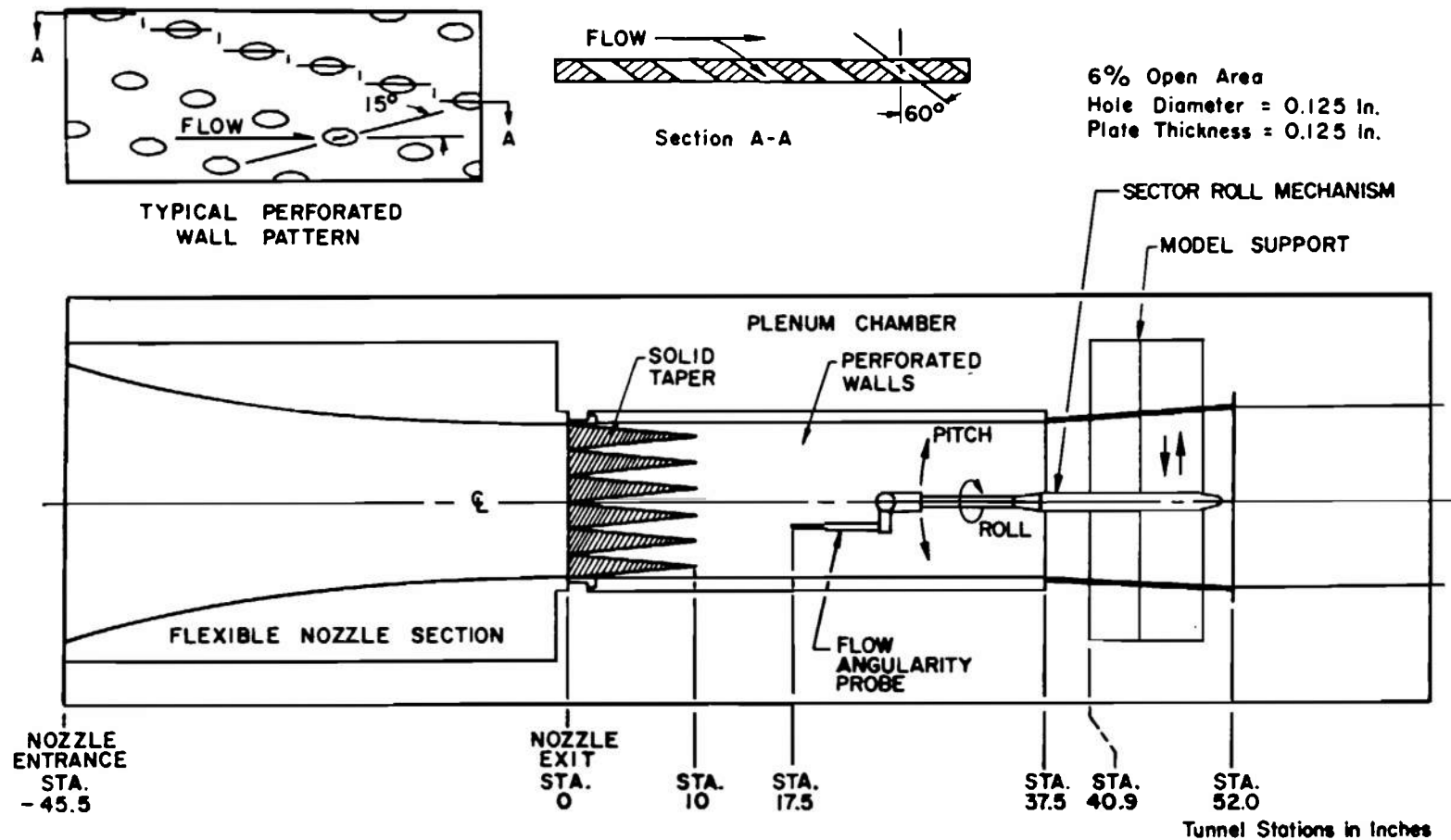


Fig. 17 Schematic of Tunnel 1T Test Leg

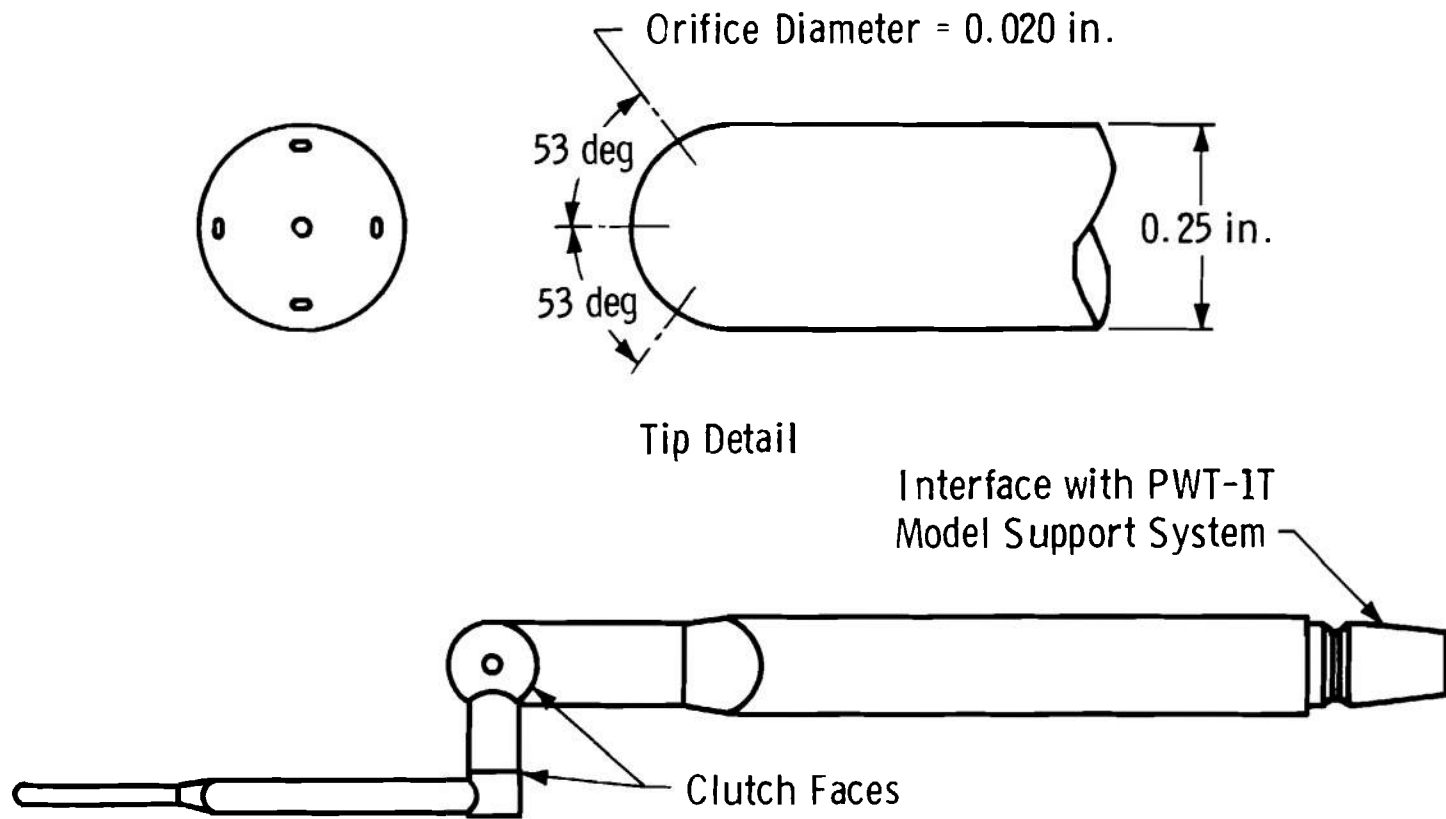


Fig. 18 Flow Angularity Probe and Support Mechanism

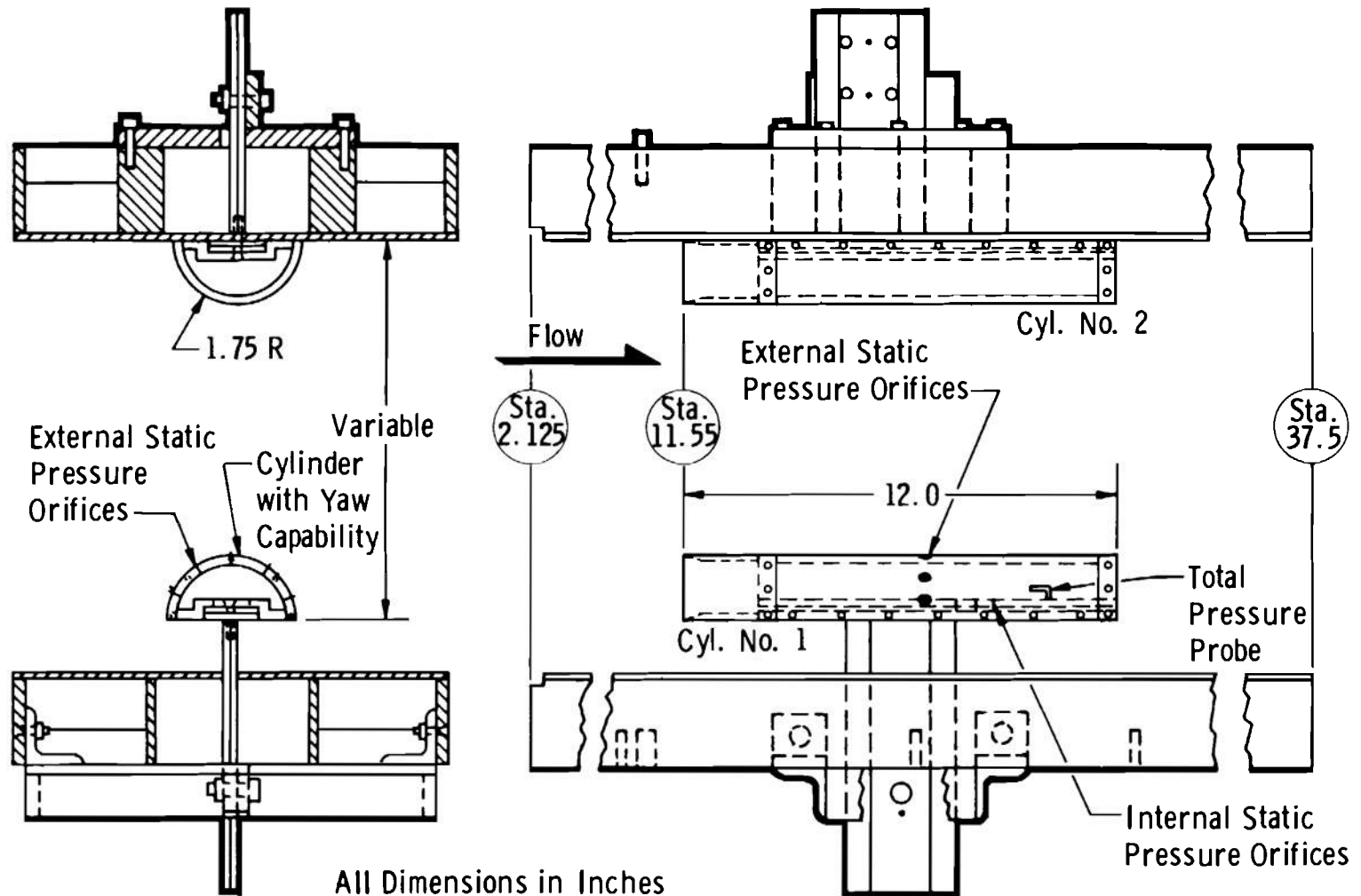


Fig. 19 Schematic of the Dual Hollow Circular Cylinder Installation

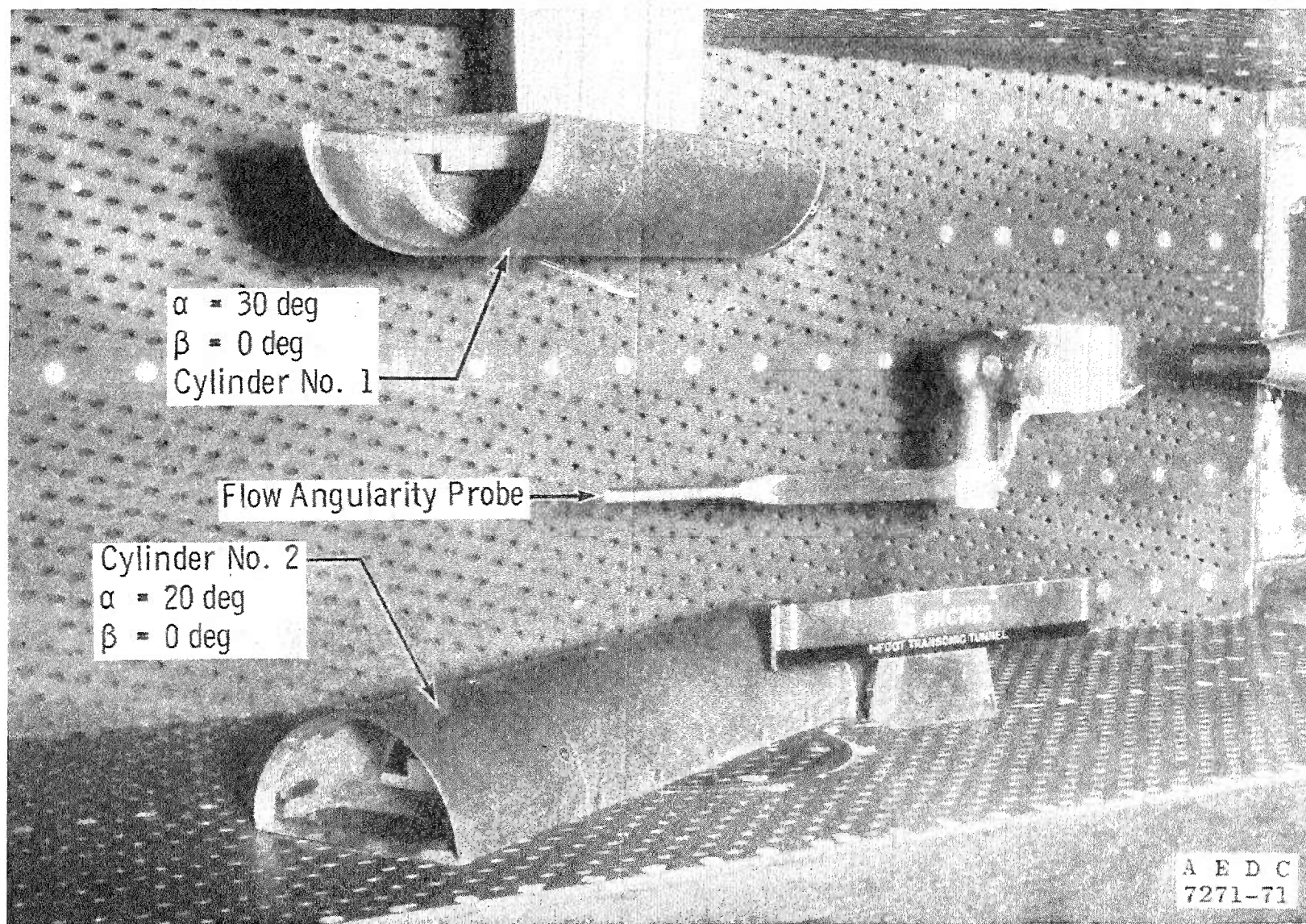
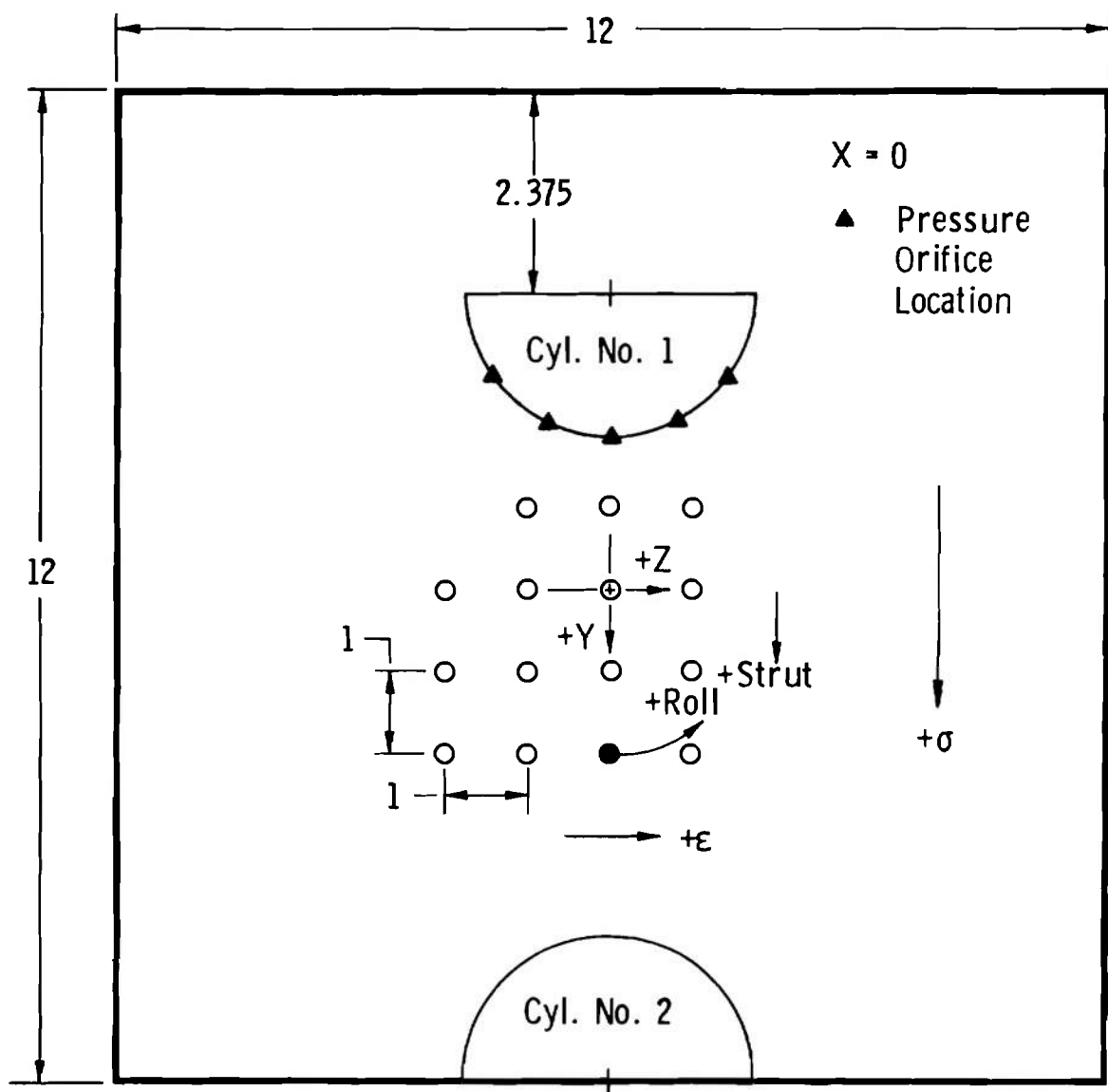


Fig. 20 Dual Hollow Cylinders Installed in the AEDC 1-ft Transonic Wind Tunnel



All Dimensions in Inches

- Probe Tip Position for Strut and Roll Mechanism Zero Position for 9.625 in. Spacing Outside to Outside

Fig. 21 Probe Survey Grid for the Dual Hollow Circular Cylinder Wind Tunnel Test

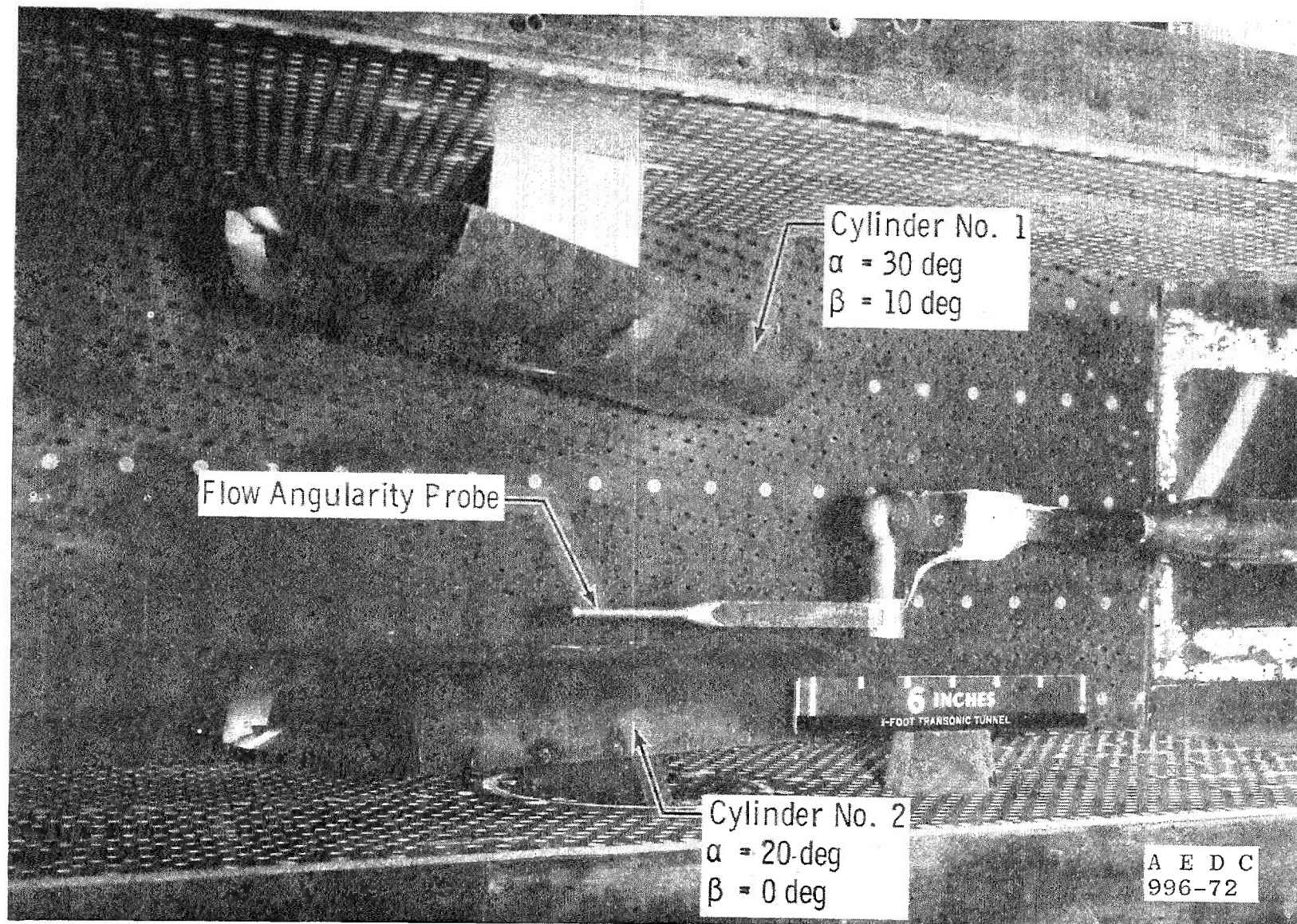
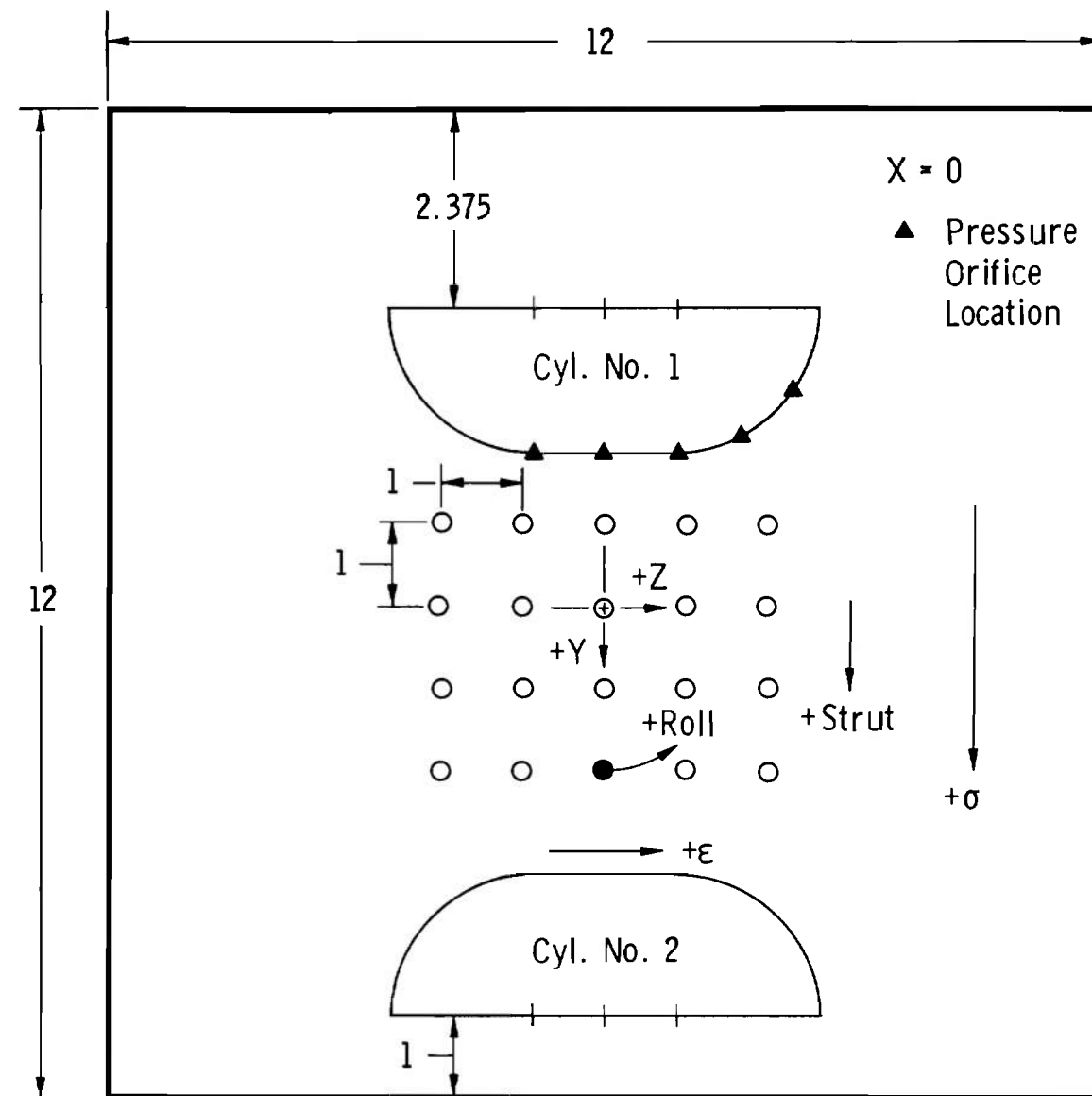


Fig. 22 Modified Hollow Cylinders Installed in the AEDC PWT-1T



All Dimensions in Inches

- Probe Tip Position for Strut and Roll Mechanism Zero Position for 8.625 in. Spacing Outside to Outside

Fig. 23 Probe Survey Grid for the Modified Hollow Cylinder Wind Tunnel Test

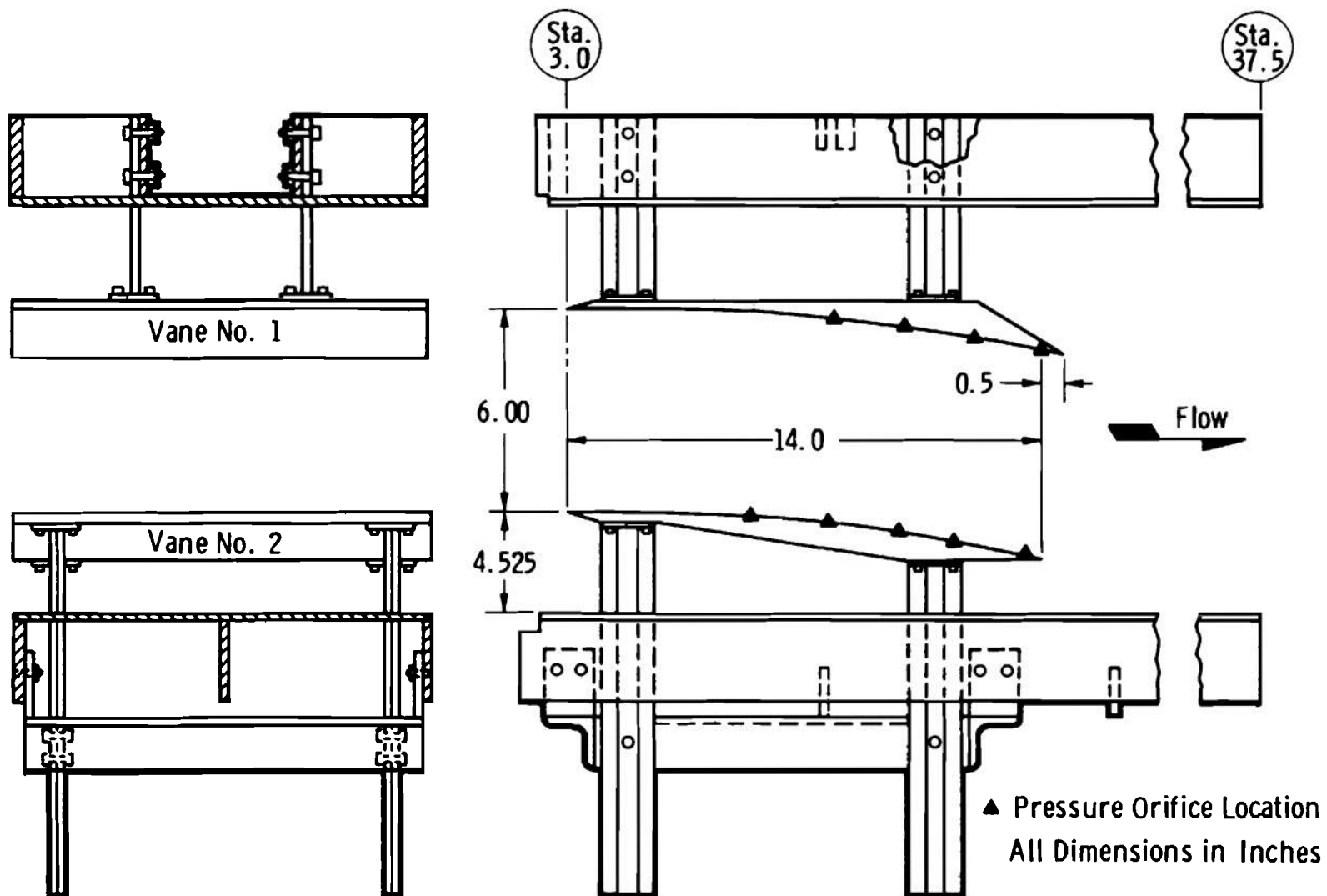


Fig. 24 Schematic of the Large Turning Vane Installation

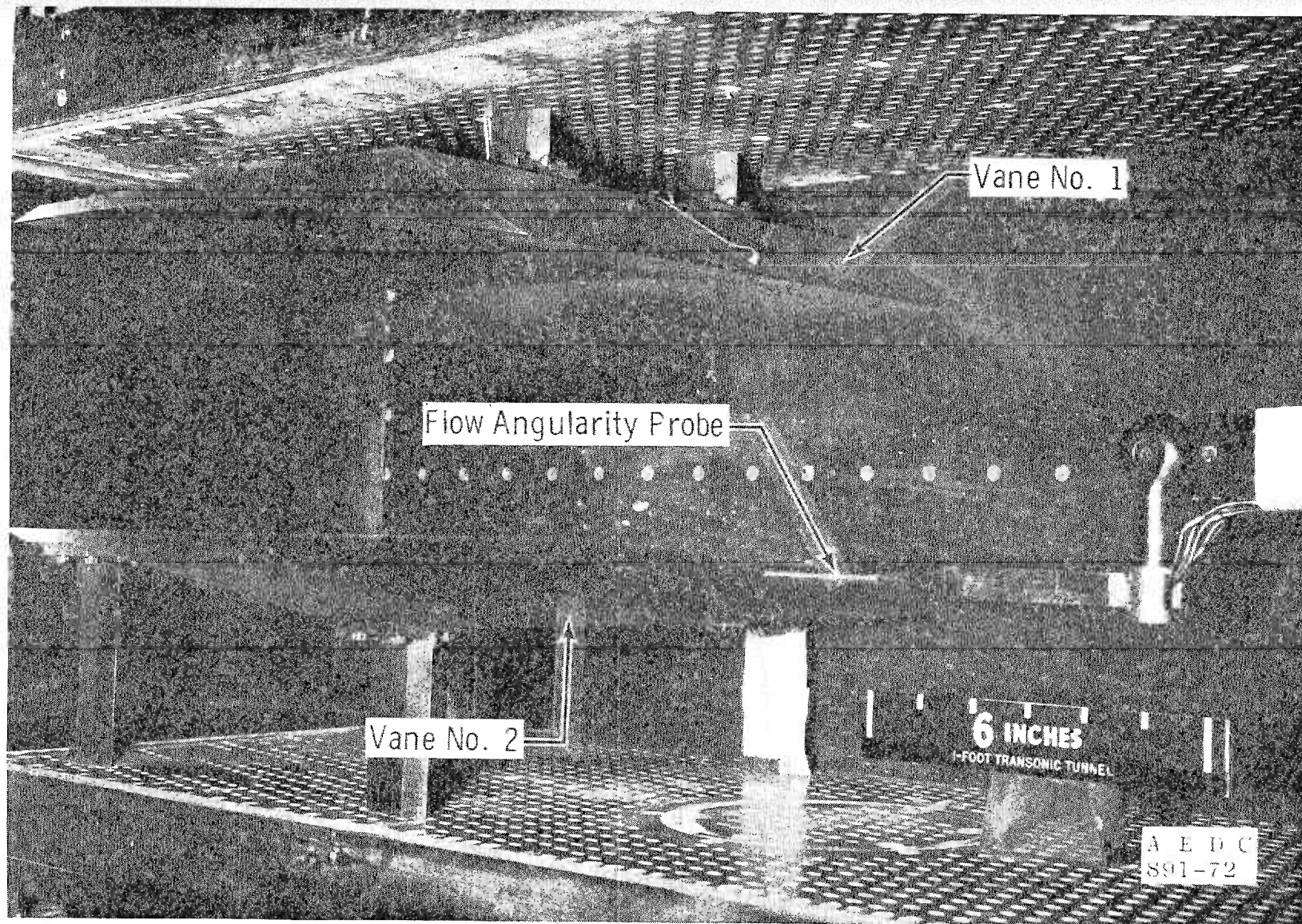
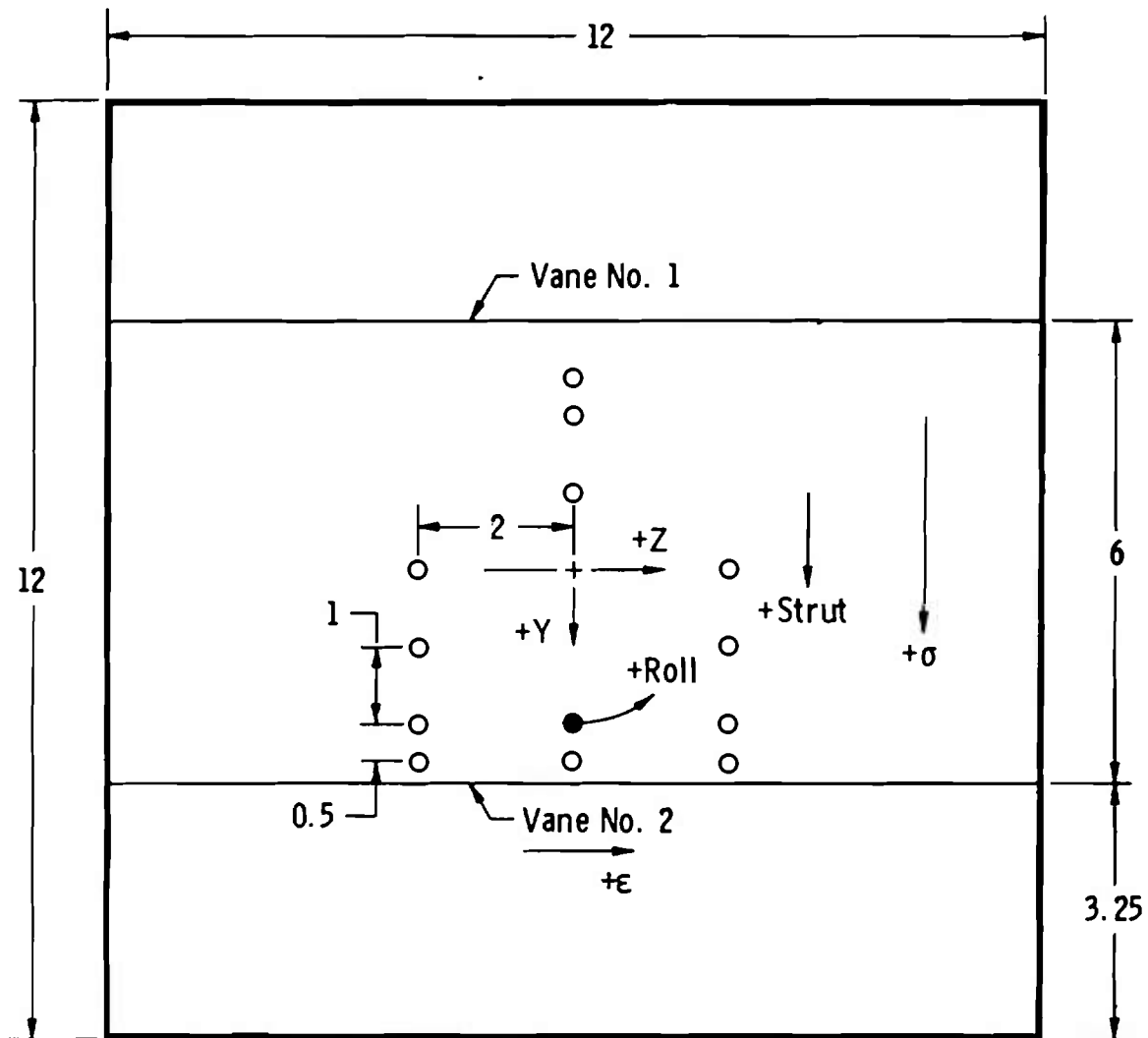


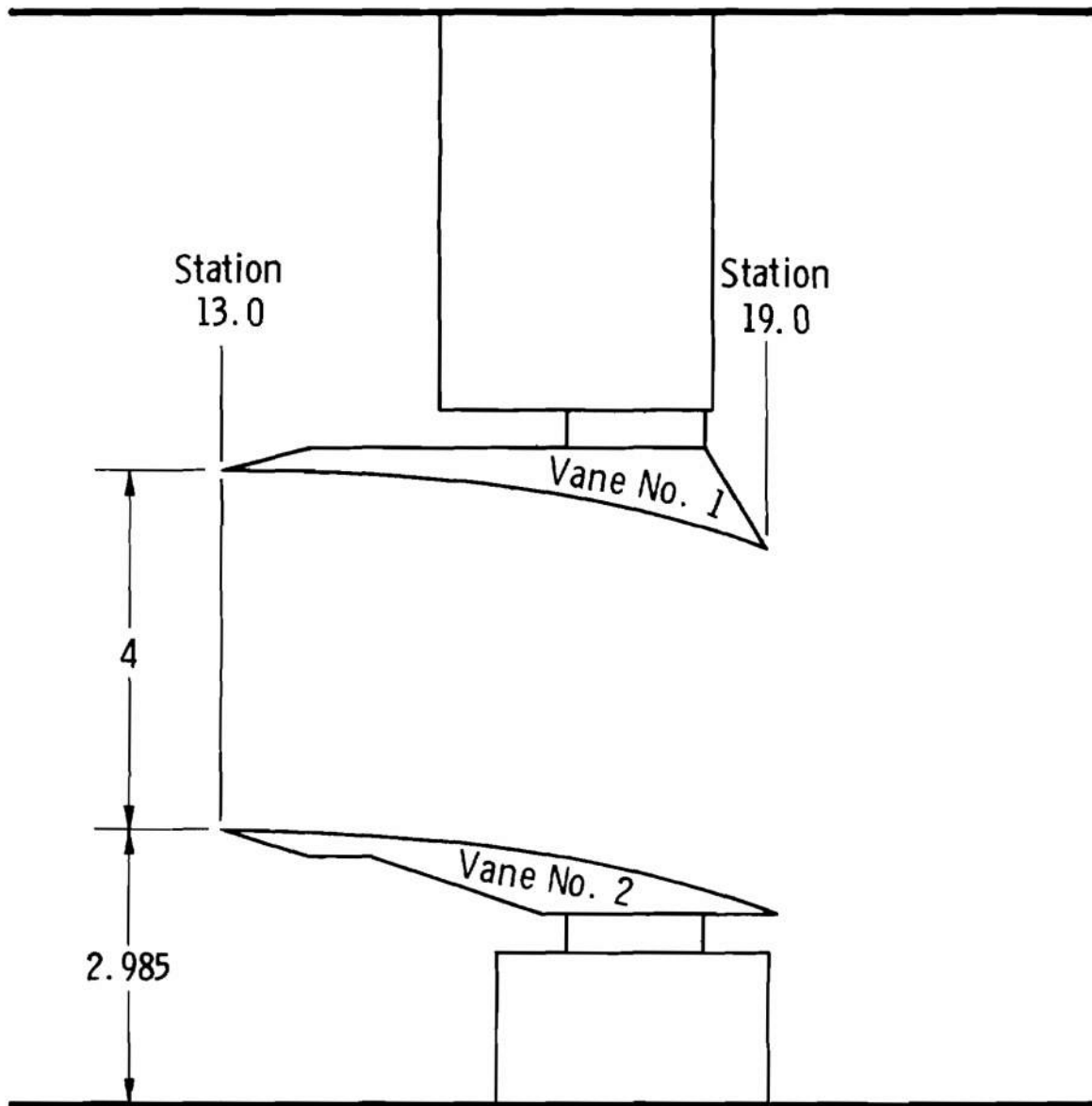
Fig. 25 Large Turning Vanes Installed in the AEDC PWT-1T



All Dimensions in Inches

- Probe Tip Position for Strut and Roll Mechanism Zero Survey Taken at Trailing Edge of Vane No. 2

Fig. 26 Probe Survey Grid for the Large Turning Vane Wind Tunnel Test



All Dimensions in Inches

Fig. 27 Schematic of the Small Turning Vane Installation

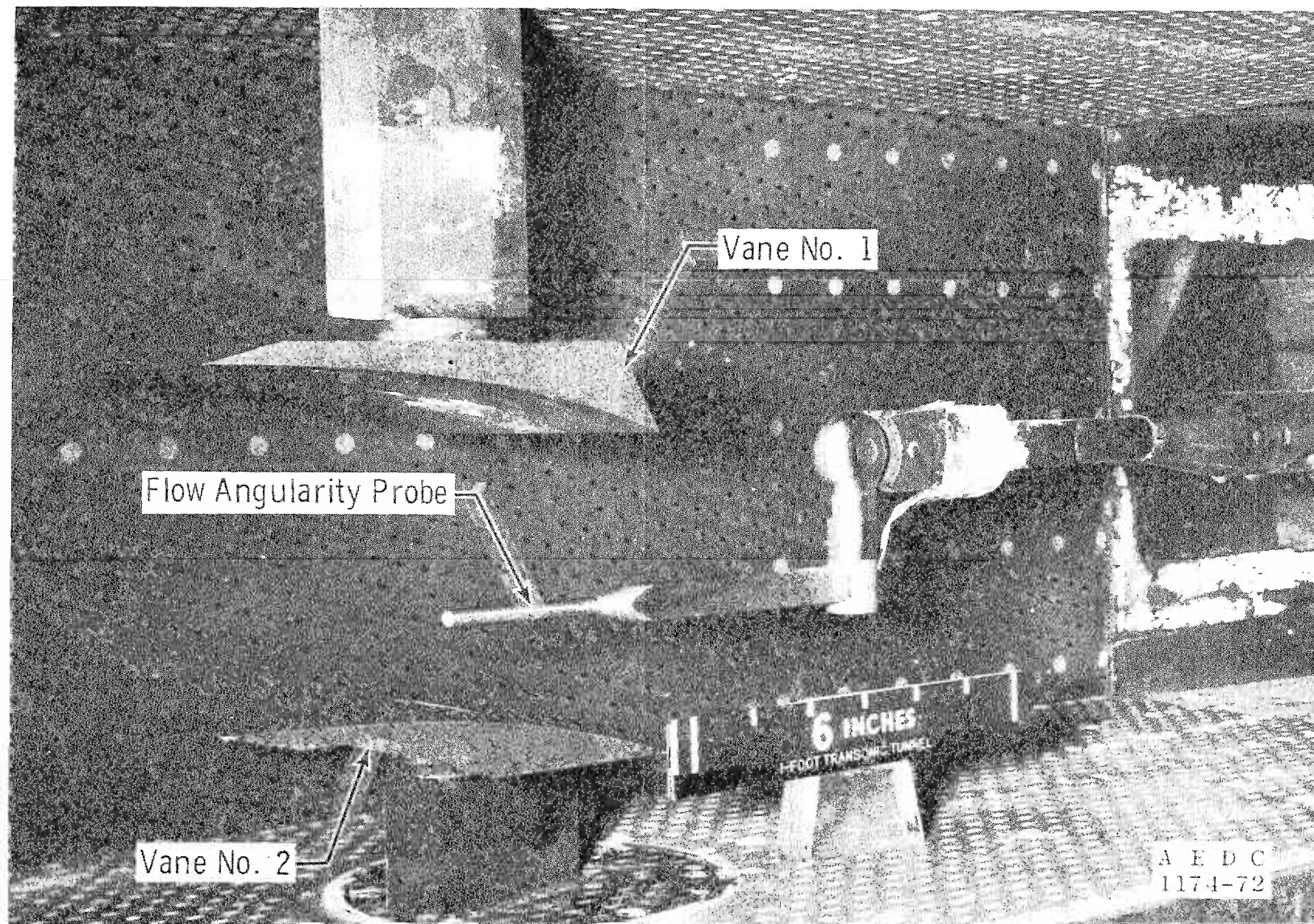
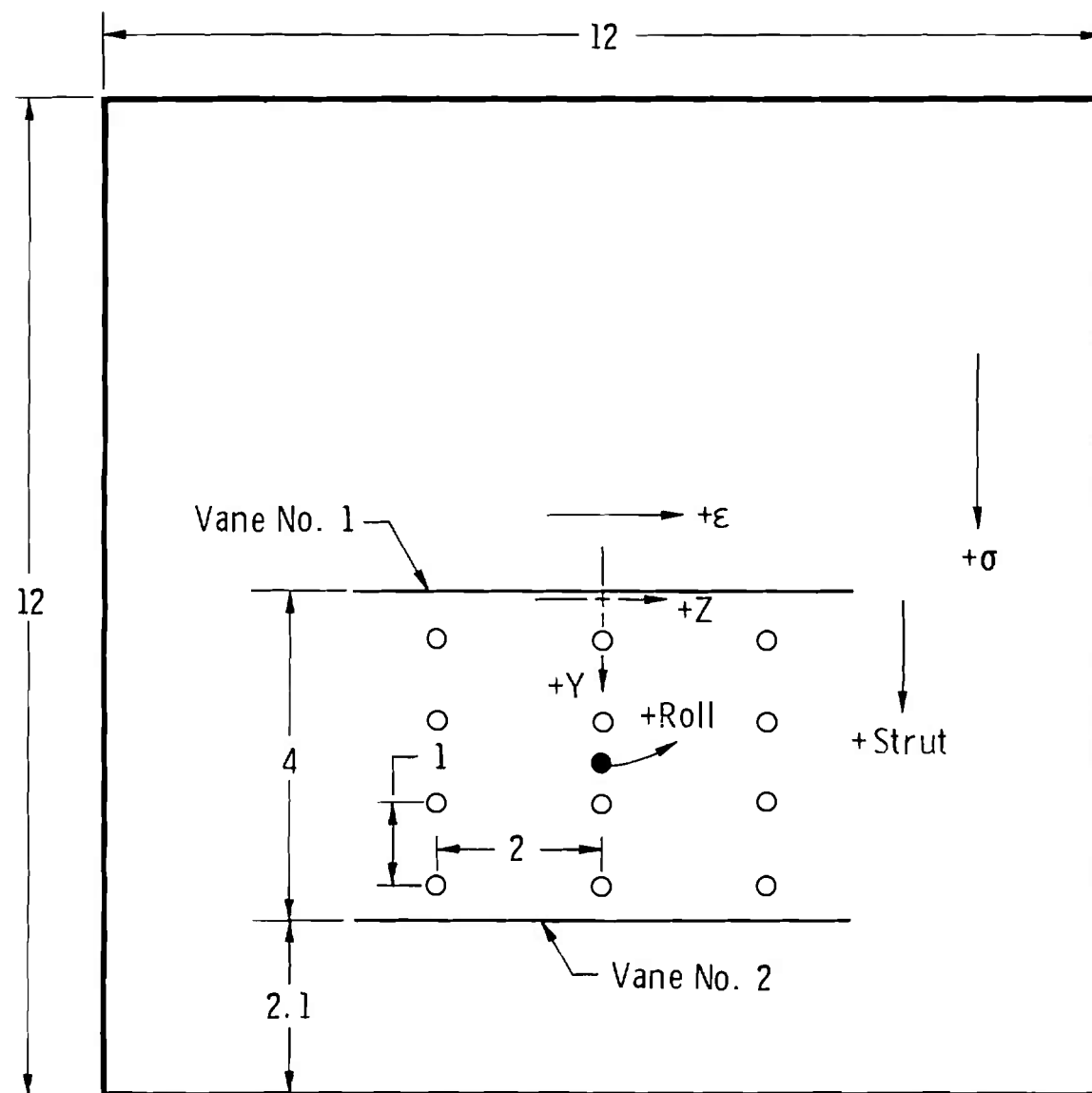


Fig. 28 Tunnel Turning Vanes Installed in the AEDC PWT-1T



All Dimensions in Inches

- Probe Tip Position for Strut and Roll Mechanism Zero Survey Made at Trailing Edge of Vanes

Fig. 29 Probe Survey Grid for the Small Turning Vane Wind Tunnel Test

$$\theta = \tan^{-1} \sqrt{\tan^2 \epsilon + \tan^2 \sigma}$$

$$\psi = \tan^{-1} \tan \sigma / \tan \epsilon$$

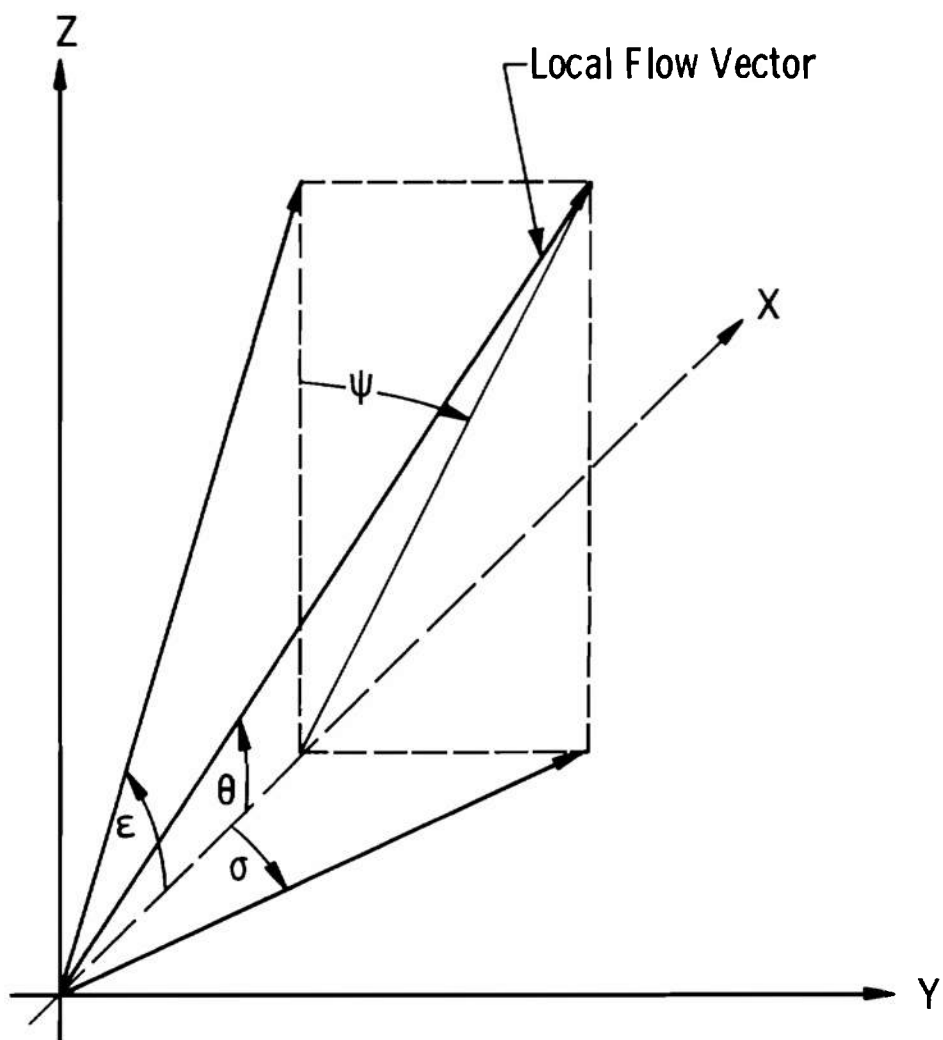


Fig. 30 Local Flow Vector Diagram

Mach Number = 0.9

Experimental Flow-Field Data \longrightarrow

Theoretical Flow-Field Data \longrightarrow

$\theta = 0 \ 5 \ 10 \ 20 \ 30 \text{ deg}$

Cylinder Diameter 56 in. Full Scale,
Cylinders Spaced 154 in.
Center-to-Center Full Scale

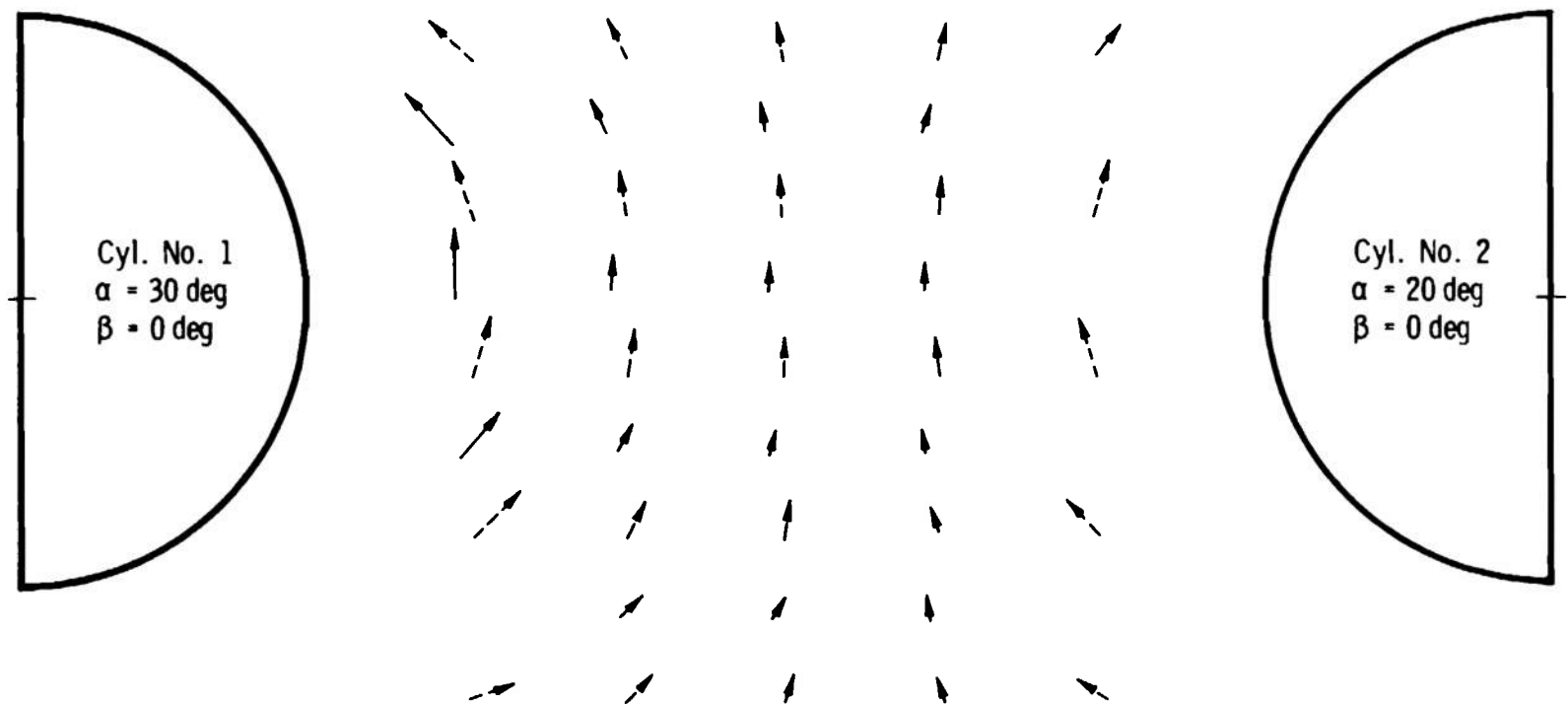


Fig. 31 Experimental and Theoretical Comparison of Local Flow Vectors for the Dual Hollow Circular Cylinders

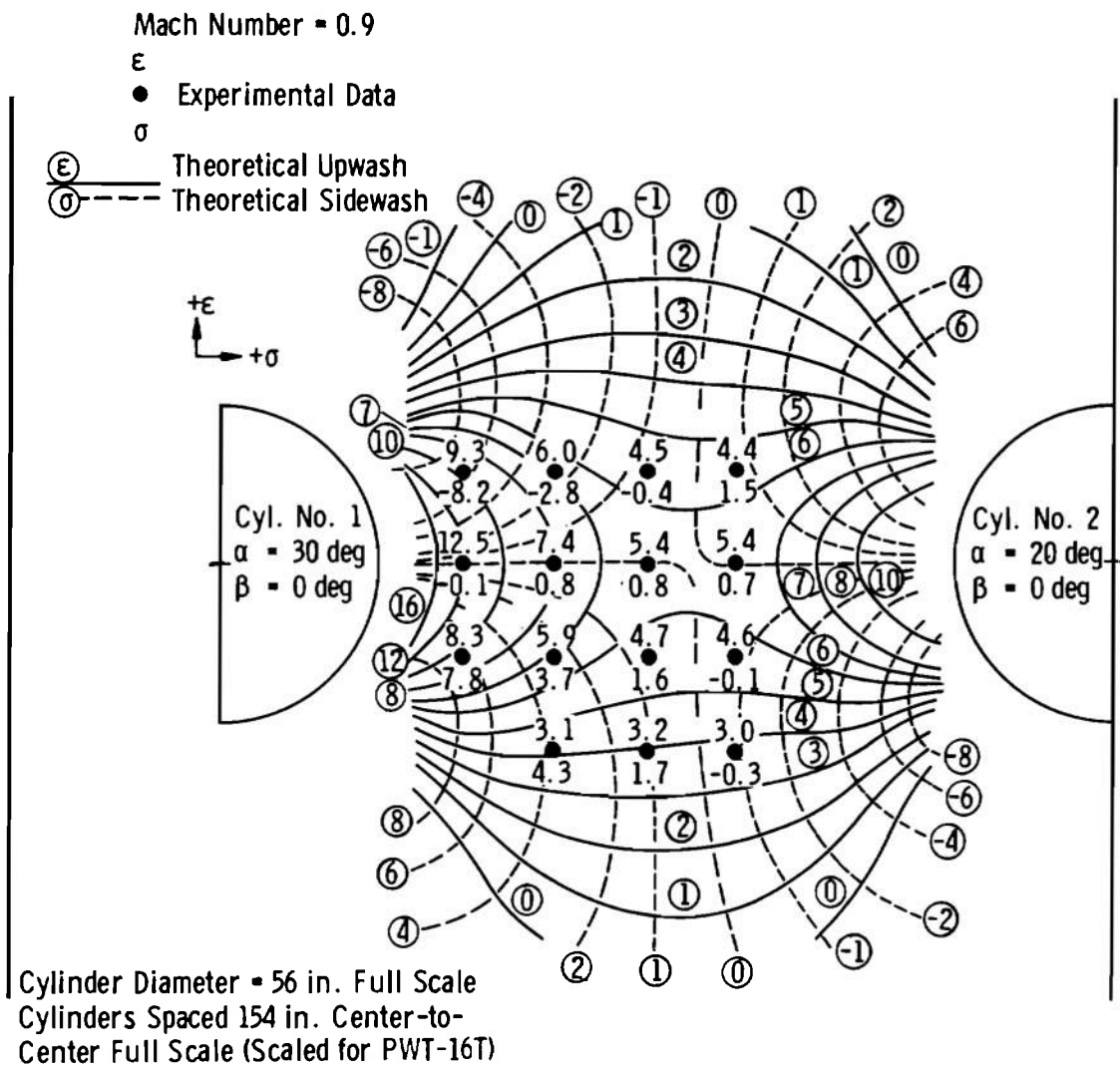


Fig. 32 Experimental and Theoretical Comparison of Upwash and Sidewash Angles for the Dual Hollow Circular Cylinders

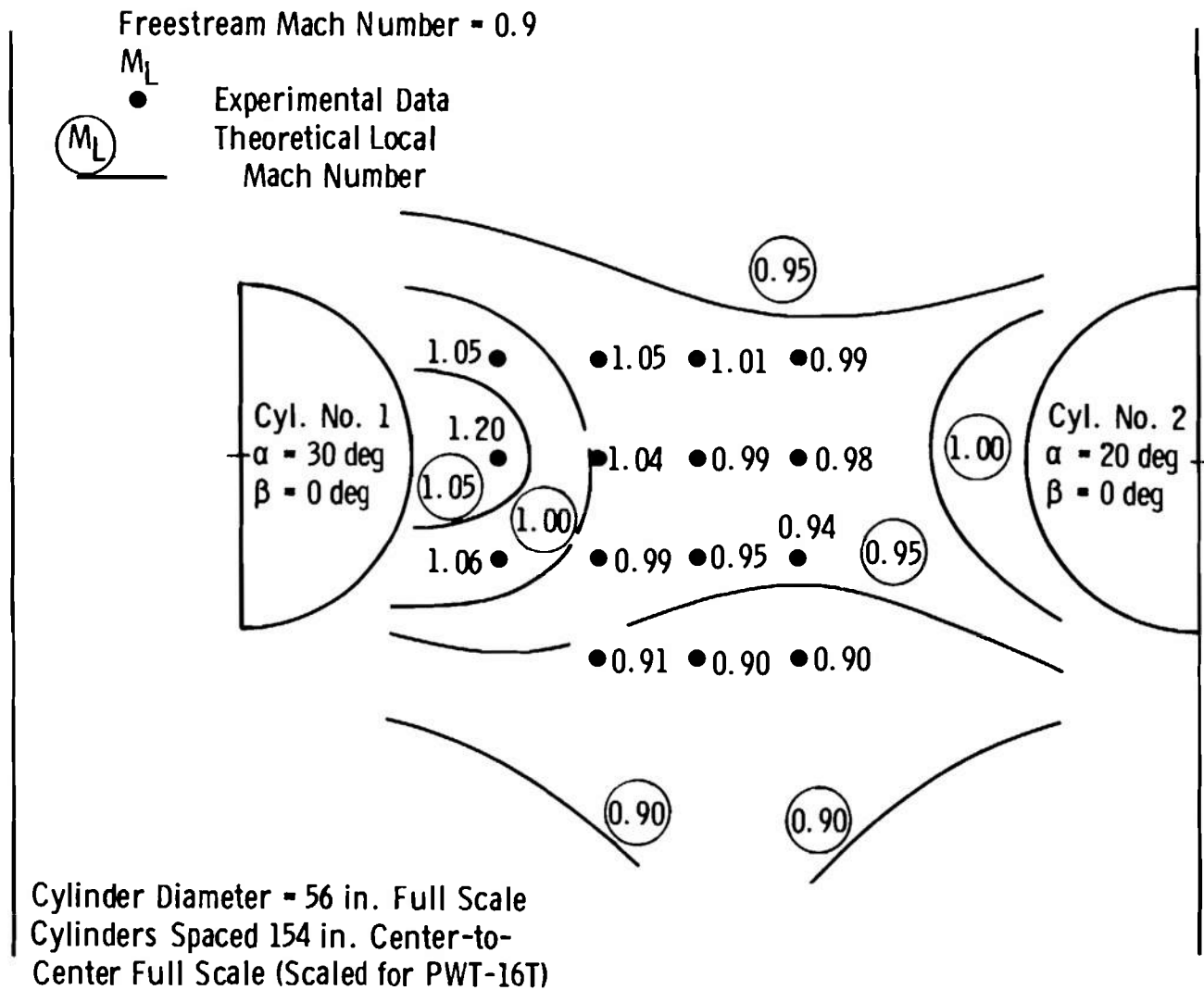


Fig. 33 Experimental and Theoretical Comparison of Local Mach Numbers for the Dual Hollow Circular Cylinders

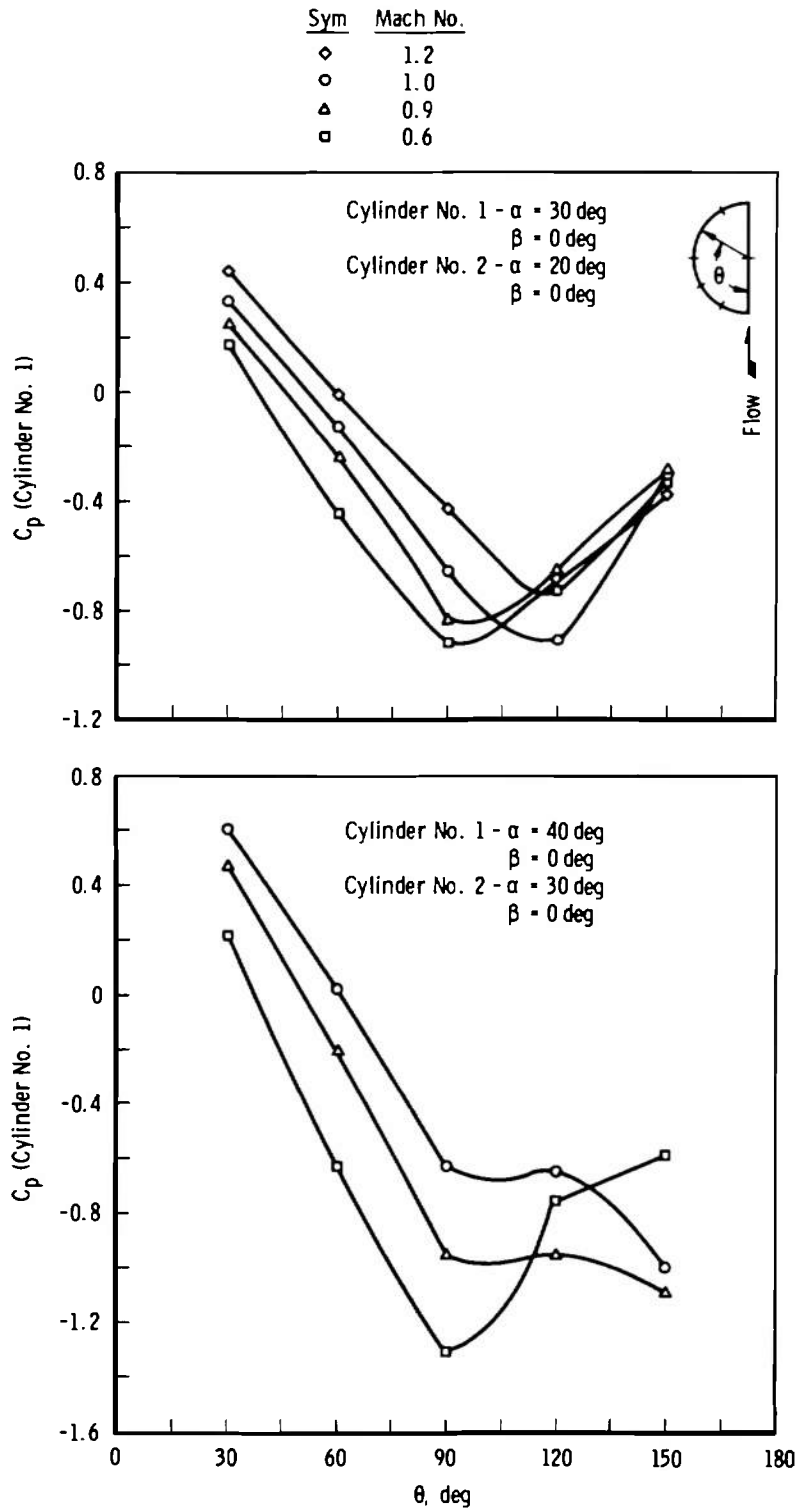
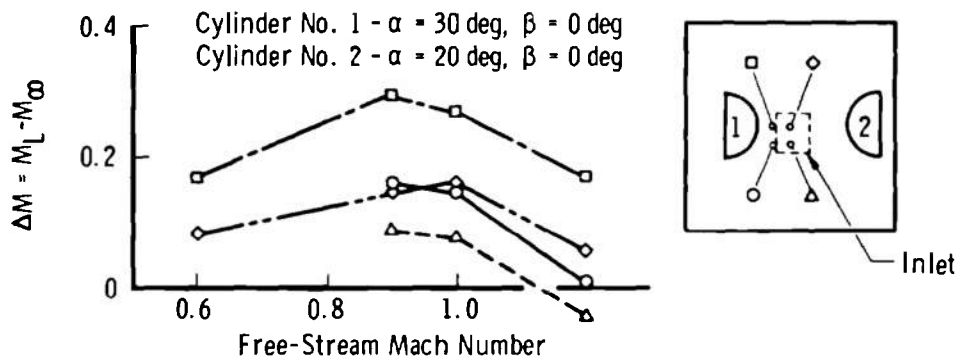
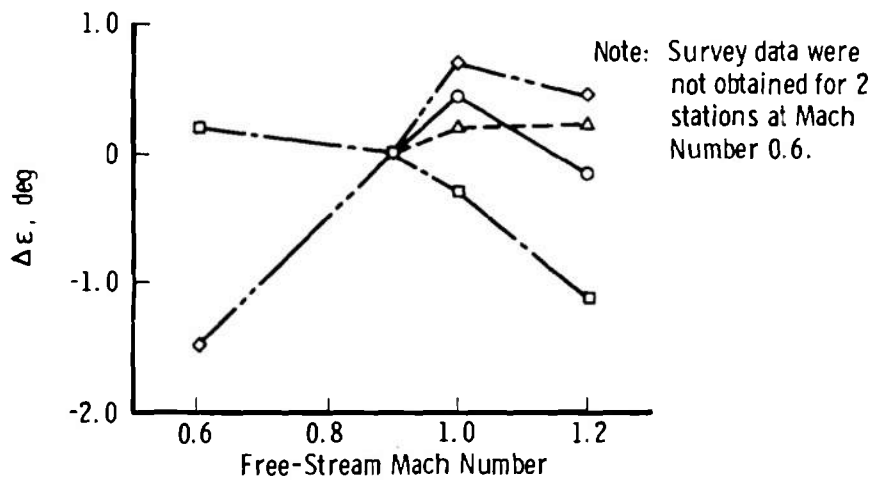


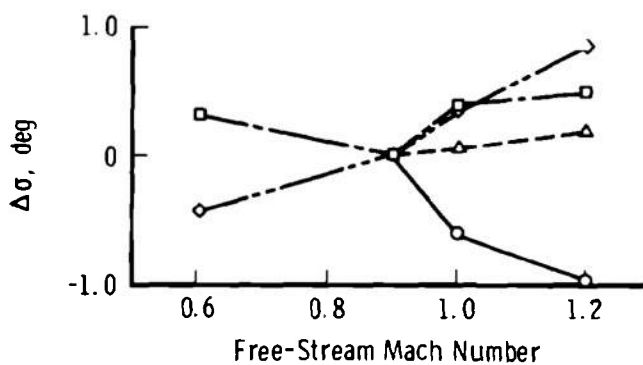
Fig. 34 Experimental Pressure Coefficients around Cylinder Number 1 of the Dual Hollow Circular Cylinder Configuration



a. Variation in Local Mach Number



b. Change in Upwash



c. Change in Sidewash

Fig. 35 Variation in Experimental Flow Field with Free-Stream Mach Number for the Dual Hollow Circular Cylinders

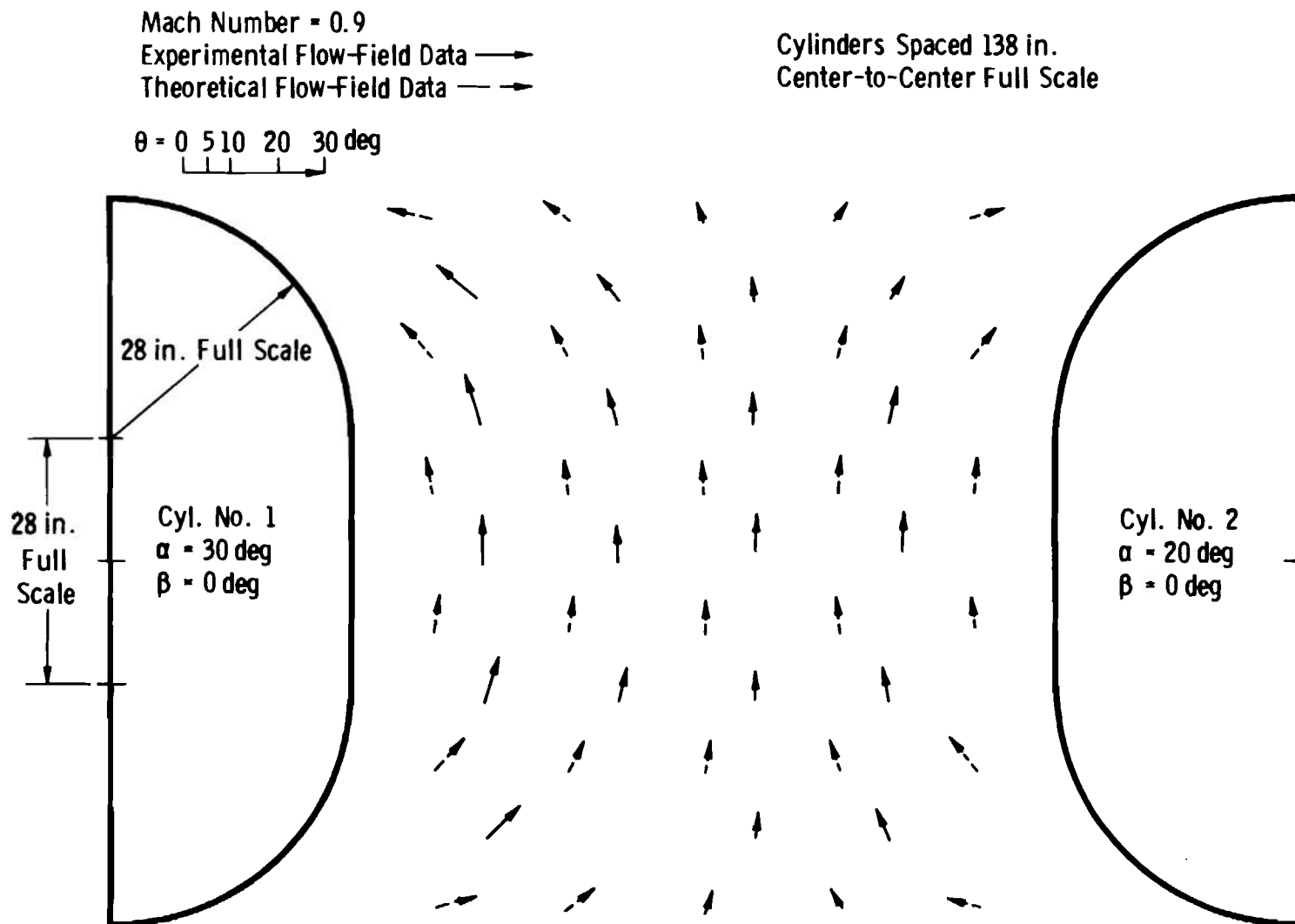


Fig. 36 Experimental and Theoretical Comparison of Local Flow Vectors for the Modified Hollow Cylinders (Cylinder No. 1, $\alpha = 30 \text{ deg}$; Cylinder No. 2, $\alpha = 20 \text{ deg}$)

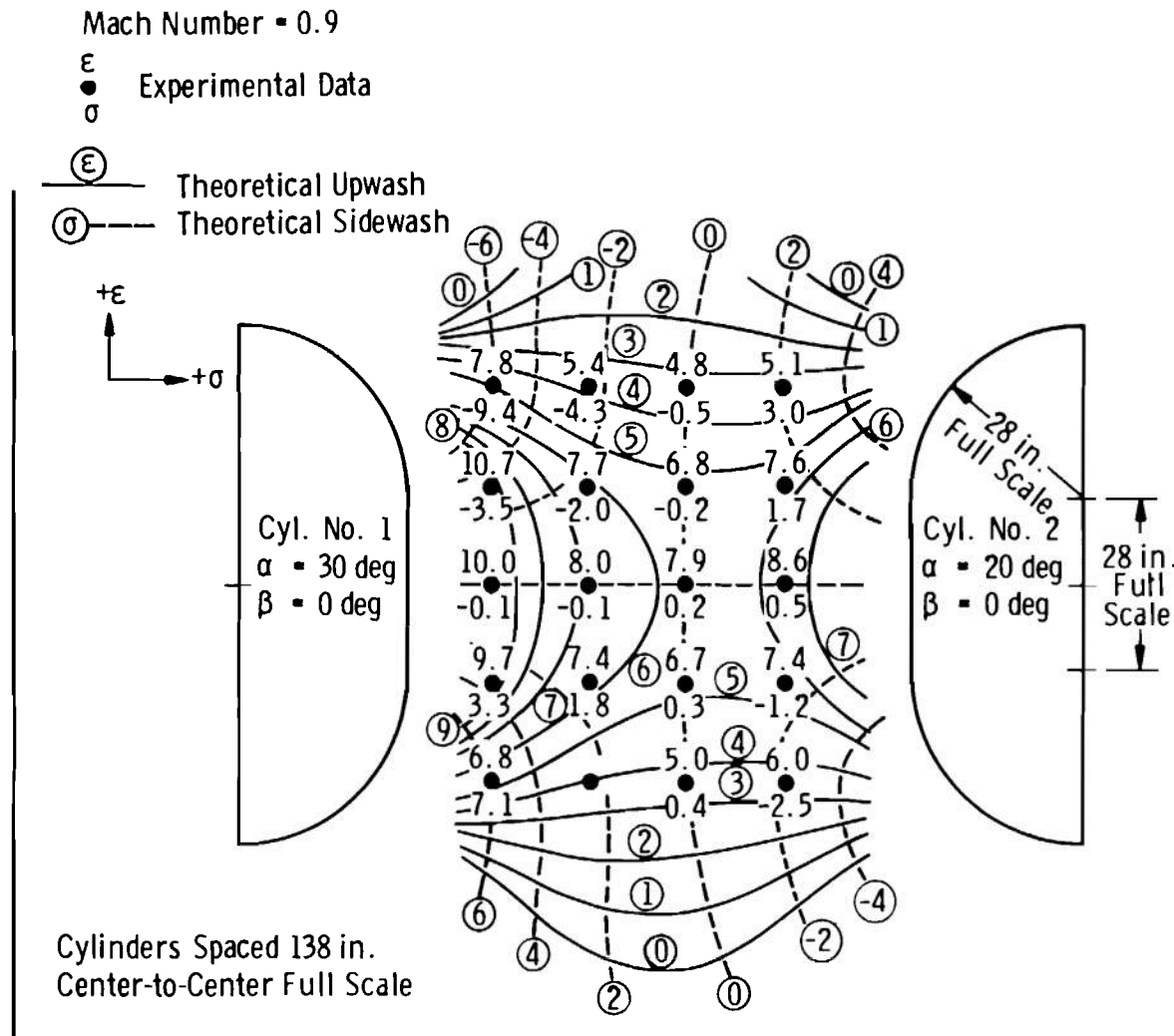


Fig. 37 Experimental and Theoretical Comparison of Upwash and Sidewash Angles for the Modified Hollow Cylinders (Cylinder No. 1, $\alpha = 30 \text{ deg}$; Cylinder No. 2, $\alpha = 20 \text{ deg}$)

Free-Stream Mach No. = 0.9

 M_L M_L

Experimental Data

Theoretical Local Mach Number

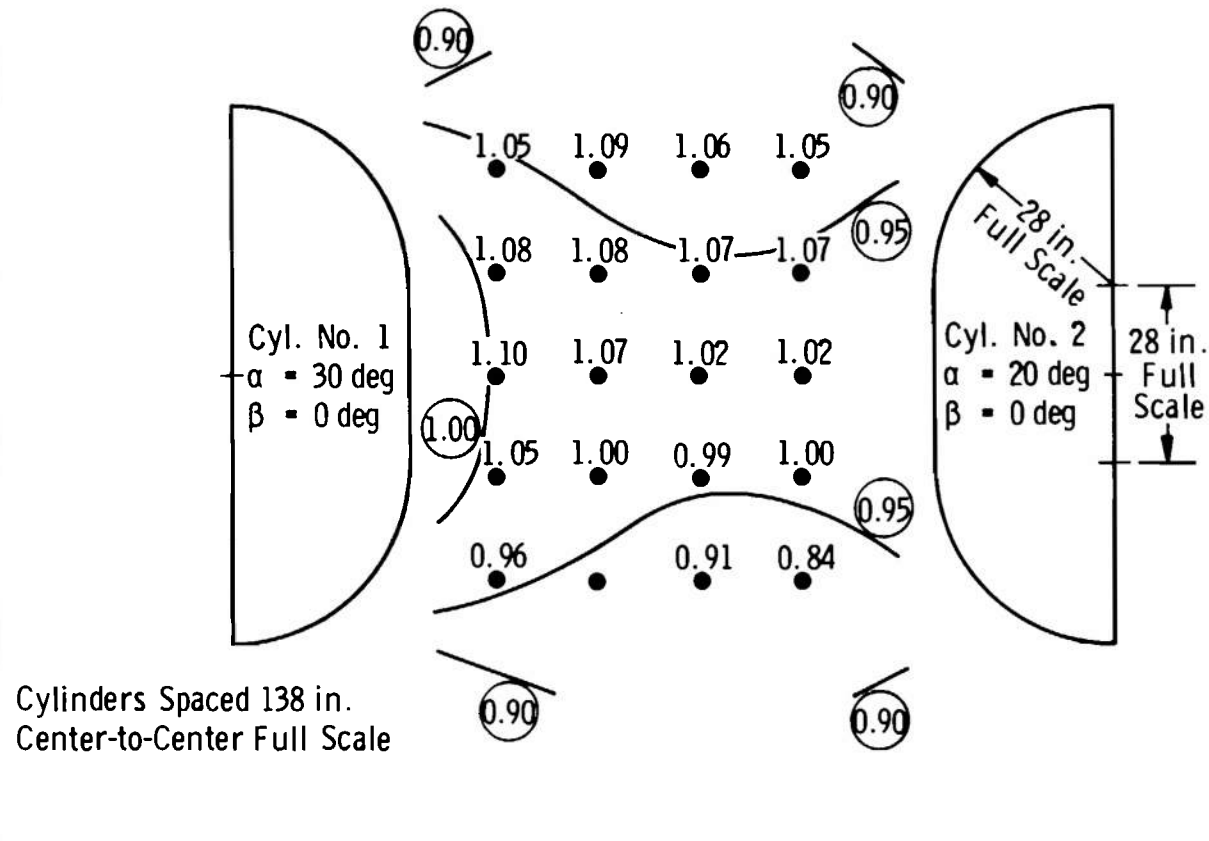


Fig. 38 Experimental and Theoretical Comparison of Local Mach Numbers for the Modified Hollow Cylinders (Cylinder No. 1, $\alpha = 30^\circ$; Cylinder No. 2, $\alpha = 20^\circ$)

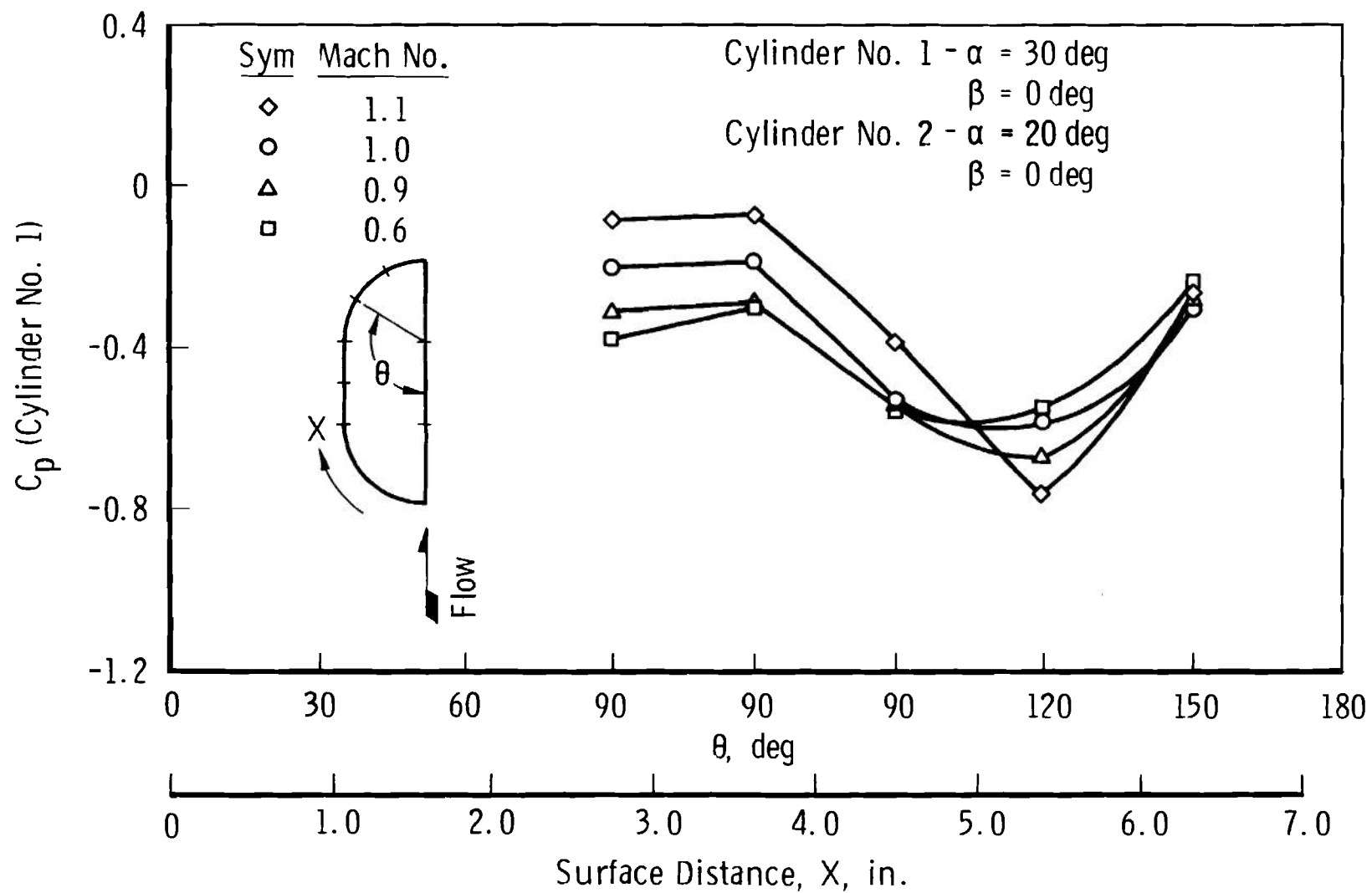


Fig. 39 Experimental Pressure Coefficients around Cylinder No. 1 of the Modified Hollow Cylinder Configuration

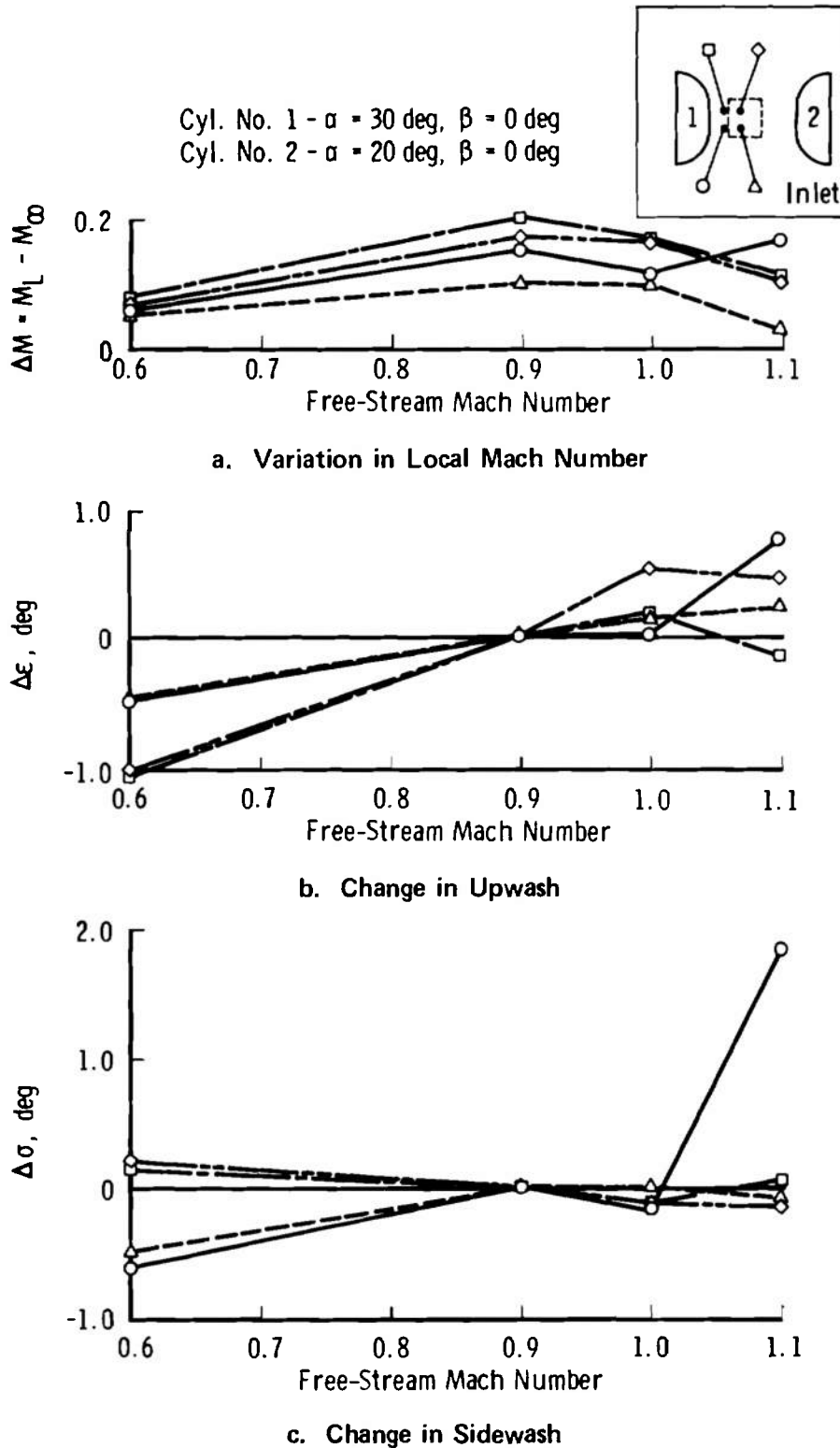


Fig. 40 Variation in Experimental Flow Field with Free-Stream Mach Number for the Modified Hollow Cylinders (Cylinder No. 1, $\alpha = 30$ deg; Cylinder No. 2, $\alpha = 20$ deg)

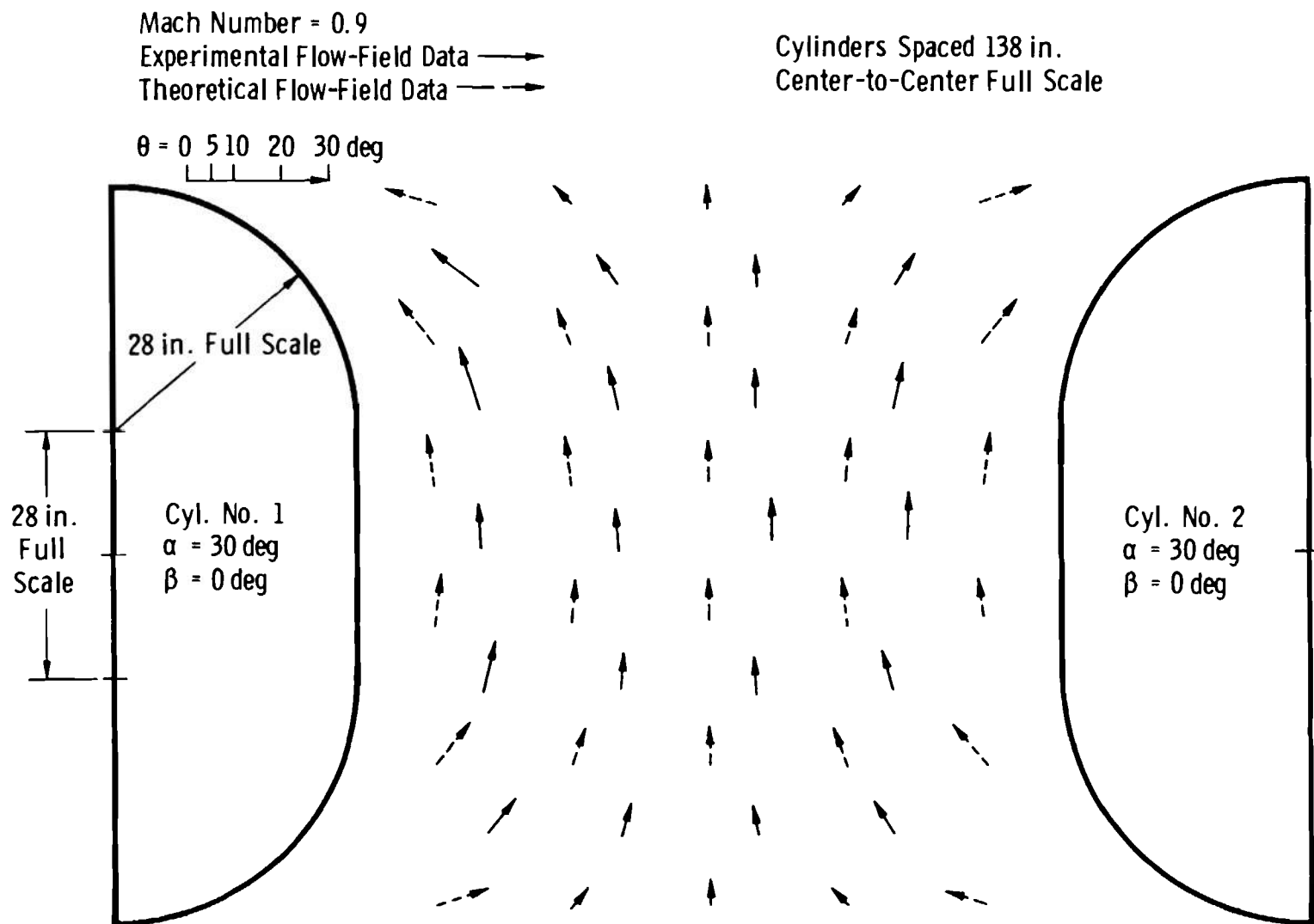


Fig. 41 Experimental and Theoretical Comparison of Local Flow Vectors for the Modified Hollow Cylinders (Cylinder No. 1, $\alpha = 30 \text{ deg}$; Cylinder No. 2, $\alpha = 30 \text{ deg}$)

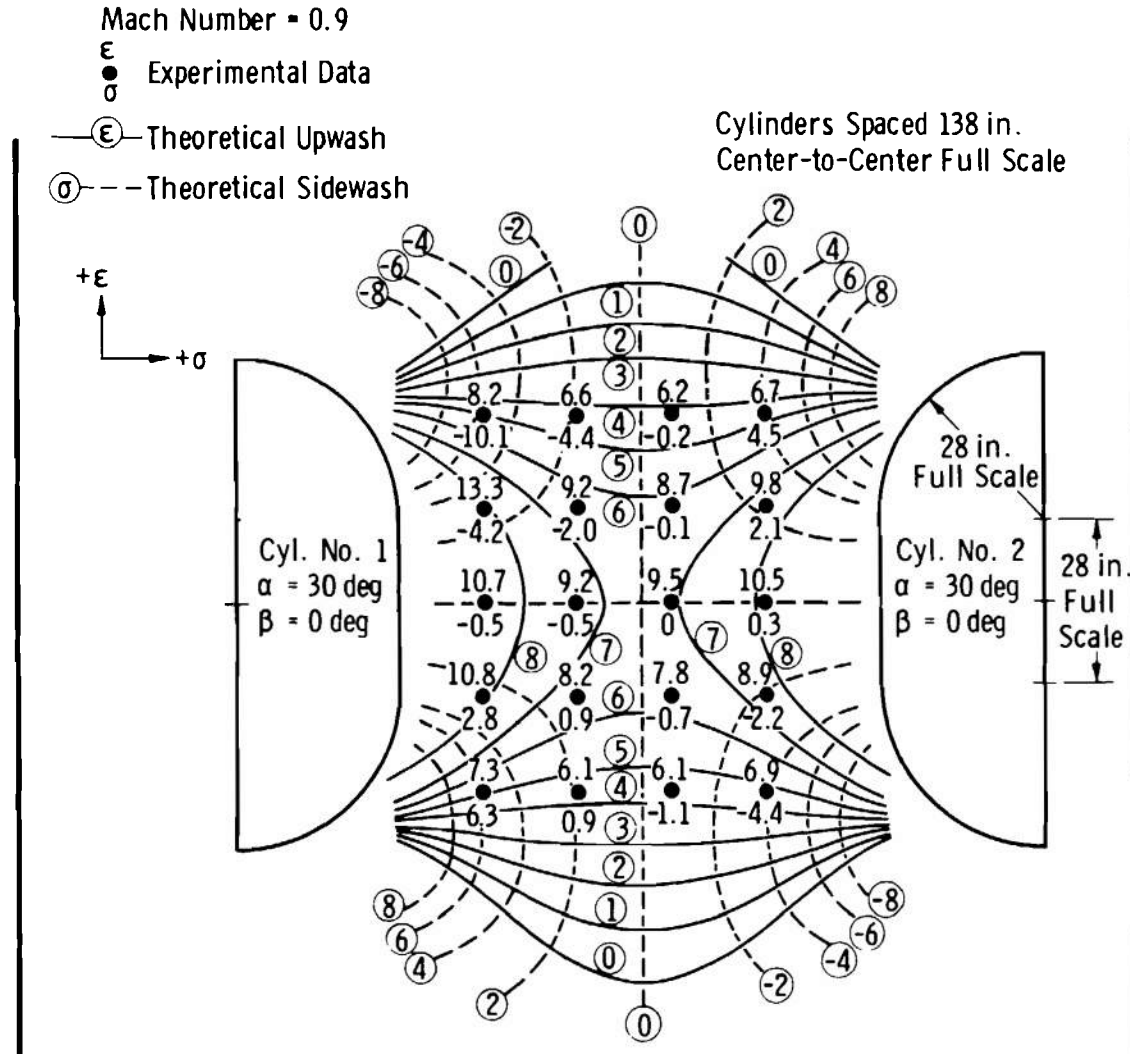


Fig. 42 Experimental and Theoretical Comparison of Upwash and Sidewash Angles for the Modified Hollow Cylinders (Cylinder No. 1, $\alpha = 30$ deg; Cylinder No. 2, $\alpha = 30$ deg)

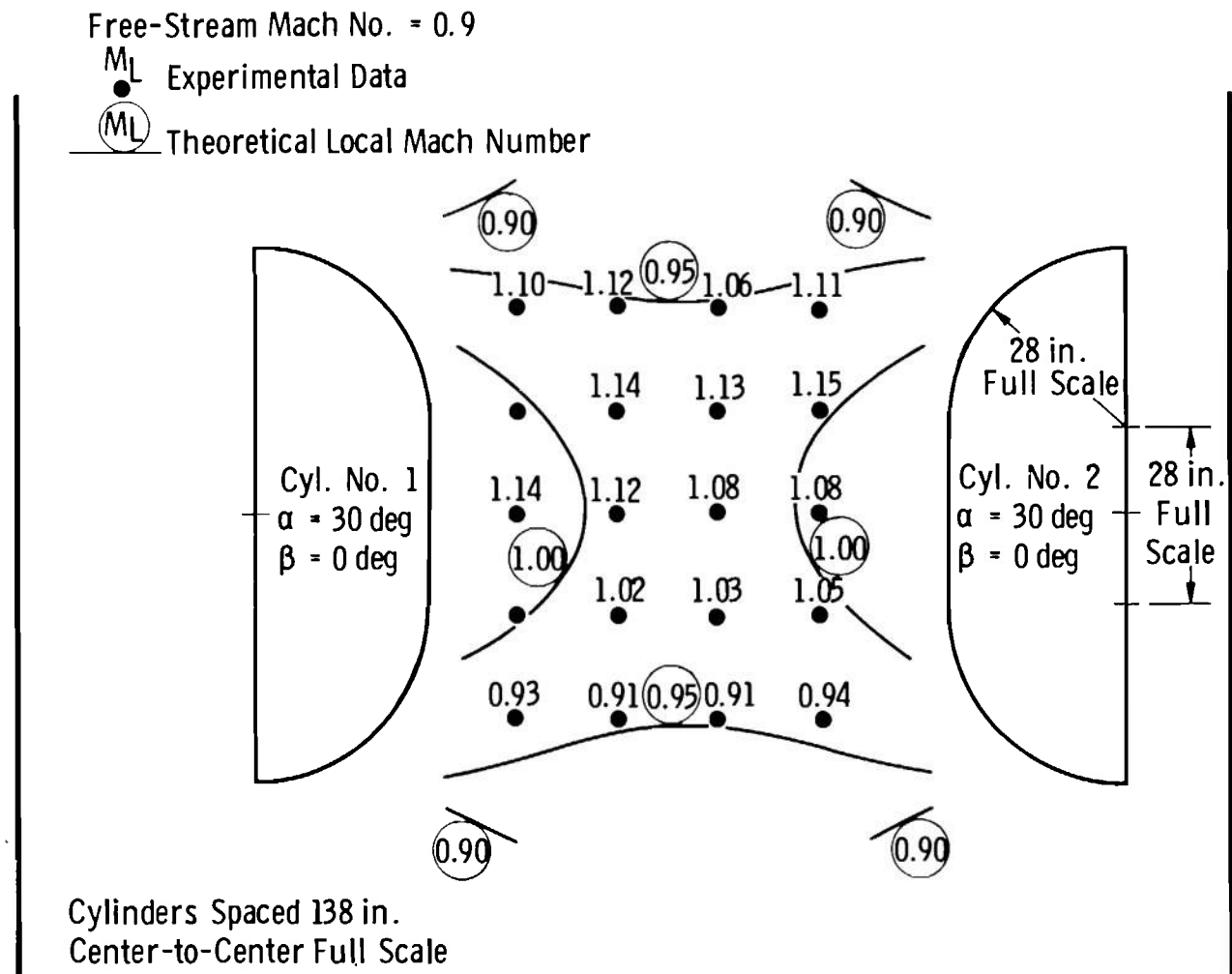
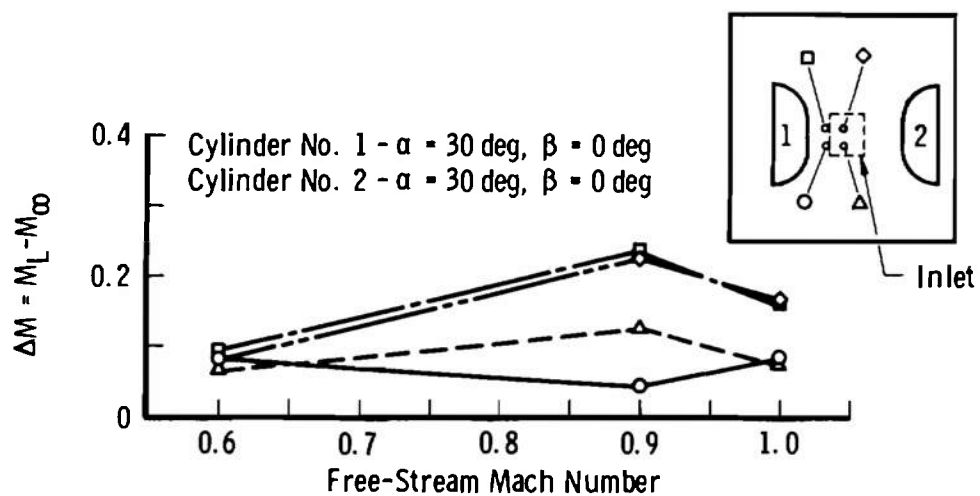
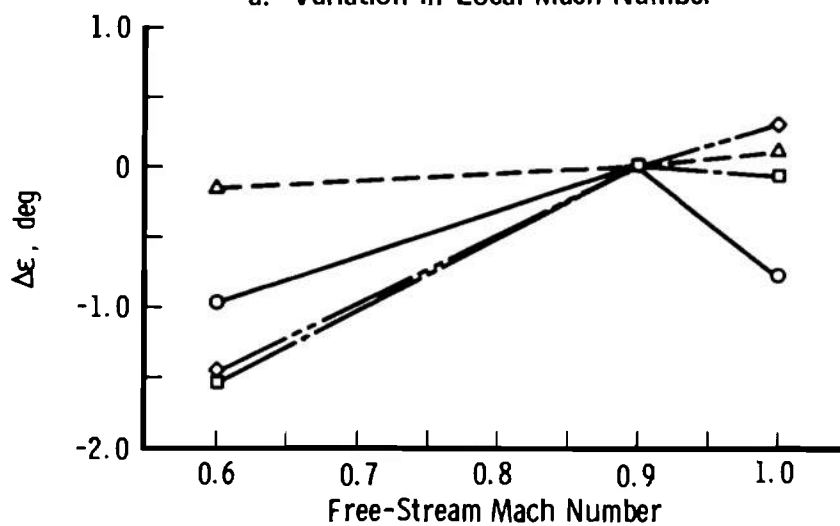


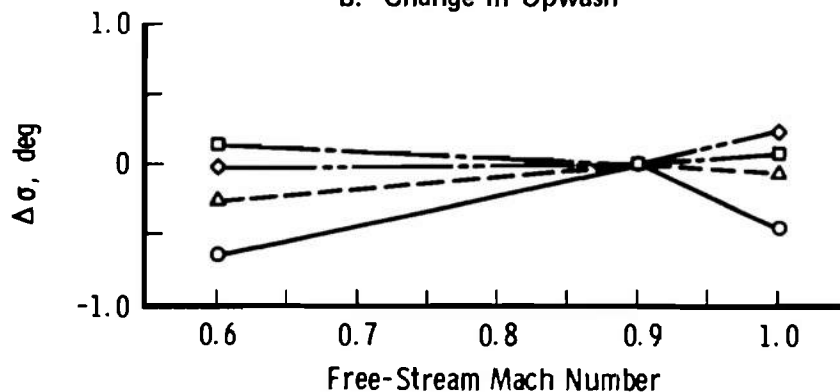
Fig. 43 Experimental and Theoretical Comparison of Local Mach Numbers for the Modified Hollow Cylinders (Cylinder No. 1, $\alpha = 30 \text{ deg}$; Cylinder No. 2, $\alpha = 30 \text{ deg}$)



a. Variation in Local Mach Number



b. Change in Upwash



c. Change in Sidewash

Fig. 44 Variation in Experimental Flow Field with Free-Stream Mach Number for the Modified Hollow Cylinders (Cylinder No. 1, $\alpha = 30$ deg; Cylinder No. 2, $\alpha = 30$ deg)

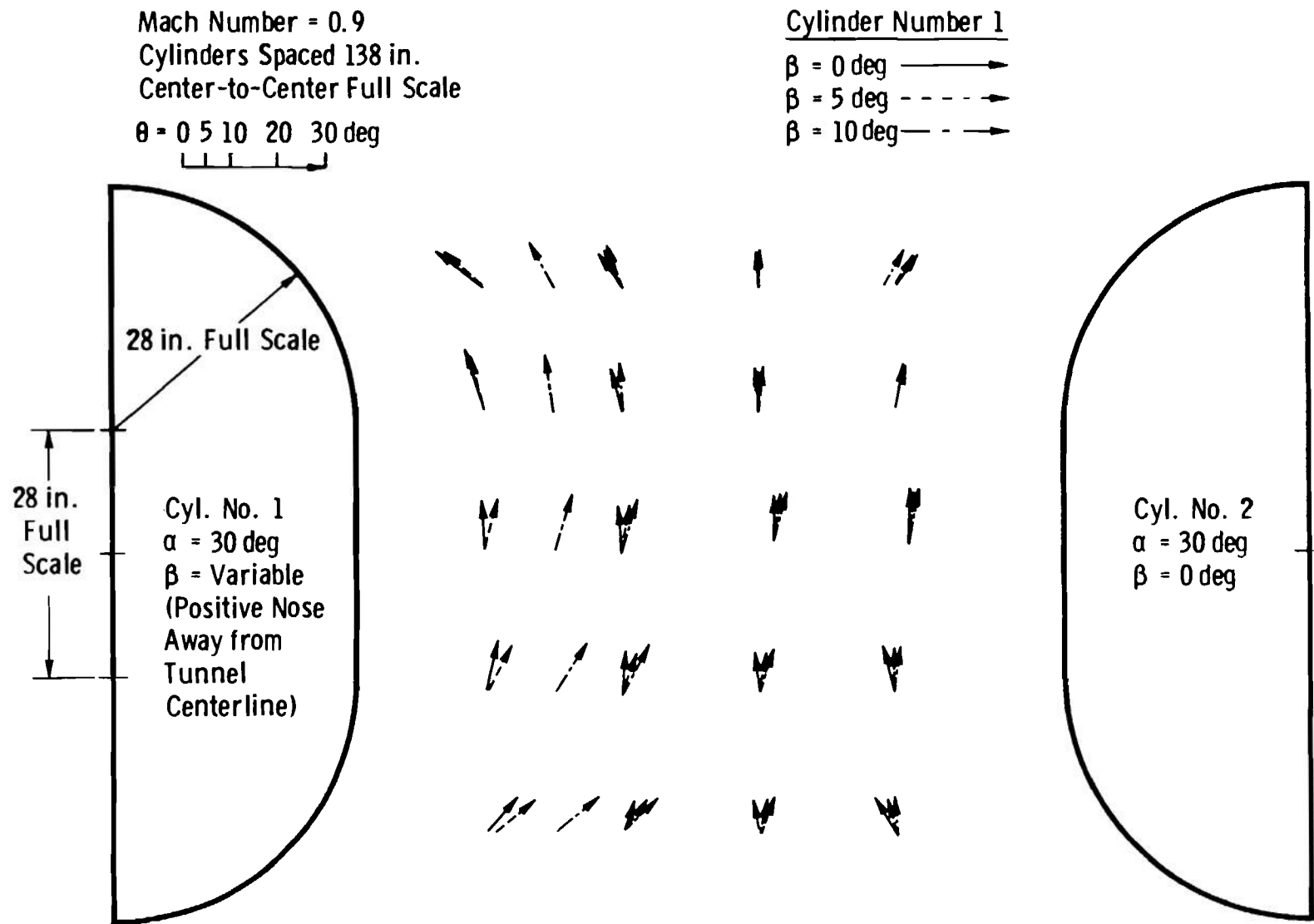


Fig. 45 Variation in Experimental Local Flow Vectors with Yaw Angles for Modified Hollow Cylinders

Mach Number = 0.9

Experimental Flow-Field Data —→

Theoretical Flow-Field Data —→

$\theta = 0 \quad 5 \quad 10 \quad 20 \quad 30 \text{ deg}$



Survey Taken at Trailing Edge of Vane No. 2

Turning Vanes Span the Tunnel, 96 in. Apart Full Scale (Fig. 24)

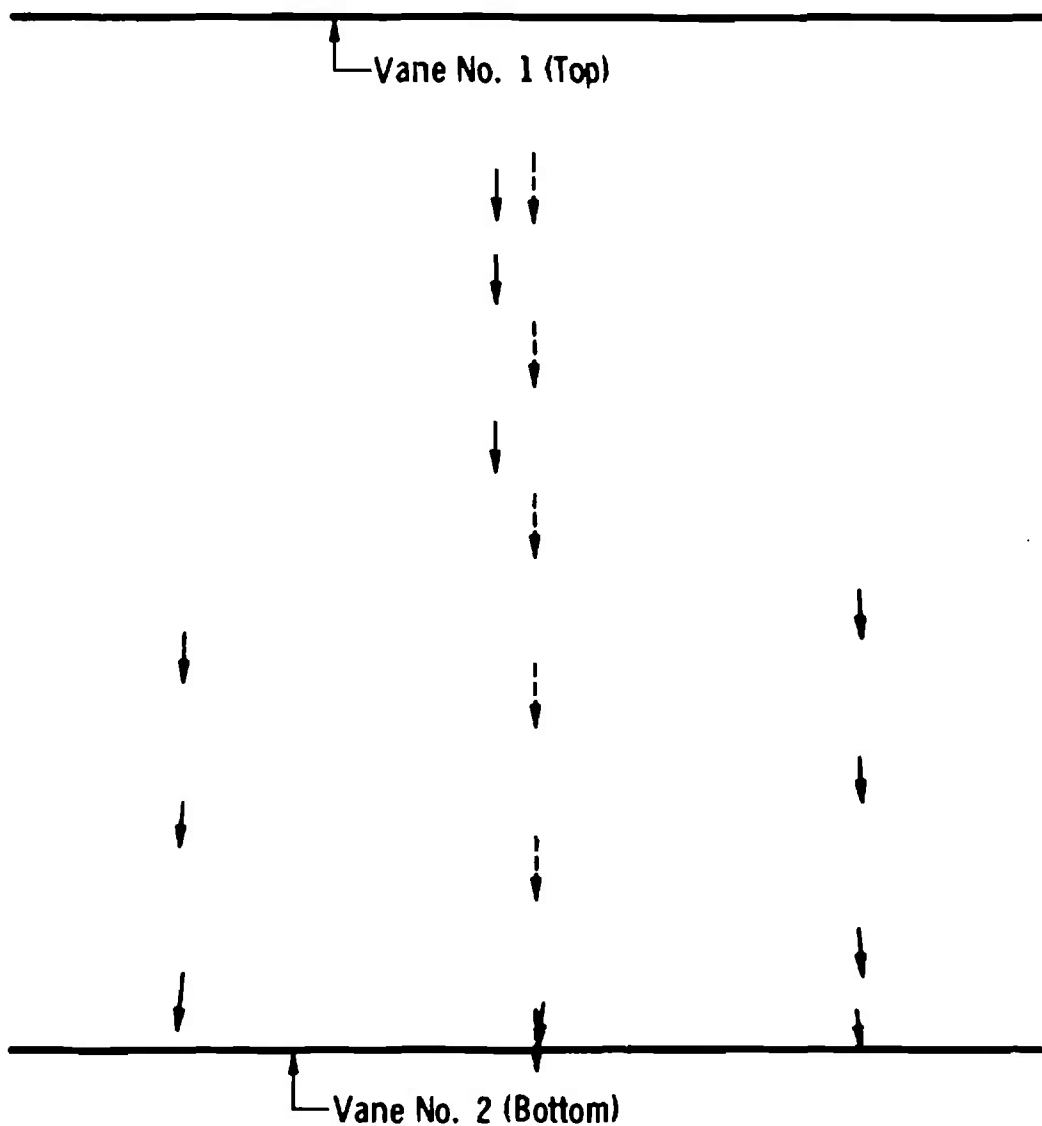
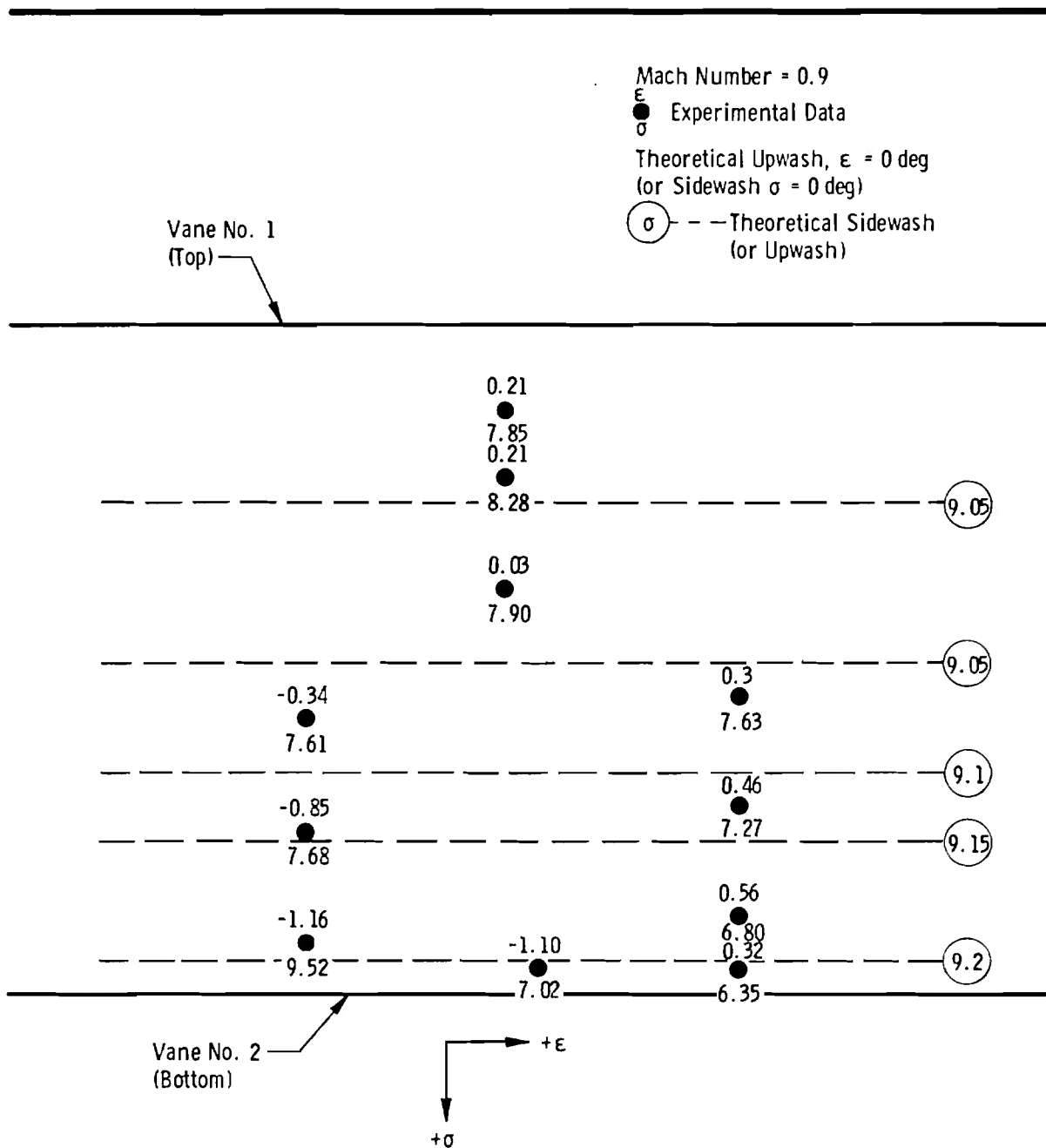


Fig. 46 Experimental and Theoretical Comparison of Local Flow Vectors for Large Turning Vanes



Survey Taken at Trailing Edge of Vane No. 2
Turning Vanes Span the Tunnel, 96 in. Apart Full Scale

Fig. 47 Experimental and Theoretical Comparison of Upwash and Sidewash Angles for the Large Turning Vanes

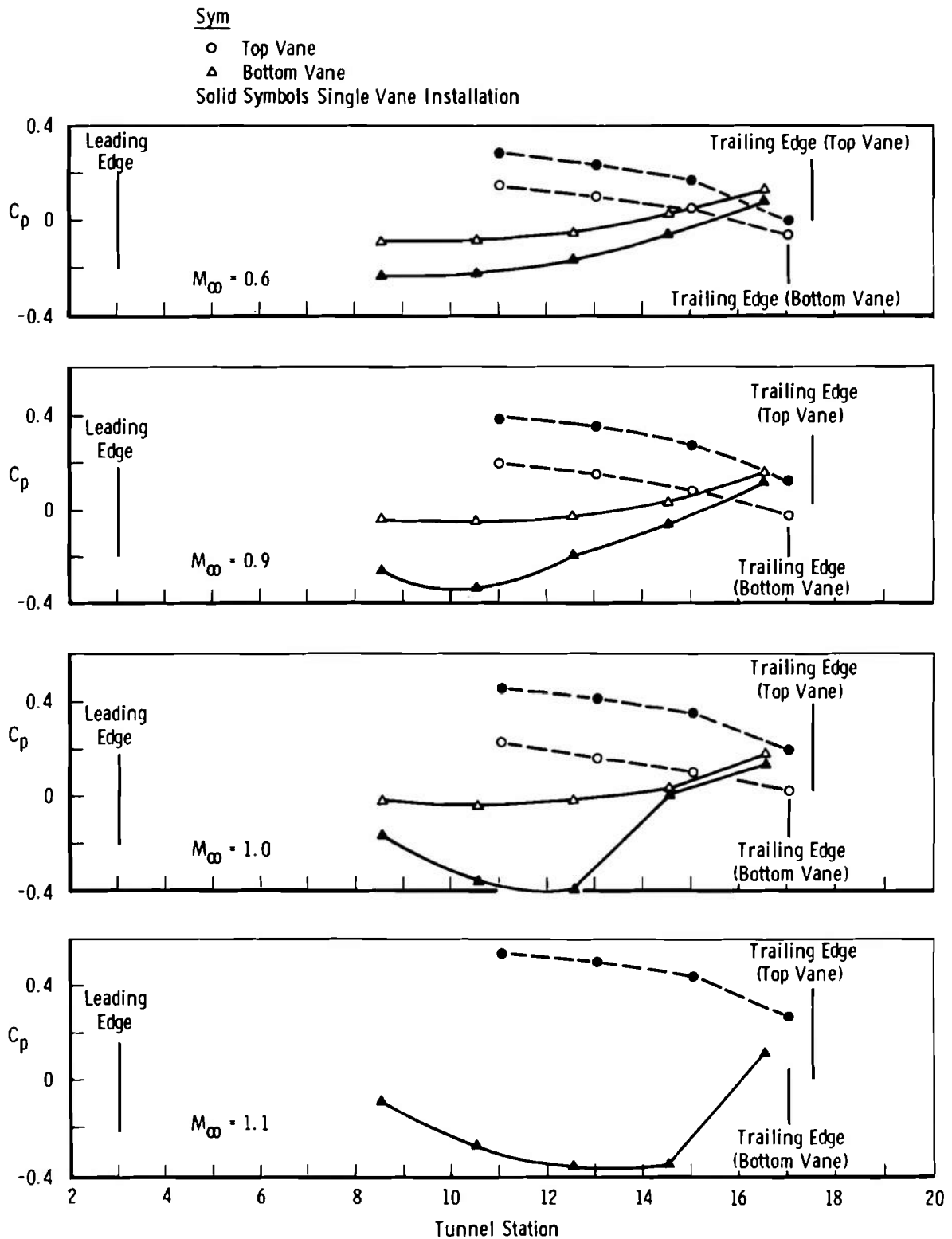


Fig. 48 Experimental Surface Pressure Coefficients for the Large Turning Vanes

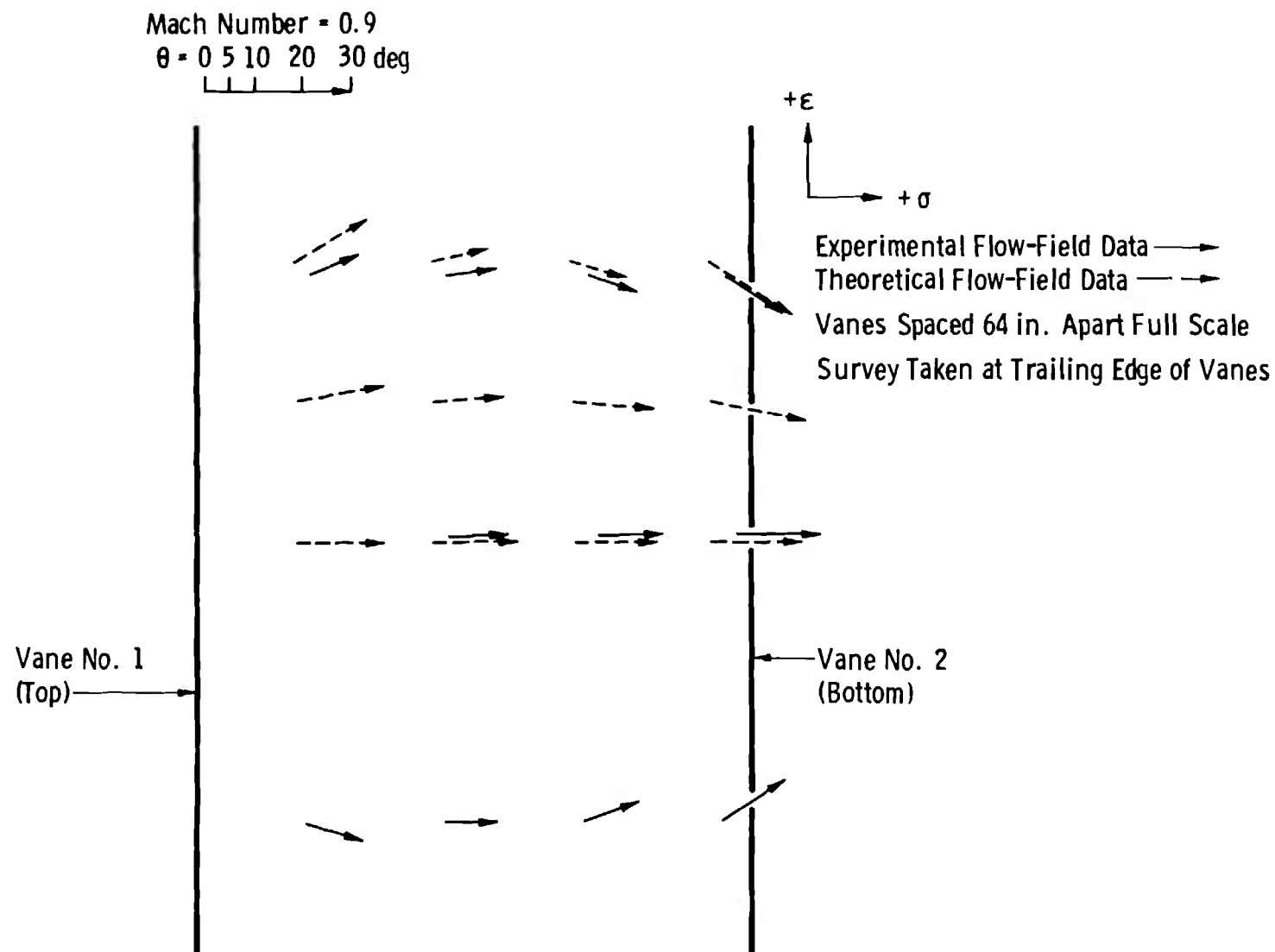


Fig. 49 Experimental and Theoretical Comparison of Local Flow Vectors for Small Turning Vanes

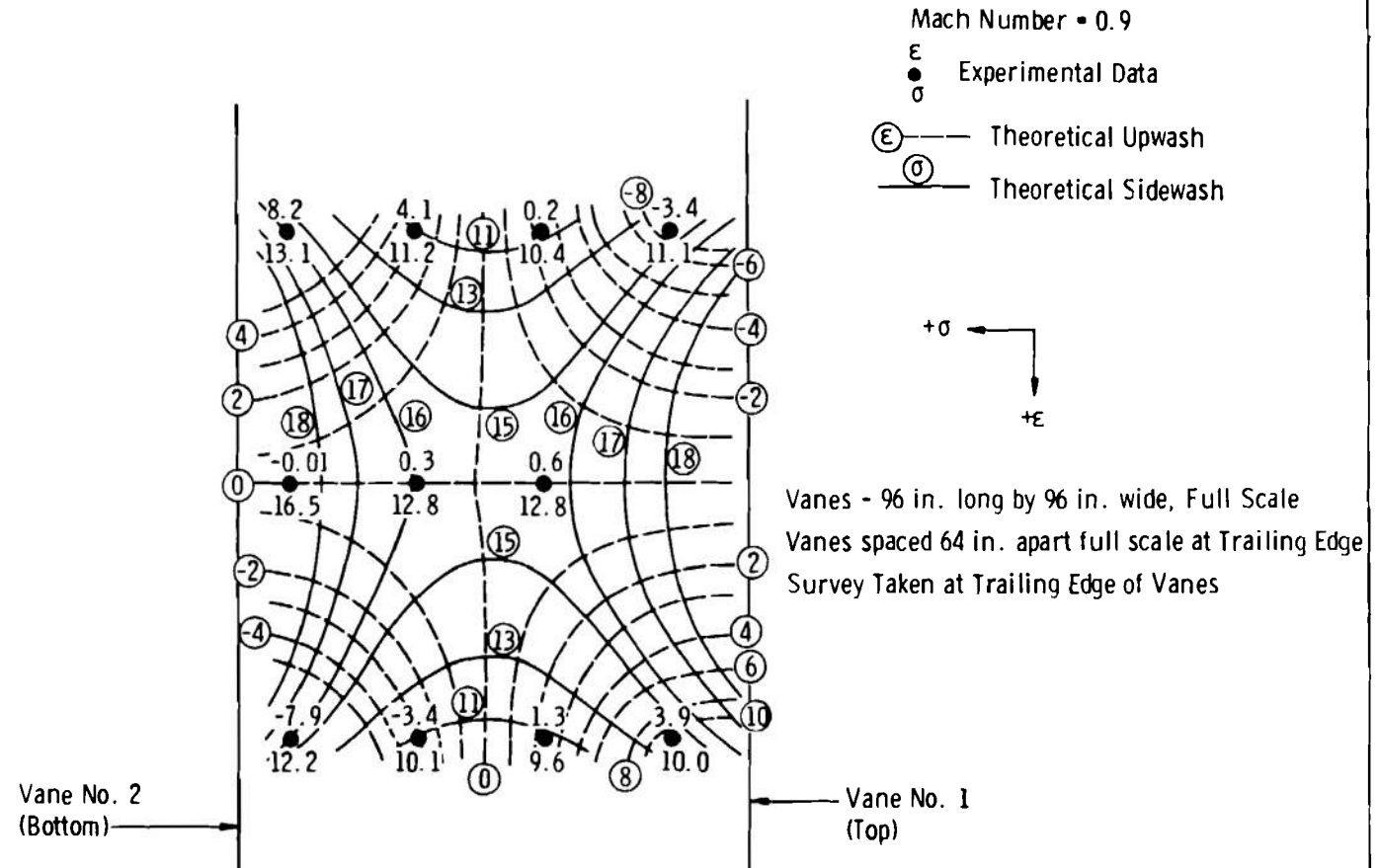


Fig. 50 Experimental and Theoretical Comparison of Upwash and Sidewash Angles for the Small Turning Vanes

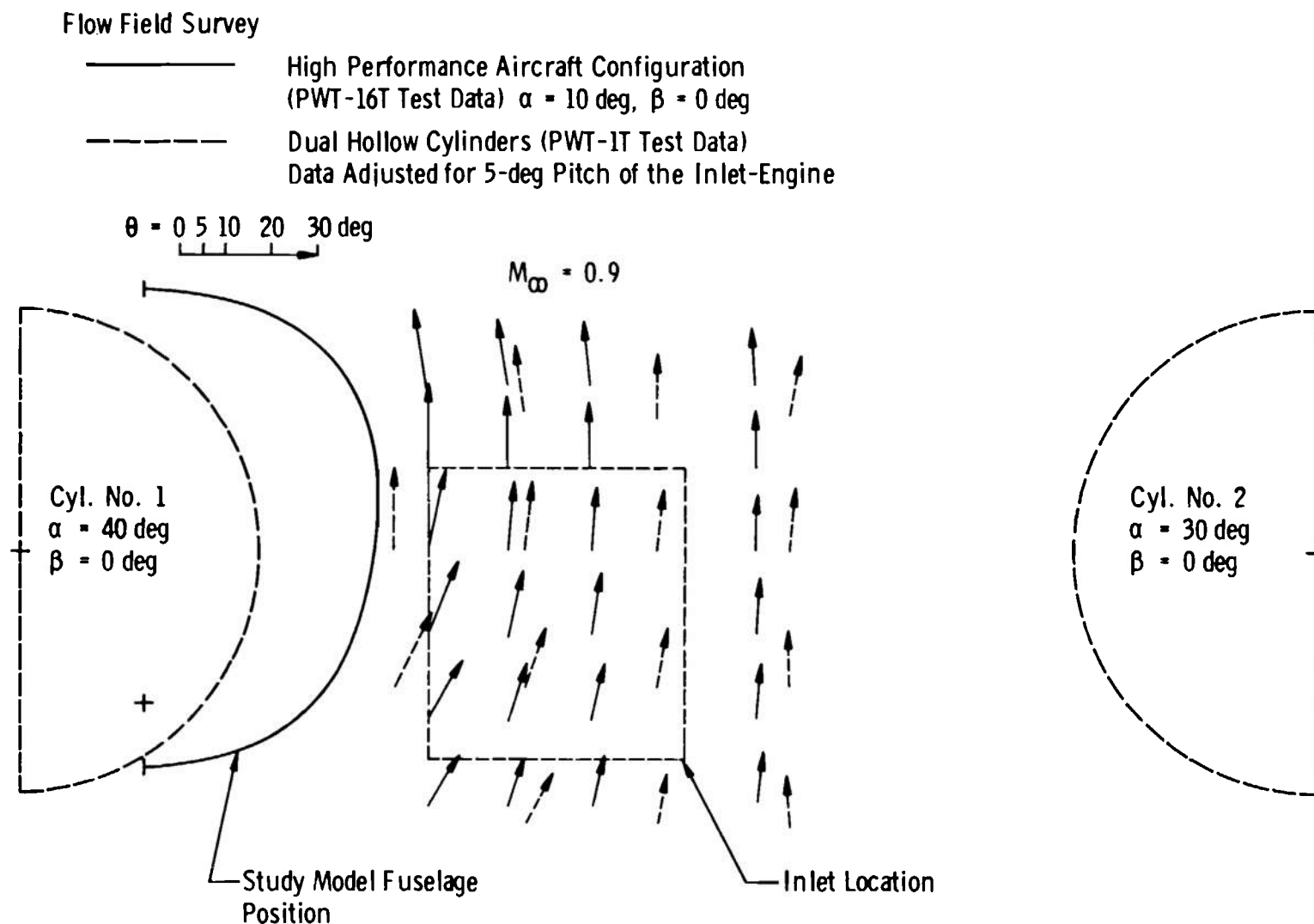


Fig. 51 Comparison of Local Flow Vectors in the AEDC PWT-16T with the Study Configuration at an Angle of Attack of 10 deg with Simulated Local Flow Vectors Taken in the AEDC PWT-1T

Flow Field Survey

- High-Performance Aircraft Configuration
 (PWT-16T Test Data) $\alpha = 19.8$ deg, $\beta = 0$ deg
 - - - Dual Hollow Cylinders (PWT-1T Test Data)
 Data Adjusted for 12-deg Pitch of the
 Inlet-Engine

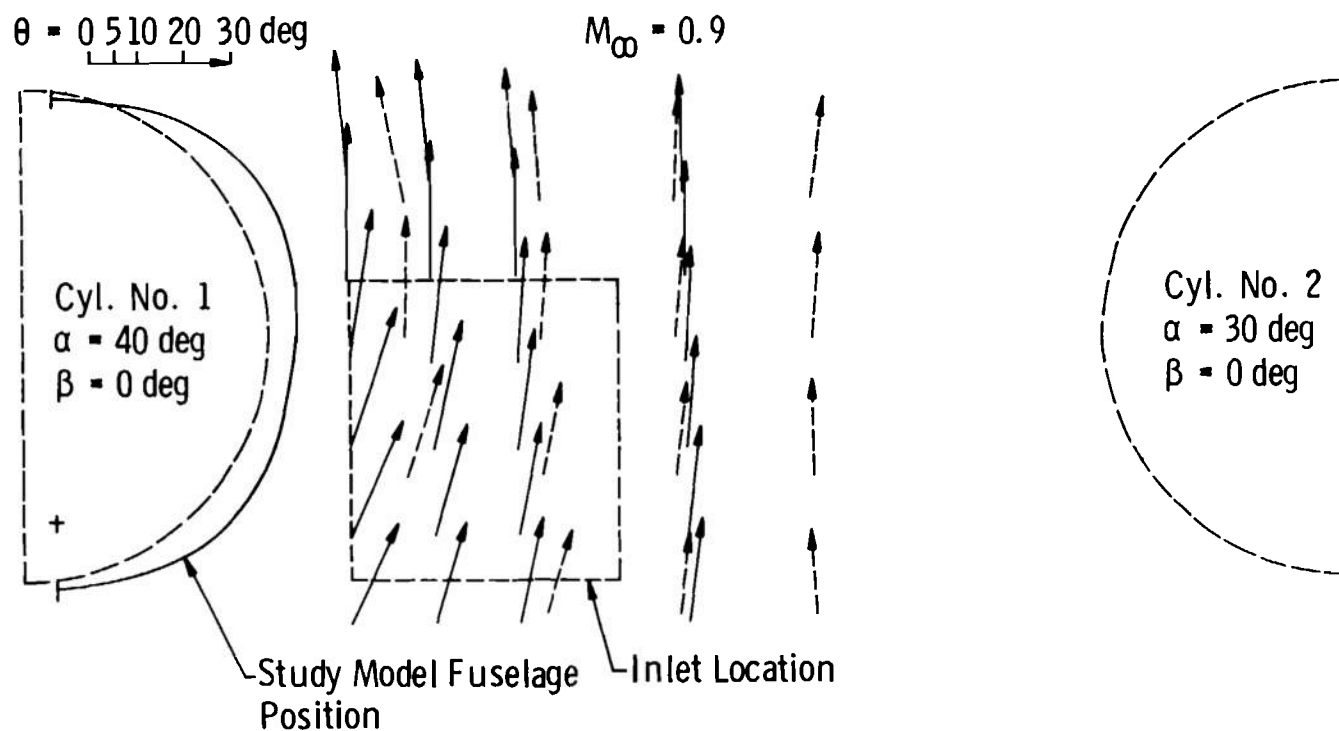


Fig. 52 Comparison of Local Flow Vectors Taken in the AEDC PWT-16T with the Study Configuration at an Angle of Attack of 19.8 deg with Simulated Local Flow Vectors Taken in the AEDC PWT-1T

Flow-Field

- Experimental, High-Performance Aircraft Configuration
(PWT-16T Test Data) $\alpha = 10$ deg, $\beta = 4$ deg, Lee Inlet
- - - Theoretical, Modified Cylinders Spaced 154 in. Center-to-Center Full Scale
(Data Adjusted for 10 deg Geometric Pitch of Inlet/Engine System.)

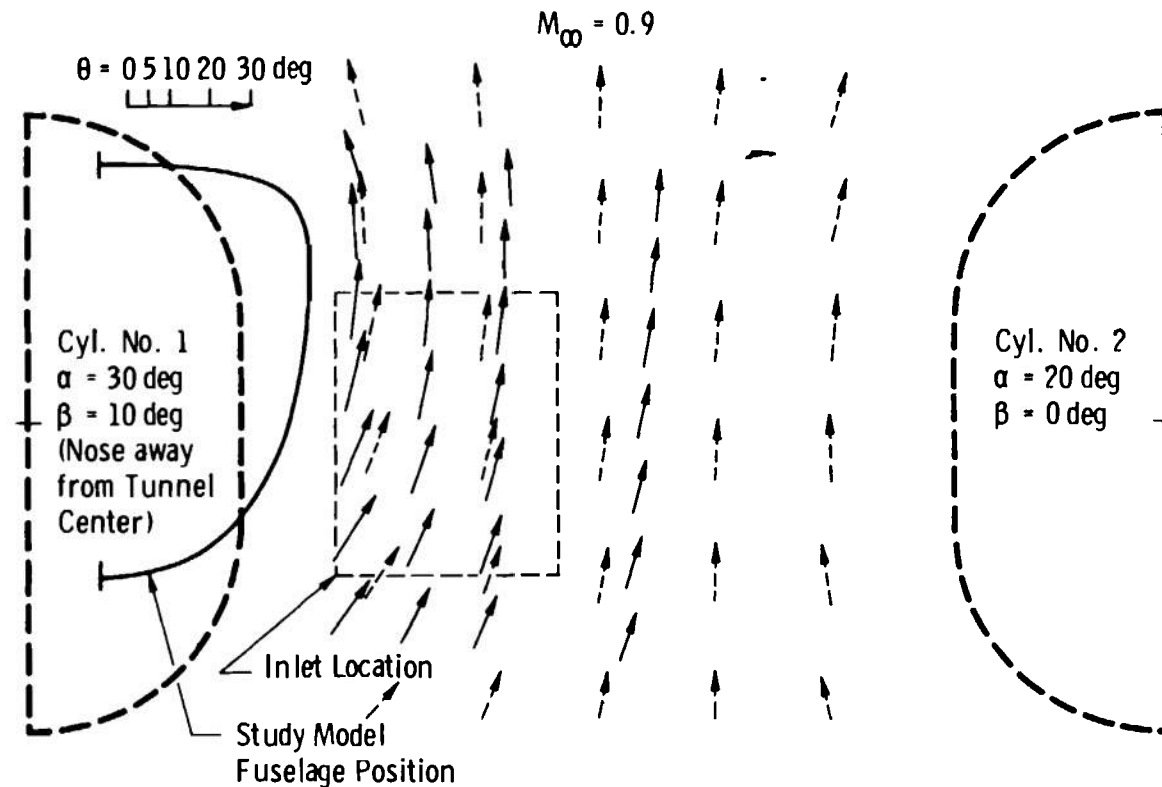


Fig. 53 Comparison of Local Flow Vectors Taken in the AEDC PWT-16T with the Study Configuration at an Angle of Attack of 10 deg and an Angle of Yaw of 4 deg with Simulated Local Flow Vectors Taken in the AEDC PWT-1T

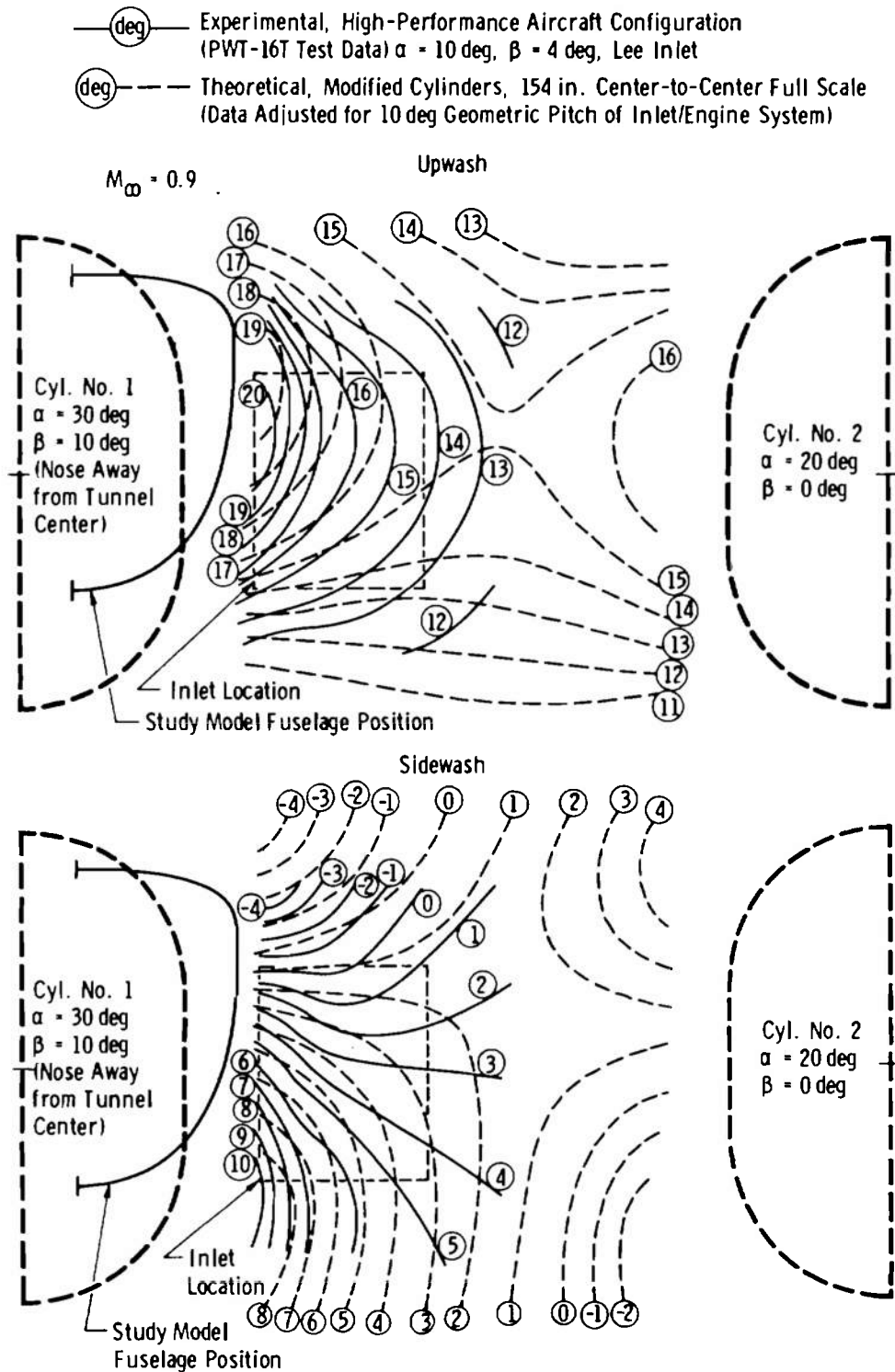


Fig. 54 Experimental and Theoretical Comparison of Upwash and Sidewash Angles for the Study Configuration and Modified Hollow Cylinders

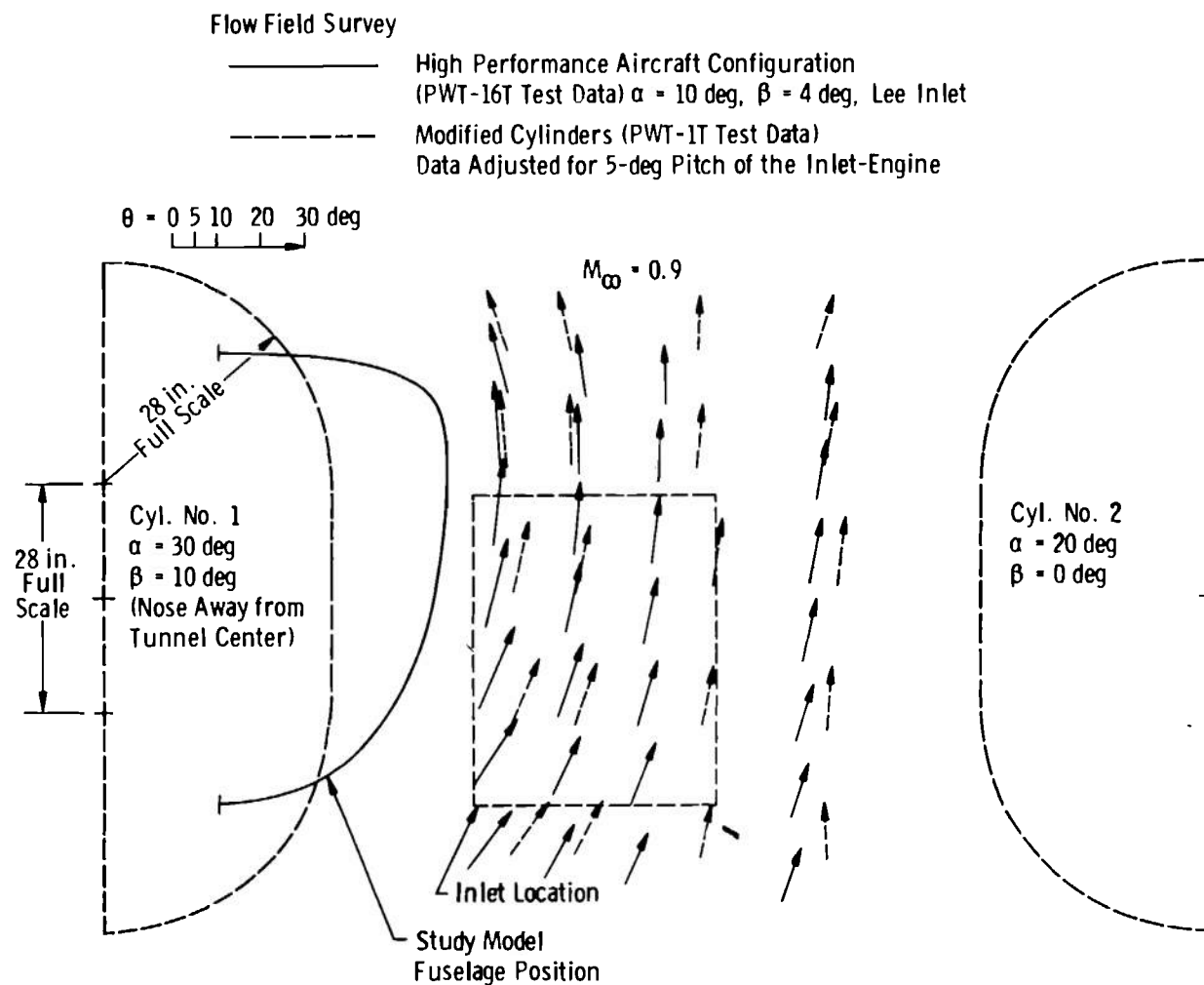
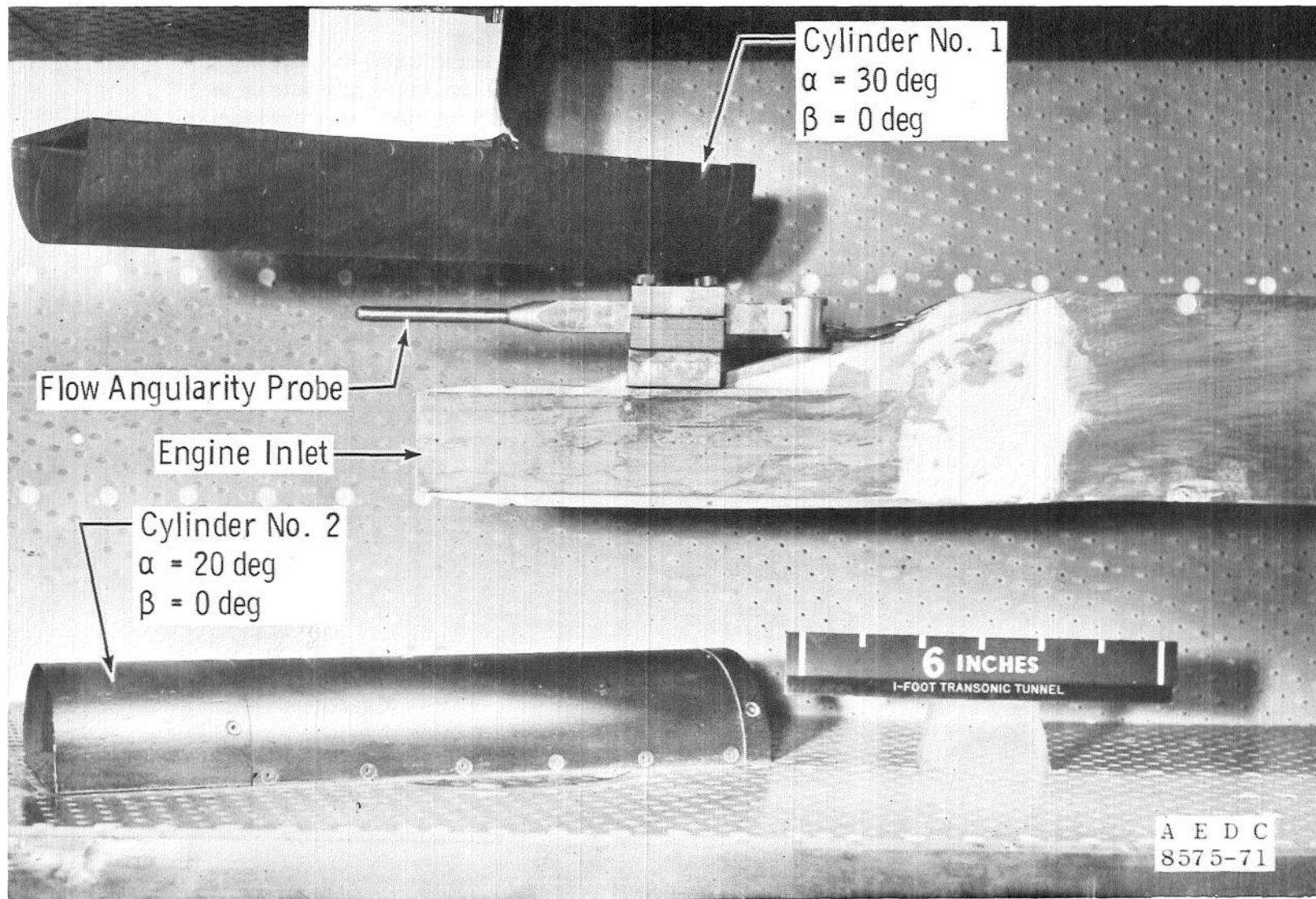
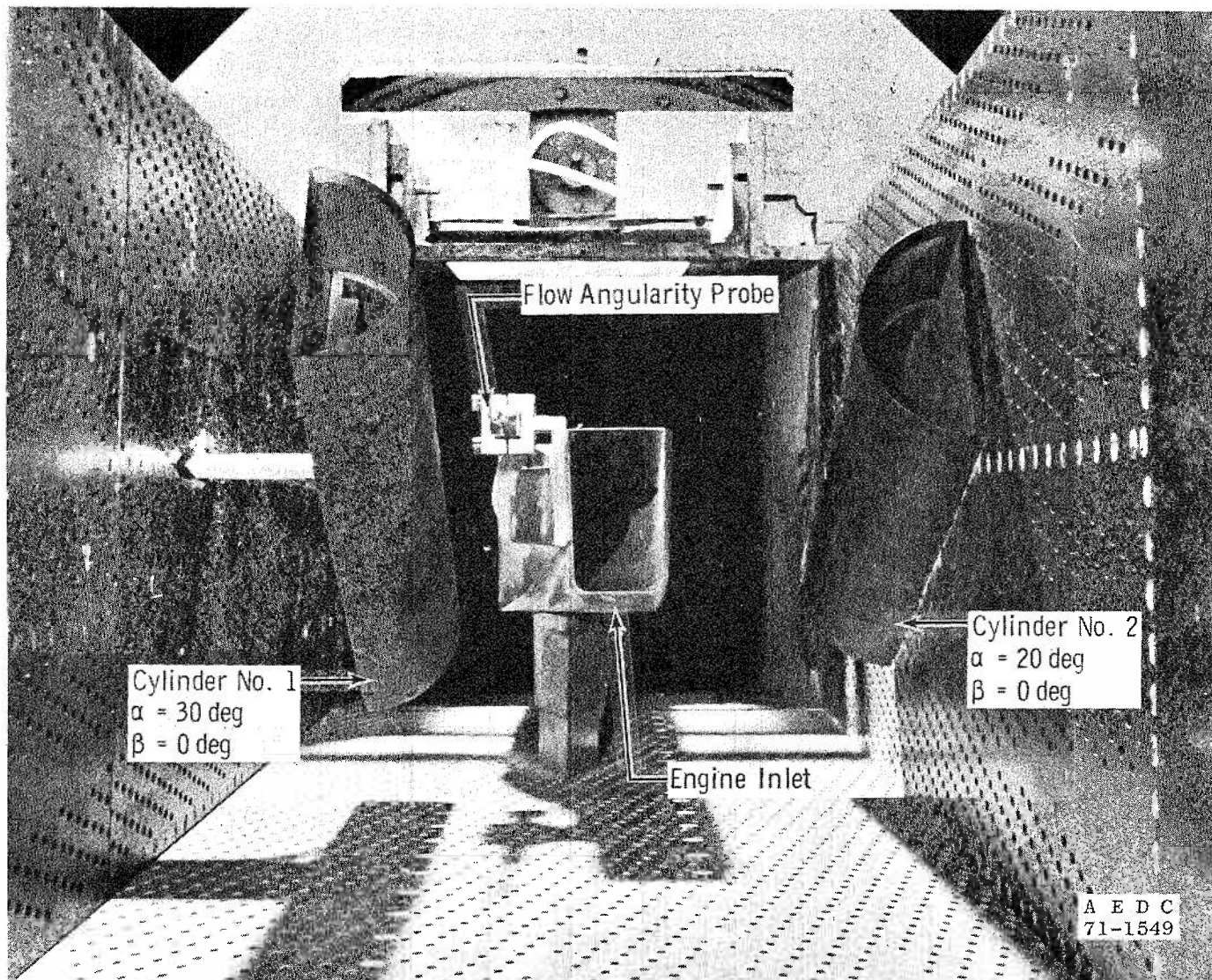


Fig. 55 Comparison of Local Flow Vectors Taken in AEDC PWT-16T with the Study Configuration at an Angle of Attack of 10 deg and an Angle of Yaw of 4 deg with Simulated Local Flow Vectors Taken in the AEDC PWT-1T

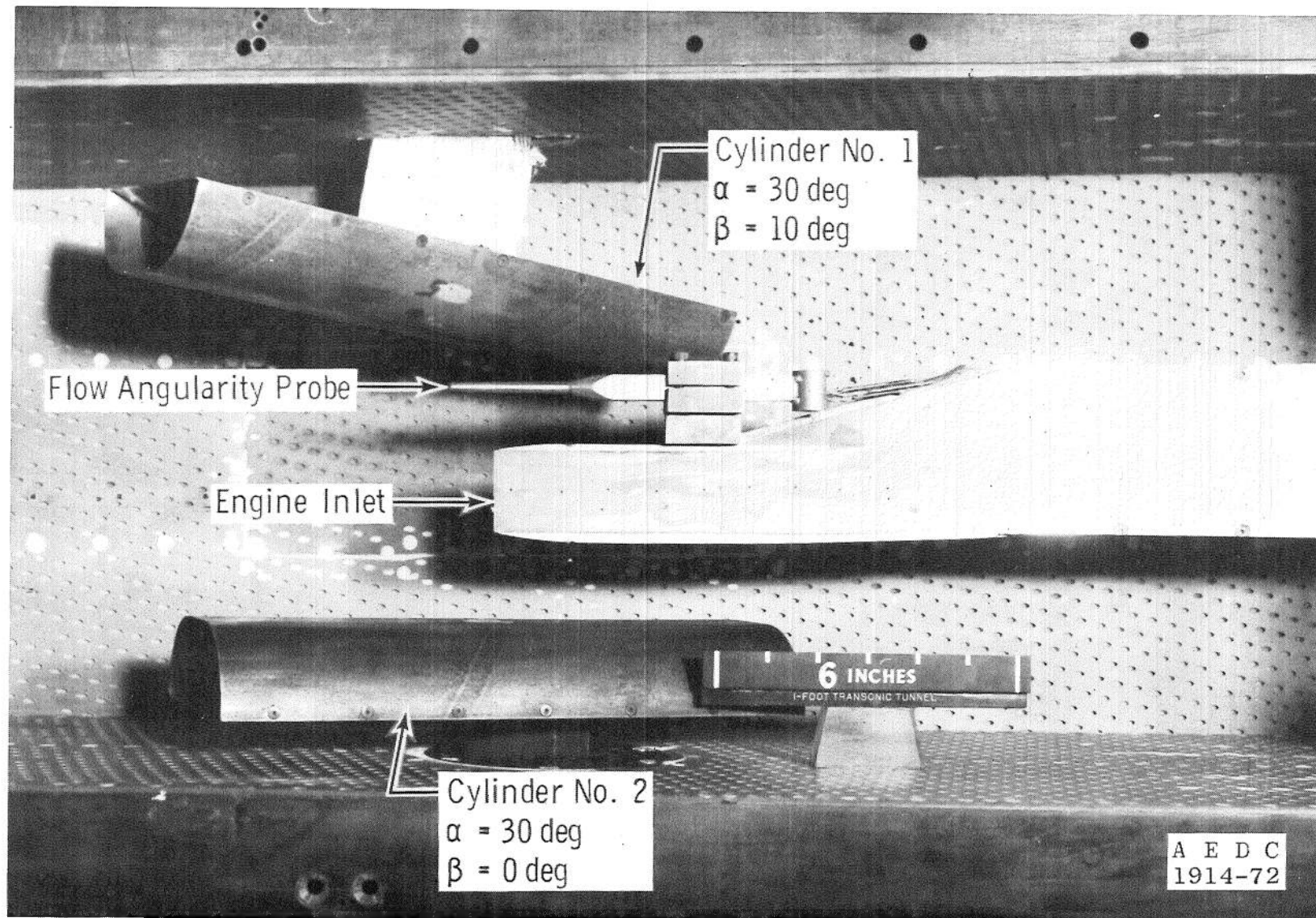


a. Viewed from Top of Inlet/Engine Model

Fig. 56 Installation of the Inlet/Engine Model with the Dual Hollow Circular Cylinders in the AEDC PWT-1T

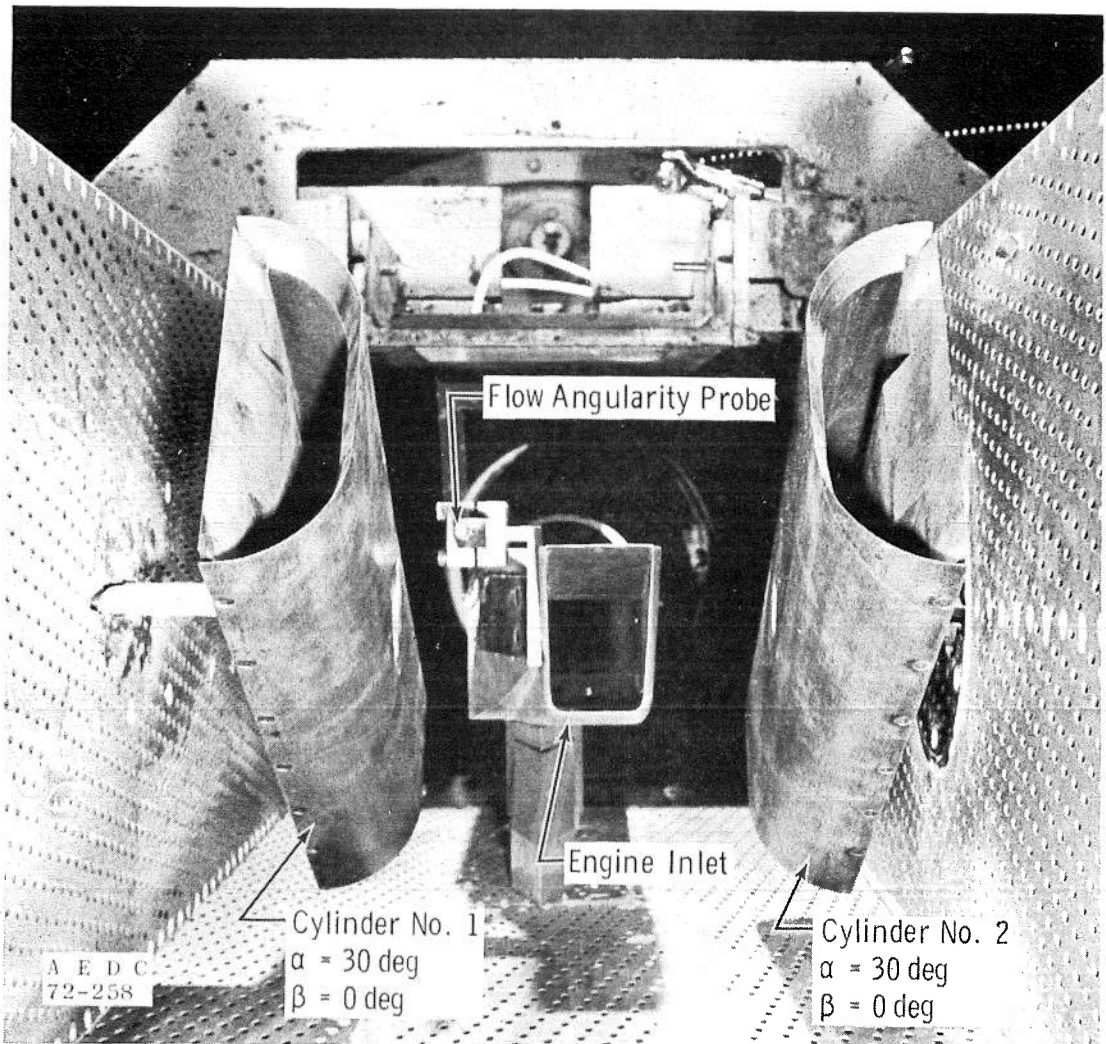


b. Viewed from Front of Inlet/Engine Model
 Fig. 56 Concluded



a. Viewed from Top of Inlet/Engine Model

Fig. 57 Installation of the Inlet/Engine Model with the Modified Hollow Cylinders in the AEDC PWT-1T



b. Viewed from Front of Inlet/Engine Model
Fig. 57 Concluded

- Cylinder No. 1, $\alpha = 30$ deg, $\beta = 0$ deg;
 Cylinder No. 2, $\alpha = 20$ deg, $\beta = 0$ deg
 △ Cylinder No. 1, $\alpha = 40$ deg, $\beta = 0$ deg;
 Cylinder No. 2, $\alpha = 30$ deg, $\beta = 0$ deg
 Open Symbols, Cylinders Only
 Solid Symbols, Cylinders with Inlet-Engine Model

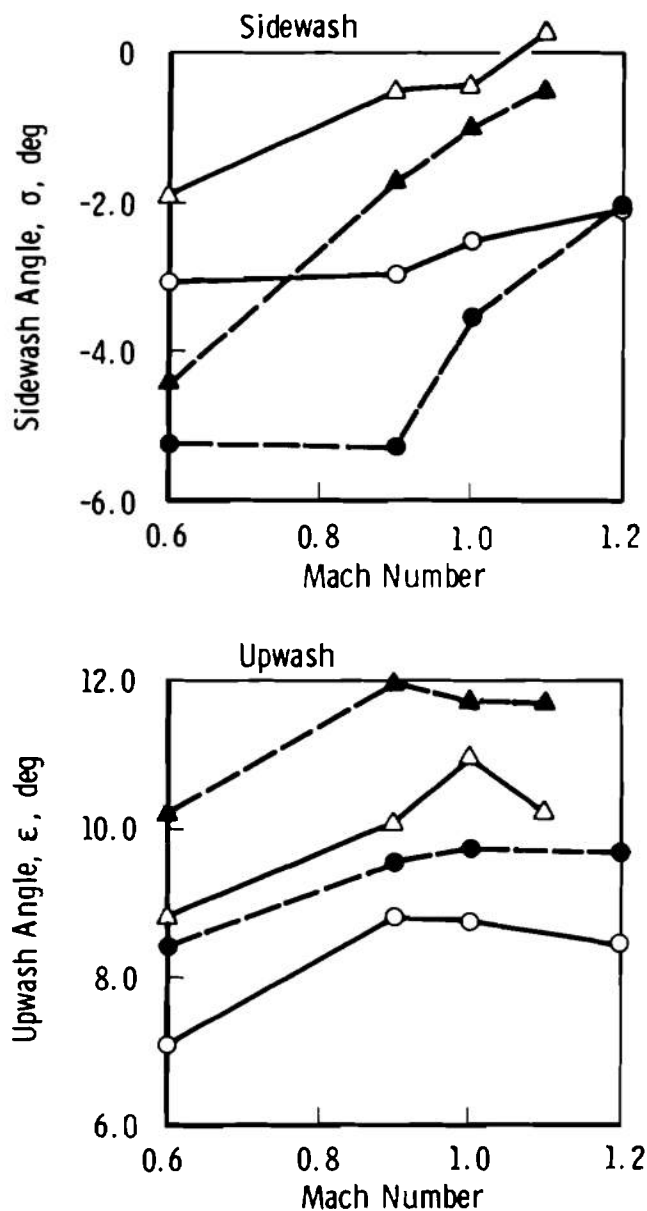


Fig. 58 Increase in Upwash and Sidewash Angles due to the Installation of the Inlet/Engine with the Dual Hollow Circular Cylinders

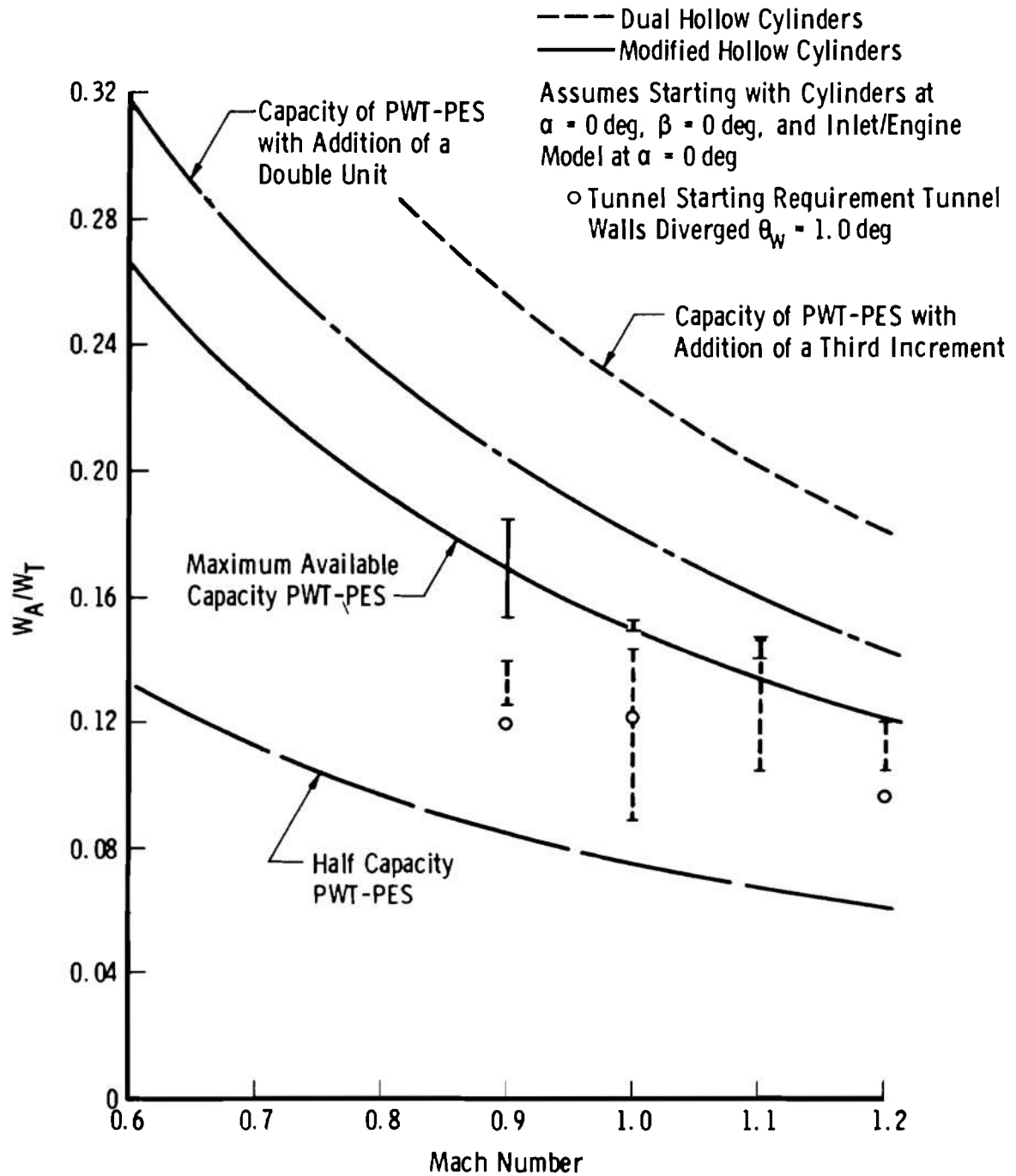


Fig. 59 Auxiliary Weight Flow Required to Operate the Tunnel with Flow Shaping Devices and Inlet/Engine Installed

APPENDIX II

VORTEX-LATTICE PROGRAM FOR 3-D POTENTIAL FLOW PROBLEMS

NOMENCLATURE

a_*	Speed of sound at critical conditions
\vec{C}	Defined by Eq. (II-3)
CP	Pressure coefficient, Eq. (II-23)
k	Ratio of specific heats, C_p/C_v
M	Local Mach number, Eq. (II-22)
M_∞	Free-stream Mach number
\vec{v}	Velocity
\vec{v}_∞	Free-stream velocity, O. or unit velocity in X-direction
$\left. \begin{matrix} u \\ v \\ w \end{matrix} \right\}$	Velocity components
$\vec{v}_k \cdot \vec{n}_k$	Vector dot product of the velocity and the unit normal at the K'th control point
γ	Strength of a horseshoe vortex
η	Strength of a horizontal vortex segment of the model
MNSUM	Total number of independent horseshoe vortices of the model

GENERAL INFORMATION

The program is written in FORTRAN and is run on the IBM 370/155.

Purpose

This program was originally written at Boeing (Ref. 5). At ARO it was modified several times by several different people, to add Goethert's rule, restart capability, etc. Use of the program became complicated. Some of the options were no longer available but still were included in the input. Internal coding was patchwork and inefficient. Therefore, the program has been completely rewritten.

The program computes velocities and streamlines in 3-D potential flow problems. The boundary conditions to be specified are the free-stream velocity and the vector dot product of the velocity and the normal to the boundary. Compressibility can be accounted for using Goethert's rule.

The program has been used to compute subsonic flow around wings and airplanes and to compute flow around various configurations in wind tunnels. It has also been used to compute flow fields of V/STOL aircraft.

Assumptions

The boundary is represented by a lattice network of vortices. The lattice is analyzed by the program into the correct number of independent horseshoe loops, and a control point is located on the boundary for each loop. Then, the strengths of the loops are calculated so that the boundary conditions are satisfied at the control points. When the strengths are known, the velocity at any point in the field can be computed using the Biot-Savart law.

Limitations

The boundary is represented by a network of vortices. The velocity is very large at points near a vortex. Near the boundary the velocity is almost wholly the effect of one or two vortices, not representative of the real boundary in that locality; therefore, the velocity is not accurate. Moving away from the boundary, the velocity is the effect of several vortices, and the solution becomes accurate. One can investigate the flow closer to the boundary by making a finer lattice; however, this rapidly increases computer time.

The program is for potential flow problems; however, compressibility can be accounted for using Goethert's rule. Good results have been obtained for Mach numbers up to 0.9.

The program is limited to steady flow.

METHOD

Introduction

Consider the problem of calculating the subsonic flow about a wing. To use this program, the wing must be modeled by a lattice network of vortices which are input to the program. The program analyzes the lattice into the correct number of independent horseshoe loops. For each loop, a control point is calculated and a unit vector normal to the wing at the control point. The strengths of the horseshoe vortices are determined such that the velocity at the control points is perpendicular to the normal vectors. Once the strengths of the vortices are known, the velocity at any point can be computed from the Biot-Savart law.

In the above problem, there is a free-stream velocity and the boundary condition that, at the surface of the wing, the flow is parallel to the surface. The program can also be used for problems where there is flow through a surface as in the case of a fan-in-wing configuration (Ref. 6), flow in a wind tunnel with porous walls, or the efflux tube of V/STOL aircraft. The free-stream velocity can be set to zero or be set to unit magnitude in the direction of the x-axis.

The Model

A model is input to the program in several parts, divided according to the convenience or experience of the user. A part is illustrated in Fig. II-1. The figure is shown flat, rectangular, and horizontal, but the lattice can be twisted, stretched, and rotated as desired to lie on the boundary surface. The number of points and the coordinates of each point are input. The number of points for the part shown would be input as follows:

$M = 4$ One more than the number of vertical lines

$N = 5$ The number of horizontal lines

$ITR = 3$ The number of points along a horizontal line
minus M , called extra points

For any part, $M \geq 2$, $N \geq 2$, and $ITR \geq 0$.

The coordinates are input in the following order. First for $J = 1$, the coordinates at $I = 1, 2, \dots, M + ITR$ are input. Next for $J = 2$, the coordinate at $I = 1$ to $I = M + ITR$ are input. Then the same for $J = 3$ and so on to $J = N$. All the coordinates for the first part are input, then the second, and so on for all parts.

The part shown in Fig. II-1 is analyzed by the program into 12 horseshoe vortices as shown in Fig. II-2. Note that the number of independent horseshoe vortices is $(M - 1)(N - 1)$. All the horseshoe vortices for a given part trail off from the last point to infinity at a given direction. The direction is input for each part via the variables AX , AY , and AZ , that is, the angle in degrees that the trails make with the X , Y , and Z axes, respectively. A trail can be made to fall along a curve by using extra points, that is $ITR > 0$. A lattice with no trailing vortices can be made by using extra points to make the last points of all the horizontal lines coincide; thus, all the trails will fall along each other and cancel out. That is, the net strength of the trail (singular since all the trails coincide) will be zero.

The program locates a control point in the center of the first 4 points of each horseshoe vortex, represented by X's in Fig. II-2 and computes a unit normal at those points. If there is flow through the body, then the vector dot product of the velocity and the unit normal at each control point is input. They are input in the following order: First for $J = 1$, the velocity dot normals at control points $I = 1, 2, \dots, M - 1$ are input.

Next for $J = 2$, they are input for $I = 1$ to $I = M - 1$. Then the same for $J = 3$ and so on to $J = N = 1$. All the velocity dot normals for the first part are input, then the second, and so on for all parts.

The description in this section uses terms such as vertical, horizontal, rectangle, etc., referring to the figures. It is to be remembered that an actual part can have any orientation, for example, rotated 90 deg, rotated 180 deg, stretched, twisted, and have a completely different appearance than the figures, determined completely by the coordinates input.

Theory

The velocity at a point induced by a horseshoe vortex is given by the Biot-Savart law

$$\vec{v} = \frac{\gamma}{4\pi} \int \frac{\vec{r} \times d\vec{s}}{r^3} \quad (\text{II-1})$$

where the line integral is over the vortex filament, \vec{r} is the vector from the point to the vortex, and $d\vec{s}$ is of arc length magnitude and is tangent to the vortex filament.

The velocity at any point is equal to the free-stream velocity plus the sum of the velocity induced at that point by each horseshoe vortex. Therefore, the velocity at the K'th point is

$$\vec{v}_k = \vec{v}_\infty + \sum_{j=1}^{\text{MNSUM}} \vec{v}_{kj} \quad (\text{II-2})$$

where \vec{v}_{kj} is the velocity induced at the K'th point by the J'th horseshoe vortex and MNSUM is the number of vortices. The velocity induced by a vortex is directly proportional to its strength, so define

$$\vec{C} \triangleq \frac{\vec{v}}{\gamma} \quad (\text{II-3})$$

then Eq. (II-2) becomes

$$\vec{v}_k = \vec{v}_\infty + \sum_{j=1}^{\text{MNSUM}} \vec{C}_{kj} \gamma_j \quad (\text{II-4})$$

Consider the case where the K'th point refers to the K'th control point and take the dot product of both sides of Eq. (II-4) with \vec{n}_k and rearrange

$$\sum_{j=1}^{\text{MNSUM}} [\vec{C}_{kj} \cdot \vec{n}_k] \gamma_j = \vec{v}_k \cdot \vec{n}_k - \vec{v}_\infty \cdot \vec{n}_k \quad (\text{II-5})$$

The $\vec{v}_k \cdot \vec{n}_k$ is either 0 or input. The free-stream velocity is either 0 or input. The \vec{n}_k are computed. \vec{C}_{kj} is the velocity induced at the K'th control point by the J'th vortex when its strength is one; therefore, it can be computed. Thus, everything in Eq. (II-5), except γ_j , is either known or can be calculated, and Eq. (II-5) is a linear algebraic set of equations which can be solved for the strengths of the vortices.

When strengths are known, the velocity at any point K can be obtained from Eq. (II-2). Streamlines are calculated from velocities by integrating

$$\frac{d\vec{r}}{dr} = \frac{\vec{v}}{v} \quad (II-6)$$

Symmetry

Consider a system that is symmetrical with respect to a plane. Number half of its vortices from 1 to MNSUM and the other half from MNSUM+1 to 2*MNSUM where 2*MNSUM corresponds to 1, 2*MNSUM-1 corresponds to 2, and so on to MNSUM+1 corresponds to MNSUM. Equation (II-5) becomes

$$\sum_{j=1}^{2*MNSUM} [\vec{C}_{kj} \cdot \vec{n}_k] \gamma_j = \vec{v}_k \cdot \vec{n}_k - \vec{v}_\infty \cdot \vec{n}_k \quad (II-7)$$

Define

$$i = 2*MNSUM+1-j \quad (II-8)$$

$$\ell = 2*MNSUM+1-K \quad (II-9)$$

By symmetry, it is seen that \vec{v}_∞ is parallel to the plane of symmetry and that

$$\gamma_i = -\gamma_j \quad (II-10)$$

$$\vec{v}_\ell \cdot \vec{n}_\ell = \vec{v}_k \cdot \vec{n}_k \quad (II-11)$$

$$\vec{v}_\infty \cdot \vec{n}_\ell = \vec{v}_\infty \cdot \vec{n}_k \quad (II-12)$$

$$\vec{C}_{\ell i} \cdot \vec{n}_\ell = \vec{C}_{kj} \cdot \vec{n}_k \quad (II-13)$$

By changing the free index to m, combining corresponding terms on the left hand side, and using Eqs. (II-8) and (II-10), then Eq. (II-7) becomes

$$\sum_{j=1}^{MNSUM} [(\vec{C}_{mj} - \vec{C}_{mi}) \cdot \vec{n}_m] \gamma_j = \vec{v}_m \cdot \vec{n}_m - \vec{v}_\infty \cdot \vec{n}_m \quad (II-14)$$

It is seen that Eq. (II-14) yields the same equation for $m = k$ and for $m = \ell$. Therefore, one can solve Eq. (II-14) for γ_j for j from 1 to MNSUM and use Eq. (II-10) for the rest of the γ 's.

Computing the coefficients for a symmetrical system takes only half as long since the coefficients for only half of the equations need be computed. Solving the system takes only about one-eighth as long, since the time to solve the equations goes up approximately like the cube of the number of equations. The program can be used with no symmetry, symmetry with respect to the XY plane, symmetry with respect to the XZ plane, or symmetry with respect to both the XY and XZ plane. The latter case requires only one-fourth as long to compute the coefficients and about 1/64th as long to solve the equations as an equivalent nonsymmetrical case.

Goethert's Rule

All input and output to the program is in the physical reference system. Internally, however, a transformation is made to account for compressibility according to

$$x' = \frac{x}{\sqrt{1 - M_\infty^2}} \quad (\text{II-15})$$

$$y' = y \quad (\text{II-16})$$

$$z' = z \quad (\text{II-17})$$

Velocity components in the transformed plane (u' , v' , w') are obtained and then are transformed back to the physical plane according to

$$u = \frac{u' - M_\infty^2}{1 - M_\infty^2} \quad (\text{II-18})$$

$$v = \frac{v'}{\sqrt{1 - M_\infty^2}} \quad (\text{II-19})$$

$$w = \frac{w'}{\sqrt{1 - M_\infty^2}} \quad (\text{II-20})$$

Transformations in the x-direction are different than transformations in the y and z directions, because \vec{v}_∞ is in the x direction. These transformations are according to Goethert's rule as given in Ref. 7.

Equations for Local Flow Data That Are Output by the Program

The flow data output by the program for a given point are x , y , z , u , v , w , $|\vec{v}|$, M , $\tan^{-1} v/u$, $\tan^{-1} w/u$, CP, and $M - M_\infty$. The coordinates of the point are x , y , z , and the components of the velocity are u , v , w . The magnitude of the velocity is

$$|\vec{v}| = \sqrt{u^2 + v^2 + w^2} \quad (II-21)$$

The local Mach number is computed by

$$M = \frac{|\vec{v}| M_\infty}{\sqrt{1 + \frac{k-1}{2} M_\infty^2 (1 - |\vec{v}|^2)}} \quad (II-22)$$

The pressure coefficient by

$$CP = 1 - |\vec{v}|^2 \quad (II-23)$$

The flow angularity is determined by $\tan^{-1} v/u$ and $\tan^{-1} w/u$. These parameters are computed as indicated as is $M - M_\infty$.

Equation (II-22) is derived from Eqs. (50) and (58) of Ref. 8. Since the free-stream velocity is of unit magnitude, the above mentioned Eq. (50) becomes in the free-stream

$$\left(\frac{1}{a^*}\right)^2 = \frac{\frac{k+1}{2} M_\infty^2}{1 + \frac{k-1}{2} M_\infty^2} \quad (II-24)$$

Equation (58) of Ref. 8 is

$$M^2 = \frac{\frac{2}{k+1} \frac{|\vec{v}|^2}{a_*^2}}{1 + \frac{k-1}{k+1} \frac{|\vec{v}|^2}{a_*^2}} \quad (II-25)$$

By eliminating a_* and solving for M , one obtains Eq. (II-22).

Effect of a Vortex Segment or a Vortex Ray

Once γ 's have been obtained it would be very inefficient to compute Eq. (II-1) for each horseshoe vortex and add the results to calculate a velocity. Instead, the net strength of each segment and ray is computed, and Eq. (II-1) is evaluated just once over each segment and ray of the model. Note that the strength of each vertical segment (Fig. II-2) is the strength of its respective horseshoe vortex. The strength of a horizontal segment, however, is the algebraic sum of the strengths of each horseshoe vortex, of which the segment is a part. Let η_{ij} be the net strength of a horizontal horseshoe segment where j denotes the horizontal line and i which segment of the line. It is seen from Fig. II-2 that

$$\eta_{ij} = \zeta_1 + \zeta_2 + \zeta_3 \quad (II-26a)$$

where

$$\zeta_1 = \begin{cases} \gamma_{i-1,j} & i > 1 \\ 0 & i = 1 \end{cases} \quad (\text{II-26b})$$

$$\zeta_2 = \begin{cases} \gamma_{i,j-1} & j > 1 \\ 0 & j = 1 \end{cases} \quad (\text{II-26c})$$

$$\zeta_3 = \begin{cases} -\gamma_{ij} & j < N \\ 0 & j = N \end{cases} \quad (\text{II-26d})$$

Since the model is made up completely of vortex segments and vortex rays (the trailing vortices), only two formulas are needed by the program to evaluate Eq. (II-1), one where the curve C corresponds to a line segment and the other when it is a ray. In Fig. II-3, the line segment extends from point A to point B, and C is the point at which the velocity is desired. Equation II-1 results in

$$\vec{v} = \frac{\gamma}{4\pi a} (\cos \theta_1 + \cos \theta_2) \vec{u} \quad (\text{II-27})$$

where \vec{u} is a unit vector, which for the case shown in Fig. II-3, is directed into the paper. The formula for a ray is easily obtained by letting θ_2 approach zero. Thus, it is identical to Eq. (II-27) except $\cos \theta_2$ is replaced by 1.

RESULTS

Figure 14 shows the model that was used in the sample problem. The model is symmetrical with respect to the XY plane, and only one-half of the model is shown. Figure 15 contains contour plots of the flow angularity computed by the program for this model. Printed output for this shot follows the program listing.

INPUT PREPARATION AND OUTPUT DESCRIPTION

Card Input Data

Card input to the program is indicated below in "pseudo-FORTRAN." The format of each card is given in parenthesis after READ. Definitions of variables follow the "FORTRAN."

```

1      INPUT TO VORTEX LATTICE PROGRAM
2
3      READ (213) IREST, MINGO
4      READ (A80) TITLE
5      READ (413) NW, LXY, LXZ, L900
6      READ (E12.0) RER
```

```

7      READ (2E12.0) M∞, k
8
9      DO 10 K = 1, NW
10     READ (3I3, 3X, 3E12.0), M, N, ITR, AX, AY, AZ
11
12     BODY COORDINATES
13     DO 16 K=1,NW
14     DO 16 J=1,N(K)
15     DO 16 I=1,M(K)+1TR(K)
16     READ (3E12.0) XB, YB, ZB
17
18     VELOCITY DOT NORMALS
19     IF (L900-0) GO TO 23
20     READ (6E12.0) (((  $\vec{v} \cdot \vec{n}$ , I=1,M(K)-1), J=1,N(K)), K=1,NW)
21
22     VELOCITIES
23     READ (I3) NV
24     IF (NV=0) GO TO 29
25     DO 26 J=1,NV
26     READ (3E12.0) XV,YV,ZV
27
28     STREAMLINES
29     READ (I3)NS
30     IF (NS=0) GO TO 35
31     DO 33 J=1,NS
32     READ (6E12.0,I8) XO,YO,ZO,DSO,AN,AX,NX
33     READ (6E12.0) XN,XX,YN,YX,ZN,ZX
34
35     END OF CARD INPUT

```

Definitions of above variables follow:

IREST	0 Initial shot 1 Restart in SETM 2 Restart in LSYSEQ 3 γ 's are known
MINGO	Time in minutes the program is to run.
NW	Number of model parts
LXY } LXZ }	Symmetry indicators 0 indicates no symmetry 1 indicates symmetry

L900	$0 \vec{v}_\infty = \hat{u}$, where \hat{u} is unit velocity in x-direction, $\vec{v} \cdot \vec{n} = 0$ $1 \vec{v}_\infty = \hat{u}$, $\vec{v} \cdot \vec{n}$ are read $2 \vec{v}_\infty = 0$, $\vec{v} \cdot \vec{n}$ are read
RER	If a point is within this distance of a line determined by a vortex segment, the effect of that segment is set to zero. $RER \geq 0$.
M_∞	Free-stream Mach number
k	Ratio of specific heats. If left zero, it defaults to 1.4.
M	One more than the number of vertical lines. $M \geq 2$.
N	The number of horizontal lines. $N \geq 2$.
ITR	The number of extra points - i.e., the number of points along a horizontal line minus M. $ITR \geq 0$.
AX } AY } AZ }	Angle in degrees the trailing vortices of the part make with the X, Y, and Z axis, respectively.
XB } YB } ZB }	Coordinates of points on the model
$\vec{v} \cdot \vec{n}$	If $L900 \neq 0$, then the $\vec{v} \cdot \vec{n}$ must be read in, 6 to a card.
NV	Number of points at which velocities are to be calculated
XV } YV } ZV }	Coordinates of the points at which velocities are to be calculated
NS	Number of streamlines to be calculated
XO } YO } ZO }	Coordinates of starting point of streamline
DSO	Absolute value of DSO is maximum step size used in calculating streamline. It is also the length of the initial step size. The sign, plus or minus, determines whether the downstream or upstream streamline is to be calculated.

AN	Minimum angle in degrees. If the angle between velocities at the beginning of a step and at the end of a step is less than AN, then the step size is increased unless it is already at its maximum value which is the absolute value of DSO.
AX	Maximum angle in degrees. If the angle between velocities at the beginning of a step and at the end of a step exceed AX, then the step size is decreased.
NX	Maximum number of steps. Calculation of the streamline terminates after this number of steps.
XN,XX } YN,YX } ZN,ZX }	Minimum value and maximum value for X,Y, and Z. If the streamline extends past one of these values, calculation of the streamline terminates.

Read and Write Units

<u>Unit 5</u>	Card Reader - See previous section for card input data.
<u>Unit 6</u>	Printer - All output is labeled using the same nomenclature as this report.
<u>Unit 10</u>	Direct Access Unit - This unit is used only in LSYSEQ. If it is known that a shot will terminate in SETM because of time, then Unit 10 need not be defined.
<u>Unit 11</u>	System of Equations - It is written in SETM and read by LSYSEQ. If IREST>2, then Unit 11 need not be defined. Each logical record of Unit 11 consists of one row of coefficients of the system of equations and the right hand constant. SETM computes a row, then writes it on 11; computes another row and writes it, and so on. After the last record, that is either all coefficients have been computed or else SETM must terminate because of time, in either case, Unit 11 is endfiled. See Unit 21 for more information.
<u>Unit 12</u>	When LSYSEQ terminates because of time, it writes the partially solved system of equations out on Unit 12. When the solution is complete LSYSEQ rewinds 12, writes without format γ_j , $j=1$ to MNSUM, and then endfiles 12. Note that either one or the other, either the partially solved system of equations or else the solution is written on 12. Not both. The γ 's are read from Unit 12 by AIRFL2.

Unit 13

Velocities - If it is known that a shot will terminate in SETM or LSYSEQ because of time, then Unit 13 need not be defined. Otherwise, Unit 13 must be defined, whether or not any velocities are requested. USERV computes the velocity at a point and writes a record on Unit 13; computes the velocity at the next point and writes a record on 13, and so on until all velocities requested have been computed. It then writes out a record of -1's and then endfiles 13 even if no other records were written, that is even if no velocities were requested. Each record is written without format thus: XV, YV, UV, U, V, W, $|\vec{V}|$, M, $\tan^{-1}(v/u)$, $\tan^{-1}(w/u)$, CP, $M-M_\infty$. These are the same velocity data that are printed. The program never reads Unit 13. The velocity data are saved on Unit 13 for the convenience of the user in case further processing is required, for example plotting.

Unit 14

Streamlines - If it is known that a shot will terminate in SETM or LSYSEQ because of time, then Unit 14 need not be defined. Otherwise, it must be defined, even if no streamlines are requested. STREAM, called by USERS, writes one record on Unit 14 for each point along a streamline. This record is identical to that written for velocities, that is each record is written without a format thus: XS, YS, ZS, U, V, W, $|\vec{V}|$, M, $\tan^{-1}(v/u)$, $\tan^{-1}(w/u)$, CP, $M-M_\infty$ where XS, YS, ZS are the coordinates of a point on the streamline. After computation of a streamline is finished, a record of -1's is written. After all streamlines requested have been completed, Unit 14 is endfiled. It is endfiled even if no records were written, that is even if no streamlines were requested. The program never reads Unit 14. Streamline data are saved on Unit 14 for the convenience of the user, in case further processing is required, for example plotting.

Unit 21

When restarting in SETM or in LSYSEQ, the tape written on Unit 11 in the previous shot must be mounted on Unit 21. Otherwise, Unit 21 need not be defined. When restarting in SETM, SETM reads a record from Unit 21 and writes it on Unit 11; reads the next record and writes it, and so on until it reaches end of file on Unit 21. It then proceeds computing the coefficients a row at a time and writing them on Unit 11. When restarting in LSYSEQ, before LSYSEQ is called, SETM reads the system of equations from Unit 21 and writes then on Unit 11.

Unit 22

When restarting in LSYSEQ, the tape written on Unit 12 in the previous shot must be mounted on Unit 22. Otherwise, Unit 22 need not be defined.

OPERATING INFORMATION

Restart Capability

The time in minutes a shot is to run is input via MINGO. At the very start, the program calls an assembler language subroutine, TIMEX. TIMEX sets the FORTRAN variable, JRUB equal to zero, and at the end of the allotted time sets JRUB equal to one. The variable JRUB is checked by the subroutines SETM and LSYSEQ at the end of each row of computation. If time has run out, they terminate and can be restarted. Note that the routines check at the end of a row of computation, then must write restart information on tape, thus the shot will run a little longer than the time input MINGO. This must be considered because, if the program is killed by the operating system instead of terminating normally, then it might be impossible to restart it. Also, note that the program checks only the time while calculating the coefficient matrix (SETM) and while solving the system of equations (LSYSEQ). Once the system of equations have been solved (γ 's are obtained), the program will start calculating the velocities and streamlines ordered. It will continue until killed or until finished. However, once γ 's are obtained, one can always restart, calculating velocities at left over points or restarting a streamline where it left off.

Running Time

The time in minutes for a run can be roughly estimated as follows:

$$\begin{aligned}\text{Time in SETM} &\approx C1 * (KS * MNSUM)**2 \\ \text{Time in LSYSEQ} &\approx C2 * MNSUM**3 \\ \text{Time in USERV} &\approx C3 * KS * MNSUM * NV \\ \text{Time in USERS} &\approx 2 * C3 * KS * MNSUM * NS * \overline{NX}\end{aligned}$$

where

KS=	1	no symmetry
	2	symmetry with respect to one plane
	4	symmetry with respect to two planes

NX is the maximum number of steps for a streamline and \overline{NX} is the average of the NX's for all streamlines.

For the 370/155, the constants are

$$\begin{aligned}C1 &= 1.8 \times 10^{-4} \\ C2 &= 1.7 \times 10^{-6} \\ C3 &= 2.6 \times 10^{-5}\end{aligned}$$

Also useful in estimating time is the fact that SETM requires approximately the same amount of time for each row of computation. However, LSYSEQ requires less and less time for successive rows.

End of Shot Indication

The last line of printed output gives the reason for termination.

For example:

1. 371 OF 430 IN SETM
2. 106 OF 430 IN LSYSEQ
3. JOB COMPLETED
4. SINGULAR MATRIX
5. DIMENSIONED BY 11000, REQUIRES 12000
6. ZERO NORMAL 3 7 2

In Example 1, the program should be restarted with IREST=1. In Example 2, the program should be restarted with IREST=2. In Example 3, all requested work was completed. If additional velocities or streamlines are desired, one can restart with IREST=3. The only times Example 4 has occurred were for bad or wrong modeling. Example 5 can be eliminated either by reducing the model or increasing the dimension (see the next section for redimensioning information.) Best use of storage is made when all model parts are approximately the same size, that is all parts have approximately the same M, N, and ITR. Thus, Example 5 can sometimes be eliminated by a more judicious division of the parts. Example 6 is caused by a modeling error where the first four points of a horseshoe vortex are colinear. The three integers following the diagnostic locate which horseshoe vortex is in error.

PROGRAMMING INFORMATION

Flow Diagram and Modification Hints

A flow diagram of the program which shows where each subroutine is called is shown in Fig. II-4. The diagram goes from left to right and from top to bottom. For example, USERV calls VELLAB, then VELOCITY, then VELOUT, but does not call STREAM. USERS calls VELLAB, then STREAM, and STREAM calls VELOCITY, then VELOUT.

The program was written modular in form for easy modification. Figure II-4 and the following section should be helpful if modification is necessary. As an example of a modification which has been made: The coordinates for one large model were calculated by another program and written on tape. BODY1 was then modified to read the coordinates off the tape instead of cards.

Another example: It was easier to program which points velocities were desired rather than prepare a deck with the coordinates. Therefore, USERV was modified by replacing the READ statement with statements producing the coordinates.

Another easy change which could be made: Suppose some other parameters which were functions of the components u , v , and w were desired instead of or in addition to the parameters now calculated, M , $|\vec{v}|$, $M-M_\infty$, etc. Then one need only modify VELOUT to compute and output the desired quantities and modify VELLAB to label them properly.

To redimension the program, only two statements need be changed. They are the dimension statement in the main program and the integer statement in subroutine SCRIMP. SCRIMP computes how much storage is required by the model then checks to see if the storage is available. This is the purpose of the integer statement in SCRIMP.

Brief Description of the Subroutine

TIMEX is an assembler language routine. When called, it sets the FORTRAN variable JRUB equal to zero, sets a clock, then returns. Execution of the program continues as usual. When the allotted time, NSEC, has elapsed, then the clock sets JRUB equal to one. The variable JRUB is checked by SETM and LSYSEQ after each row of computation. If zero, they continue. If one, they terminate.

TIMEX must be supplied by the user according to the particular timing technique of the computer used. Its function is simple and clear. It sets JRUB to zero when called, and JRUB must change to one after the elapsed time, NSEC. One could if necessary, by sacrificing the restart capability, just write a FORTRAN subroutine which sets JRUB to zero and just leave it zero. Alternately, one could modify SETM and LSYSEQ so that instead of checking JRUB, they compute a given number of rows, then terminate.

SCRIMP computes how much storage is needed by each array. The storage for each array is allocated in the single array X of the main program. If the storage requirement exceeds the dimension, then SCRIMP writes a message and terminates the shot.

CHAIN is called by the main program with all arguments being the X array subscripted with the beginning location of the corresponding dummy argument. These beginning locations were supplied by SCRIMP. CHAIN, in turn, calls the subroutines as shown in Fig. II-4 with the proper arguments.

BODY1 reads the body coordinates, sets \vec{v}_∞ according to L900, and either reads $\vec{v} \cdot \vec{n}$ or sets them to zero according to L900.

AIRFL1 prints the input and sets the value of some constants. It also replaces AX, AY, and AZ with their cosines producing a unit vector in the direction of the trailing vortices.

STRECH stretches the model according to Goethert's rule.

BODY2 computes and outputs the control points and unit normal vectors.

SETM computes the coefficients and right hand constants of the system of equations represented by Eq. (II-5). This is done one row at a time and is output on Unit 11.

AIRFL2 calls LSYSEQ to effect the solution of the system of equations. If the system is singular then AIRFL2 writes a message and terminates. Otherwise, AIRFL2 reads the γ 's from Unit 12 and computes the η 's. It prints the γ 's and η 's and returns. If IREST \geq 2, then it skips calling LSYSEQ and begins by reading the γ 's, then proceeds as before.

USERV reads NV, then for each point: (1) reads the coordinate of the point, (2) obtains the velocity at the point by calling VELOCITY, then (3) outputs by calling VELOUT. Before returning it writes a record of -1's on Unit 13 then endfiles 13.

USERS reads NS, then for each streamline requested: (1) reads the streamline data, (2) calls stream, then (3) writes a record of -1's on Unit 14. Before returning, it endfiles 14.

LSYSEQ uses direct access and solves a large system of equations. If direct access is not available, then LSYSEQ must be replaced by some other subroutine using a different method. Such a routine is usually available in most computer centers. The system of equations is on Unit 11, without format, with one row of coefficients and the right hand constant per record. LSYSEQ reads Unit 11 and solves the system of equations. It then writes the solution on Unit 12 in one record without format.

DAFILE is an assembler language routine which is equivalent to the DEFINE FILE statement. It was necessitated by the requirement that the arguments of the DEFINE FILE statement be constants. DAFILE performs exactly the same function as DEFINE FILE except its arguments need not be constants.

STREAM performs a numerical integration of Eq. (II-6) and outputs via VELOUT. The method used is improved Euler.

VELOCITY computes the velocity at a point.

VELOUT computes $|\vec{V}|$, M, CP, etc., and prints. It also outputs on a designated unit.

VELLAB is an entry of VELOUT and just prints a label for the printed output of VELOUT.

SEGM and RAY compute the velocity induced by a vortex segment and a vortex ray, respectively.

YEYM and ZEMZ replace the coordinates of the model by the coordinates of its reflection with respect to the XZ plane and the XY plane, respectively.

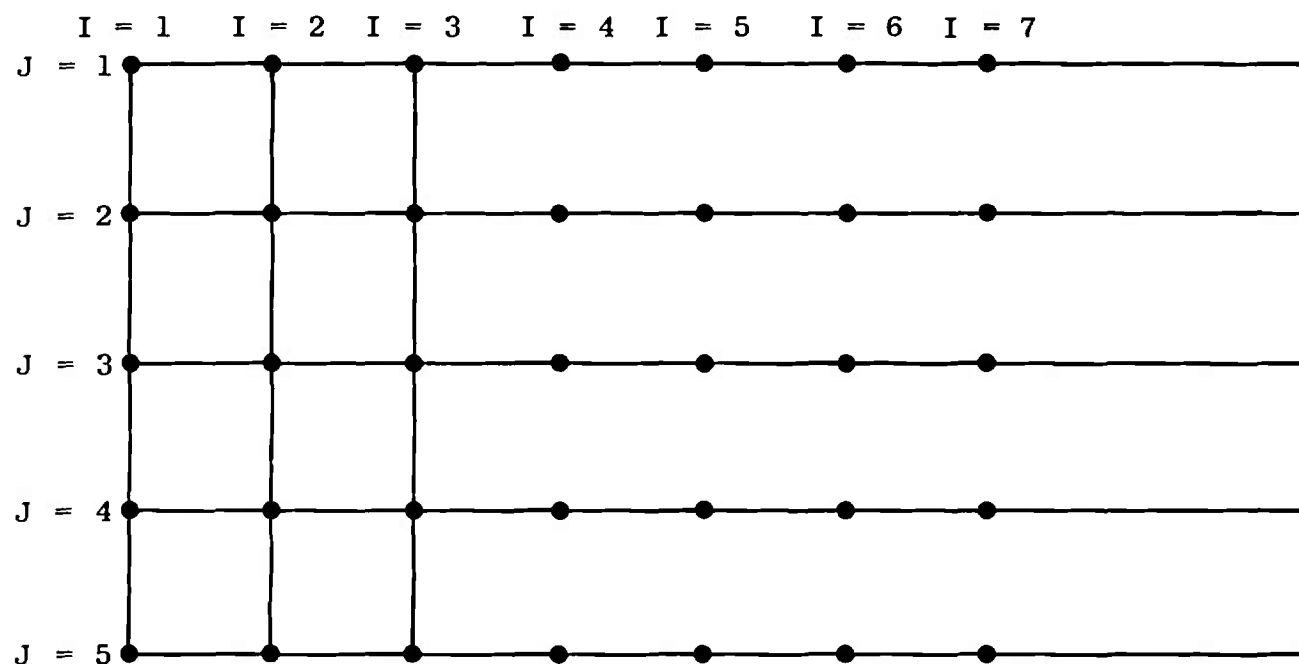


Fig. II-1 Illustrative Model Cart

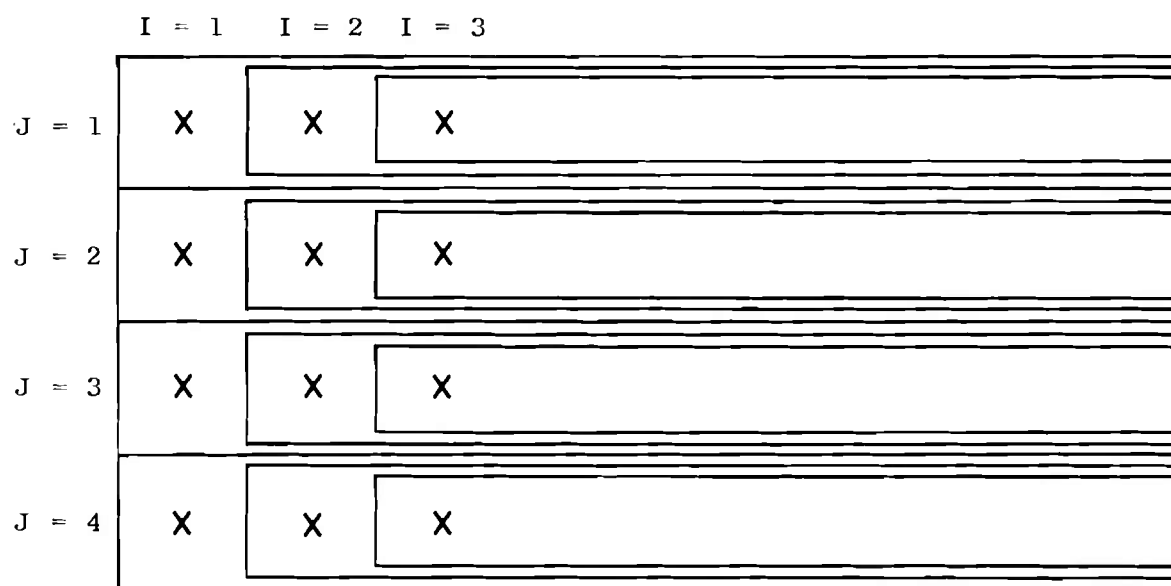
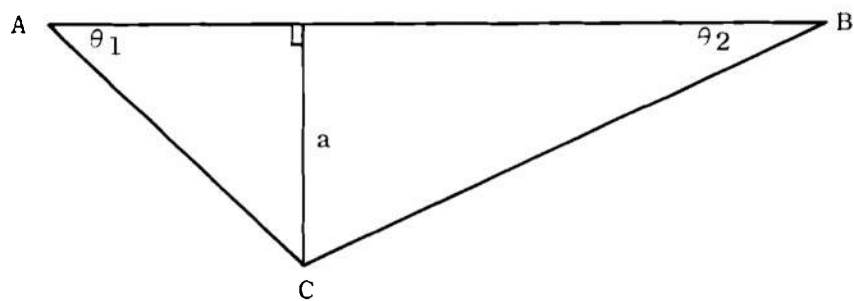


Fig. II-2 Analysis into Horseshoe Vortices

Fig. II-3 Vortex Segment AB and Point C

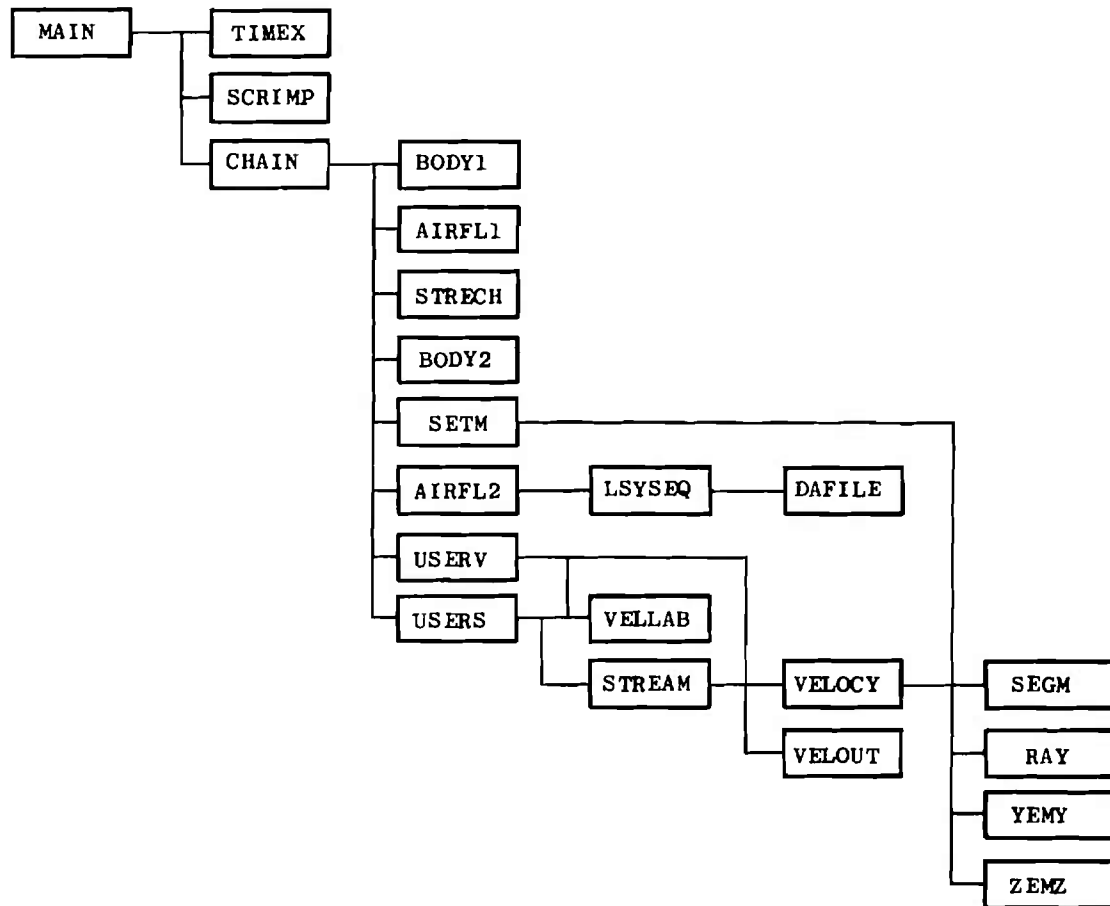


Fig. II-4 Flow Diagram of Program

Program Listing and Sample Run

Following is a program listing and a sample run. Figure 14 shows the model of the sample run. Figure 15 contains contour plots of the flow angularity.

G LEVEL	20	MAIN	DATE = 73018	12/02/34
C	SEP00211	DC TODD 08/10/71 PW5146 RL PALKD		B 1
C	TIDY VDRTEX	LATTICE PGM		B 2
		DIMENSION X(11000)		B 3
		D(MENSION M(1)		B 4
		EQUIVALENCE (X(1),M(1))		B 5
		COMMON /CMMNA/ MINGO,JRUB,IREST,MNSUM,NWCODE,LXY,LXZ,L900		B 6
		COMMON /CMMNB/ RER,T(TLE(20),FS,AM,AGAM,AMS,F1,F2		B 7
		COMMON /CMMNC/ IV,JV,KV,LTOT,LA,LB,LC,LD,LE,LF,LG,LH,LI,LJ,LK,LL,L		B 8
		IM,LN,LO,LP,LQ,LR,LS		B 9
		D(MENSION LRA(1)		B 10
		EQUIVALENCE (LRA(1),LA)		B 11
		READ (5,40) IREST,MINGO		B 12
		NSEC=60*M(NGO		B 13
		CALL T(MEX (NSEC,JRUB)		B 14
		READ (5,30) TITLE		B 15
		READ (5,40) NWCODE,LXY,LXZ,L900		B 16
		READ (5,50) RER,FS		
		READ (5,50) AM,AGAM		B 18
		IF (AGAM.EQ.0.) AGAM=1.4		B 19
		LA=NWCDE		B 20
		DO 10 K=2,6		B 21
10		LRA(K)=LRA(K-1)+NWCDE		B 22
		DO 20 K=1,NWCODE		B 23
20		READ (5,60) M(K),M(LA+K),M(LB+K),X(LC+K),X(LD+K),X(LE+K)		B 24
		CALL SCR(MP (M(1),M(LA+1),M(LB+1))		B 25
		CALL CHA(N (M(1),M(LA),M(LB),X(LC),X(LD),X(LE),X(LF),X(LG),X(LH),X		B 26
		I(LI),X(LJ),X(LK),X(LL),X(LM),X(LN),X(LO),X(LP),X(LQ),X(LR))		B 27
		WRITE (6,70)		B 28
		STOP		B 29
30		FDRMAT (20A4)		B 31
40		FORMAT (24I3)		B 32
50		FORMAT (6E12.0)		B 33
60		FDRMAT (3I3,3X,3E12.0)		B 34
70		FORMAT (14HAJDB COMPLETED)		B 35
		END		B 36-

G LEVEL	20	SCRIMP	DATE = 73018	12/02/34
		SUBROUT(NE SCRIMP (M,N,ITR)		C 1
		DIMENSION M(1), N(1), (TR(1)		C 2
		COMMON /CMMNA/ KL,JRUB,(REST,MNSUM,NWCODE		C 3
		COMMON /CMMNC/ IV,JV,KV,LTOT,L(1)		C 4
		INTEGER ND(M/11000/		
		MNSUM=0		C 5
		IV=0		C 6
		JV=0		C 7
		KV=0		C 8
		DO 10 K=1,NWCDE		C 9
		MNSUM=MNSUM+(M(K)-1)*(N(K)-1)		C 10
		(V=MAXO(IV,M(K)+(TR(K))		C 11
		JV=MAXO(JV,M(K))		C 12
		KV=MAXO(KV,N(K))		C 13
10		CONTINUE		C 14
		DO 20 K=1,6		C 15
20		L(K)=L(K)+1		C 16
		LA=(V*KV*NWCODE		C 17
		DO 30 K=7,9		C 18
30		L(K)=L(K-1)+LA		C 19
		LA=JV*KV*NWCODE		C 20
		DO 40 K=10,19		C 21
40		L(K)=L(K-1)+LA		C 22
		LTOT=L(19)		C 23
		IF (LTOT.GT.ND(M) GO TO 50		C 24
		RETURN		C 25
50		WRITE (6,60) ND(M,LTOT		C 26
		STOP		C 27
60		FORMAT (15HODIMENSIONED BY,(6,10H, REQU(RES,(6,1H.)		C 29
		END		C 30-

G LEVEL	20	CHAIN	DATE = 73018	12/02/34
		SUBROUTINE CHAIN (M,N,(TR,AX,AY,AZ,X,Y,Z,XI,ETA,ZETA,BX,BY,BZ,G,H,	D	1
		IXB,ZB)	D	2
		DIMENSION M(1), N(1), ITR(1), AX(1), AY(1), AZ(1), XB(1), ZB(1), X	D	3
		1(1), Y(1), Z(1), X(1), ETA(1), ZETA(1), BX(1), BY(1), BZ(1), G(1)	D	4
		2, H(1))	D	5
		CALL BODY1 (M,N,(TR,AX,AY,AZ,X,Y,Z,H)	D	6
		CALL AIRFL1 (M,N,(TR,AX,AY,AZ,X,Y,Z,H)	D	7
		CALL STRECH (M,N,ITR,AX,AY,AZ,X,Y,Z)	O	8
		CALL BODY2 (M,N,X,Y,Z,XI,ETA,ZETA,BX,BY,BZ,H)	D	9
		CALL SETM (M,N,(TR,AX,AY,AZ,X,Y,Z,XI,ETA,ZETA,BX,BY,BZ,G,H)	D	10
		CALL AIRFL2 (M,N,G,H,XB,ZB)	D	11
		CALL USERV (M,N,ITR,AX,AY,AZ,X,Y,Z,G,H)	D	12
		CALL USERS (M,N,ITR,AX,AY,AZ,X,Y,Z,G,H)	D	13
		RETURN	D	14
		END	D	15-

G LEVEL	20	BODY1	DATE = 73018	12/02/34
		SUBROUTINE BODY1 (M,N,ITR,AX,AY,AZ,X,Y,Z,G)	E	1
		DIMENSION M(1), N(1), ITR(1), AX(1), AY(1), AZ(1), G(1)	E	2
		DIMENSION X((V,KV,1), Y((V,KV,1), Z((V,KV,1)	E	3
		COMMON /CMMNA/ KL,JRUB,[REST,MNSUM,NWCODE,LXY,LXZ,L900	E	4
		COMMON /CMMNB/ RER,TITLE(20),FS		
		COMMON /CMMNC/ (V,JV,KV	E	5
		DO 10 K=1,NWCODE	E	6
		M1=M(K)+ITR(K)	E	7
		N1=N(K)	E	8
		DO 10 J=1,N1	E	9
		DO 10 I=1,M1	E	10
10		READ (5,50) X((I,J,K),Y((I,J,K),Z((I,J,K)	E	11
		IF(L900.EQ.0)FS=1.		
		IF(L900.EQ.1)FS=1.		
		IF(L900.EQ.2)FS=0.		
		IF (L900.EQ.0) GO TO 20	E	12
		IF(L900.EQ.3)GO TO 20		
		READ (5,50) (G(J),J=1,MNSUM)	E	13
		GO TO 40	E	14
20		DO 30 J=1,MNSUM	E	15
30		G(J)=0.	E	16
40		RETURN	E	17
50		FORMAT (6E12.0)	E	19
		END	E	20-

G LEVEL	20	AIRFL1	DATE = 73018	12/02/34	
---------	----	--------	--------------	----------	--

	SUBROUTINE AIRFL1 (M,N,ITR,AX,AY,AZ,X,Y,Z,G)	F	1
	DIMENSION M(1),N(1), ITR(1), AX(1), AY(1), AZ(1), G(1)	F	2
	DIMENSION X(1V,KV,1), Y(1V,KV,1), Z(1V,KV,1)	F	3
	COMMON /CMMNA/ MINGO,JRUB,IREST,MNSUM,NWCODE,LXY,LXZ,L900		
	COMMON /CMMNB/ RER,TITLE(20),FS,AM,AGAM,AMS,F1,F2	F	5
	COMMON /CMMNC/ IV,JV,KV,LTOT,MTOT	F	6
	REAL RPD/.01745329/		
	WRITE (6,30) TITLE	F	7
	WRITE (6,60)	F	8
	WRITE (6,40) NWCODE,LXY,LXZ,L900,MINGO,IREST,MNSUM,LTOT	F	9
	WRITE (6,70)	F	10
	WRITE (6,50) FS,RER,AM,AGAM	F	11
	DO 10 K=1,NWCODE	F	12
	WRITE (6,80)	F	13
	WRITE (6,90) K,M(K),N(K),ITR(K),AX(K),AY(K),AZ(K)	F	14
	WRITE (6,100)	F	15
	M1=M(K)+ITR(K)	F	16
	N1=N(K)	F	17
	DO 10 I=1,M1	F	18
10	WRITE (6,110) I,(X(I,J,K),Y(I,J,K),Z(I,J,K),J=1,N1)	F	19
	WRITE (6,120)	F	20
	LTOT=1	F	21
	MTOT=1	F	22
	RER=RER*RER	F	23
	AGAM=.5*(AGAM-1.)	F	24
	AMS=AM*AM	F	25
	F2=1./(1.-AMS)	F	26
	F1=SQRT(F2)	F	27
	DO 20 K=1,NWCODE	F	28
	AX(K)=COS(RPD*AX(K))	F	29
	AY(K)=COS(RPD*AY(K))	F	30
20	AZ(K)=COS(RPD*AZ(K))	F	31
	RETURN	F	32
30	FORMAT (1H1,20A4)	F	34
40	FORMAT (10I12)	F	35
50	FORMAT (1P10E12.4)	F	36
60	FORMAT (1H0,7X,6HNWCODE,8X,3HLXY,9X,3HLXZ,8X,4HL900,7X,5HMINGO,8X, 15HIREST,5X,5HMNSUM,8X,4HLTOT)	F	37 38
70	FORMAT (1H0,T3,9HFREE STRM,T15,3HRER,T27,2HMI,T39,1HK)		
80	FORMAT (1H0,T4,4HPART,T12,1HM,T18,1HN,T23,3HITR,T39,2HAX,T51,2HAY, 1T63,2HAZ)	F	40
90	FORMAT (4I6,6X,3F12.2)	F	41
100	FORMAT (1H0,T6,'I',T15,'X',T27,'Y',T39,'Z',T57,'X',T69,'Y',T81,'Z', 1,T99,'X',T111,'Y',T123,'Z')	F	42 43
110	FORMAT (16,6X,1P3E12.4,6X,3E12.4,6X,3E12.4/(12X,3E12.4,6X,3E12.4,6 1X,3E12.4))	F	44 45 46
120	FORMAT (1HA)	F	47
	END	F	48-

G	LEVEL	20	STRECH	DATE = 73018	12/02/34
			SUBROUTINE STRECH (M,N,(TR,AX,AY,AZ,X,Y,Z)		G 1
			DIMENSION M(1), N(1), (TR(1), AX(1), AY(1), AZ(1)		G 2
			DIMENSION X(IV,KV,1), Y(IV,KV,1), Z(IV,KV,1)		G 3
			COMMON /CMMNA/ KL,JRUB,IREST,MNSUM,NWCODE		G 4
			COMMON /CMMNB/ RER,TITLE(20),FS,AM,AGAM,AMS,F1,F2		G 5
			COMMON /CMMNC/ IV,JV,KV		G 6
			IF (AM.LE.0.) RETURN		G 7
			IF (AM.GT..9999) GO TO 30		G 8
			DO 20 K=1,NWCODE		G 9
			M1=M(K)+ITR(K)		G 10
			N1=N(K)		G 11
			DO 10 I=1,M1		G 12
			DO 10 J=1,N1		G 13
10			X(I,J,K)=F1*X(I,J,K)		G 14
			X1=F1*AX(K)		G 15
			F=1./SQRT(X1*X1+AY(K)**2+AZ(K)**2)		G 16
			AX(K)=F*X1		G 17
			AY(K)=F*AY(K)		G 18
20			AZ(K)=F*AZ(K)		G 19
			RETURN		G 20
30			WRITE (6,40) AM		G 21
			STOP		G 22
40			FORMAT (5HOMI =,1PE12.4,18H GREATER THAN ONE)		
			END		G 25-

G LEVEL 20

BODY2

DATE = 73018

12/02/34

```

SUBROUTINE BODY2 (M,N,X,Y,Z,X1,ETA,ZETA,BX,BY,BZ,G)      H  1
DIMENSION M(1), N(1), X1(1), ETA(1), ZETA(1), BX(1), BY(1), BZ(1),
IG(1)                                                    H  3
DIMENSION X(IV,KV,1), Y(IV,KV,1), Z(IV,KV,1)          H  4
DIMENSION XX(2), YY(2), ZZ(2)                          H  5
COMMON /CMMNA/ KL,JRUB,IREST,MNSUM,NWCODE              H  6
COMMON /CMMNB/ RER,TITLE(20)                           H  7
COMMON /CMMNC/ IV,JV,KV                                H  8
LAG=0                                                    H  9
L=0                                                       H 10
DO 60 K=1,NWCODE                                         H 11
M1=M(K)-1                                                H 12
N1=N(K)-1                                                H 13
DO 60 J=1,N1                                             H 14
J1=J+1                                                    H 15
DO 60 I=1,M1                                             H 16
I1=I+1                                                    H 17
L=L+1                                                     H 18
X1(L)=.25*(X(I1,J,K)+X(I1,J1,K)+X(I1,J1,K)+X(I1,J,K)) H 19
ETA(L)=.25*(Y(I1,J,K)+Y(I1,J1,K)+Y(I1,J1,K)+Y(I1,J,K)) H 20
ZETA(L)=.25*(Z(I1,J,K)+Z(I1,J1,K)+Z(I1,J1,K)+Z(I1,J,K)) H 21
XX(1)=X(I1,J1,K)-X(I1,J,K)                             H 22
YY(1)=Y(I1,J1,K)-Y(I1,J,K)                             H 23
ZZ(1)=Z(I1,J1,K)-Z(I1,J,K)                             H 24
XX(2)=X(I1,J,K)-X(I1,J,K)                             H 25
YY(2)=Y(I1,J,K)-Y(I1,J,K)                             H 26
ZZ(2)=Z(I1,J,K)-Z(I1,J,K)                             H 27
R1=XX(1)**2+YY(1)**2+ZZ(1)**2                          H 28
R2=XX(2)**2+YY(2)**2+ZZ(2)**2                          H 29
IF (R1.GT.0.) GO TO 10                                  H 30
IF (R2.EQ.0.) GO TO 40                                  H 31
KK=1                                                       H 32
GO TO 20                                                  H 33
10 IF (R2.GT.0.) GO TO 30                                H 34
KK=2                                                       H 35
20 XX(KK)=X(I1,J1,K)-X(I1,J,K)                          H 36
YY(KK)=Y(I1,J1,K)-Y(I1,J,K)                          H 37
ZZ(KK)=Z(I1,J1,K)-Z(I1,J,K)                          H 38
F=XX(KK)**2+YY(KK)**2+ZZ(KK)**2                        H 39
IF (F.EQ.0.) GO TO 40                                    H 40
X3=YY(1)*ZZ(2)-ZZ(1)*YY(2)                             H 41
Y3=ZZ(1)*XX(2)-XX(1)*ZZ(2)                             H 42
Z3=XX(1)*YY(2)-YY(1)*XX(2)                             H 43
F=X3*X3+Y3*Y3+Z3*Z3                                     H 44
IF (F.GT.0.) GO TO 50                                    H 45
40 LAG=1                                                  H 46
WRITE (6,80) I,J,K                                       H 47
GO TO 60                                                  H 48
50 F=1./SQRT(F)                                           H 49
BX(L)=F*X3                                               H 50
BY(L)=F*Y3                                               H 51
BZ(L)=F*Z3                                               H 52
60 CONTINUE                                              H 53
IF (LAG.EQ.1) STOP                                       H 54
WRITE (6,90) TITLE                                       H 55
WRITE (6,100)                                            H 56

```

G LEVEL	20	BODY2	DATE = 73018	12/02/34
	L=0			H 57
	DO 70 K=1,NWCODE			H 58
	M1=M(K)-1			H 59
	N1=N(K)-1			H 60
	DO 70 J=1,N1			H 61
	DO 70 I=1,M1			H 62
	L=L+1			H 63
70	WRITE (6,110) I,J,K,L,XI(L),ETA(L),ZETA(L),BX(L),BY(L),BZ(L),G(L)			H 64
	WRITE (6,120)			H 65
	RETURN			H 66
80	FORMAT (12H0ZERO NORMAL,315)			H 68
90	FORMAT (1H1,20A4)			H 69
100	FORMAT (1H0,T6,1HI,T12,1HJ,T18,1HK,T24,1HL,T33,2HX1,T45,3HETA,T57,			
	14HZETA,T75,2HBX,T87,2HBY,T99,2HBZ,T117,7HV DOT N)			
110	FORMAT (4I6,6X,1P3E12.4,6X,3E12.4,6X,E12.4)			H 72
120	FORMAT (1HA)			H 73
	END			H 74-

G LEVEL 20

SETM

OATE = 73018

12/02/34

```

SUBROUTINE SETM (M,N,ITR,AX,AY,AZ,X,Y,Z,XI,ETA,ZETA,BX,BY,BZ,AI,M) I 1
DIMENSION M(1), N(1), ITR(1), AX(1), AY(1), AZ(1), XI(1), ETA(1), I 2
IZETA(1), BX(1), BY(1), BZ(1), AI(1) I 3
DIMENSION H(MNSUM), X(IV,KV,1), Y(IV,KV,1), Z(IV,KV,1) I 4
COMMON /CMMNA/ KL,JRUB,IREST,MNSUM,NWCODE,LXY,LXZ I 5
COMMON /CMMNB/ REK,TITLE(20),FS I 6
COMMON /CMMNC/ IV,JV,KV,KXY,KXZ I 7
IF (IREST.GT.2) GO TO 170 I 8
IF (IREST.EQ.0) GO TO 20 I 9
DO 10 ISTART=1,MNSUM I 10
READ (21,END=2) H,DX I 11
10 WRITE (11) H,OX I 12
REWIND 21 I 13
GO TO 150 I 14
2 REWIND 21
WRITE (6,200) ISTART I 16
GO TO 30 I 17
20 ISTART=1 I 18
30 DO 40 I=1,MNSUM I 19
40 AI(I)=H(I)-FS*BX(I) I 20
DO 140 I=ISTART,MNSUM I 21
DO 50 J=1,MNSUM I 22
50 H(J)=0. I 23
JXY=1 I 24
JXZ=1 I 25
GO TO 80 I 26
60 CALL YEMY (JXZ,M,N,ITR,AX,AY,AZ,X,Y,Z) I 27
GO TO 80 I 28
70 CALL ZEMZ (JXY,M,N,ITR,AX,AY,AZ,X,Y,Z) I 29
80 PM=KXY*KXZ I 30
IT=0 I 31
DO 100 J=1,NWCODE I 32
M1=M(J)-1 I 33
M2=M(J)+ITR(J)-1 I 34
N1=N(J)-1 I 35
DO 100 K1=1,N1 I 36
K2=K1+1 I 37
DO 100 L1=1,M1 I 38
IT=IT+1 I 39
CALL SEGM (PM,X(L1,K1,J),Y(L1,K1,J),Z(L1,K1,J),X(L1,K2,J),Y(L1,K2, I 40
1J),Z(L1,K2,J),XI(I),ETA(I),ZETA(I),OX,OY,DZ) I 41
DO 90 L2=L1,M2 I 42
L3=L2+1 I 43
CALL SEGM (PM,X(L2,K1,J),Y(L2,K1,J),Z(L2,K1,J),X(L3,K1,J),Y(L3,K1, I 44
1J),Z(L3,K1,J),XI(I),ETA(I),ZETA(I),XL,YL,ZL) I 45
CALL SEGM (PM,X(L2,K2,J),Y(L2,K2,J),Z(L2,K2,J),X(L3,K2,J),Y(L3,K2, I 46
1J),Z(L3,K2,J),XI(I),ETA(I),ZETA(I),XR,YR,ZR) I 47
DX=DX-XL+XK I 48
DY=DY-YL+YR I 49
90 OZ=DZ-ZL+ZR I 50
CALL RAY (PM,X(L3,K1,J),Y(L3,K1,J),Z(L3,K1,J),AX(J),AY(J),AZ(J),XI I 51
1(I),ETA(I),ZETA(I),XL,YL,ZL) I 52
CALL RAY (PM,X(L3,K2,J),Y(L3,K2,J),Z(L3,K2,J),AX(J),AY(J),AZ(J),XI I 53
1(I),ETA(I),ZETA(I),XR,YR,ZR) I 54
DX=OX-XL+XR I 55
DY=OY-YL+YR I 56

```

G LEVEL	20	SETM	DATE = 73018	12/02/34
	0Z=0Z-ZL+ZR			I 57
100	H(I1)=H(I1)+DX*8X(I1)+DY*8Y(I1)+DZ*8Z(I1)			I 58
	IF (JXY.LT.0) GO TO 120			I 59
	IF (JXZ.LT.0) GO TO 110			I 60
	IF (LXZ.GT.0) GO TO 60			I 61
	IF (LXY.GT.0) GO TO 70			I 62
	GO TO 130			I 63
110	IF (LXY.GT.0) GO TO 70			I 64
	GO TO 130			I 65
120	IF (JXZ.LT.0) GO TO 60			I 66
130	CONTINUE			I 67
	WRITE (11) H,A1(I)			I 68
	IF (JRUB.EQ.1) GO TO 160			I 69
140	CONTINUE			I 70
150	I=MNSUM			I 71
160	END FILE 11			I 72
	REWIND 11			I 73
	IF (I.LT.MNSUM) GO TO 180			I 74
170	RETURN			I 75
180	WRITE (6,190) I,MNSUM			I 76
	STOP			I 77
190	FORMAT (1H0,15,3H OF,15,8H IN SETM)			I 79
200	FORMAT (24H0STARTING IN SETM ON ROW,15)			I 80
	END			I 81-

G LEVEL	20	SEGM	DATE = 73018	12/02/34
		SUBROUTINE SEGM (G,AX,AY,AZ,BX,BY,BZ,CX,CY,CZ,DX,DY,DZ)	J	1
		COMMON /CMMNB/ PS	J	2
		EX=BX-AX	J	3
		FY=BY-AY	J	4
		FZ=BZ-AZ	J	5
		ES=EX*EX+EY*EY+EZ*EZ	J	6
		IF (ES.EQ.0.) GO TO 10	J	7
		FX=CX-AX	J	8
		FY=CY-AY	J	9
		FZ=CZ-AZ	J	10
		FS=FX*FX+FY*FY+FZ*FZ	J	11
		IF (FS.EQ.0.) GO TO 10	J	12
		DX=EY*FZ-EZ*FY	J	13
		DY=EZ*FX-EX*FZ	J	14
		DZ=EX*FY-EY*FX	J	15
		DS=DX*DX+DY*DY+DZ*DZ	J	16
		IF (DS.LE.ES*PS) GO TO 10	J	17
		HS=(CX-BX)**2+(CY-BY)**2+(CZ-BZ)**2	J	18
		F=SQRT(FS)	J	19
		H=SQRT(HS)	J	20
		CT1=(FS-HS+ES)/F	J	21
		CT2=(FS-HS-ES)/H	J	22
		C=G*(CT1-CT2)/(25.13274*DS)	J	23
		DX=C*DX	J	24
		DY=C*DY	J	25
		DZ=C*DZ	J	26
		RETURN	J	27
10		DX=D.	J	28
		DY=D.	J	29
		DZ=D.	J	30
		RETURN	J	31
		END	J	32-

G LEVEL	20	RAY	DATE = 73018	12/02/34
		SUBROUTINE RAY (G,AX,AY,AZ,EX,EY,EZ,CX,CY,CZ,DX,DY,DZ)	K	1
		COMMON /CMMNB/ PS	K	2
		FX=CX-AX	K	3
		FY=CY-AY	K	4
		FZ=CZ-AZ	K	5
		FS=FX*FX+FY*FY+FZ*FZ	K	6
		IF (FS.EQ.0.) GO TO 10	K	7
		DX=EY*FZ-EZ*FY	K	8
		DY=EZ*FX-EX*FZ	K	9
		DZ=EX*FY-EY*FX	K	10
		DS=DX*DX+DY*DY+DZ*DZ	K	11
		IF (DS.LE.PS) GO TO 10	K	12
		CT1=(EX*FX+EY*FY+EZ*FZ)/SQRT(FS)	K	13
		C=G*(CT1+1.)/(12.56637*DS)	K	14
		DX=C*DX	K	15
		DY=C*DY	K	16
		DZ=C*DZ	K	17
		RETURN	K	18
10		DX=D.	K	19
		DY=D.	K	20
		DZ=D.	K	21
		RETURN	K	22
		END	K	23-

G LEVEL 20

YEMY

DATE = 73018

12/02/34

```

SUBROUTINE YEMY (L,M,N,ITR,AX,AY,AZ,X,Y,Z)
DIMENSION M(1), N(1), ITR(1), AX(1), AY(1), AZ(1)
DIMENSION X((V,KV,1), Y((V,KV,1), Z((V,KV,1)
COMMON /CMMNA/ (DUM(4),NWCODE
COMMON /CMMNC/ IV,JV,KV,KXY,KXZ
DO 10 K=1,NWCODE
AY(K)=-AY(K)
M1=M(K)+(TR(K)
N1=N(K)
DO 10 J=1,N1
DO 10 I=1,M1
10 Y(I,J,K)=-Y(I,J,K)
L=-L
KXZ=-KXZ
RETURN
END

```

L 1
L 2
L 3
L 4
L 5
L 6
L 7
L 8
L 9
L 10
L 11
L 12
L 13
L 14
L 15
L 16-

G LEVEL 20

ZEMZ

DATE = 73018

12/02/34

```

SUBROUTINE ZEMZ (L,M,N,ITR,AX,AY,AZ,X,Y,Z)
DIMENSION M(1), N(1), ITR(1), AX(1), AY(1), AZ(1)
DIMENSION X((V,KV,1), Y((V,KV,1), Z((V,KV,1)
COMMON /CMMNA/ (DUM(4),NWCODE
COMMON /CMMNC/ IV,JV,KV,KXY,KXZ
DO 10 K=1,NWCODE
AZ(K)=-AZ(K)
M1=M(K)+(TR(K)
N1=N(K)
DO 10 J=1,N1
DO 10 I=1,M1
10 Z(I,J,K)=-Z(I,J,K)
L=-L
KXY=-KXY
RETURN
END

```

M 1
M 2
M 3
M 4
M 5
M 6
M 7
M 8
M 9
M 10
M 11
M 12
M 13
M 14
M 15
M 16-

G LEVEL	20	AIRFL2	DATE = 73018	12/02/34
		SUBROUTINE AIRFL2 (M,N,G,H,A,B)		N 1
		DIMENSION M(1), N(1), B(1)		N 2
		DIMENSION A(MNSUM), G(JV,KV,1), H(JV,KV,1)		N 3
		COMMON /CMMNA/ (DET,JRUB,IRES,MNSUM,NWCODE		N 4
		COMMON /CMMNB/ RER,TITLE(20)		N 5
		COMMON /CMMNC/ IV,JV,KV		N 6
		IF (IRES.GT.2) GO TO 10		N 7
		CALL LSYSEQ (G,H,A,B)		N 8
		IF (IDET.EQ.0) GO TO 110		N 9
10		READ (12) A		N 10
		REWIND 12		N 11
		L=0		N 12
		DO 20 K=1,NWCODE		N 13
		M1=M(K)-1		N 14
		N1=N(K)-1		N 15
		DO 20 J=1,N1		N 16
		DO 20 I=1,M1		N 17
		L=L+1		N 18
20		G(I,J,K)=A(L)		N 19
		WRITE (6,120) TITLE		N 20
		WRITE (6,130)		N 21
		DO 30 K=1,NWCODE		N 22
		WRITE (6,140) K		N 23
		M1=M(K)-1		N 24
		N1=N(K)-1		N 25
		DO 30 I=1,M1		N 26
30		WRITE (6,150) I,(G(I,J,K),J=1,N1)		N 27
		DO 90 K=1,NWCODE		N 28
		M1=M(K)-1		N 29
		N1=N(K)		N 30
		DO 90 J=1,N1		N 31
		DO 90 I=1,M1		N 32
		IF (I.GT.1) GO TO 40		N 33
		G1=0.		N 34
		GO TO 50		N 35
40		G1=H(I-1,J,K)		N 36
50		IF (J.GT.1) GO TO 60		N 37
		G2=0.		N 38
		GO TO 70		N 39
60		G2=G(I,J-1,K)		N 40
70		IF (J.LT.N1) GO TO 80		N 41
		G3=0.		N 42
		GO TO 90		N 43
80		G3=-G(I,J,K)		N 44
90		H(I,J,K)=G1+G2+G3		N 45
		WRITE (6,170)		N 46
		DO 100 K=1,NWCODE		N 47
		WRITE (6,140) K		N 48
		M1=M(K)-1		N 49
		N1=N(K)		N 50
		DO 100 I=1,M1		N 51
100		WRITE (6,150) (,IH(I,J,K),J=1,N1)		N 52
		WRITE (6,180)		N 53
		RETURN		N 54
110		WRITE (6,160)		N 55
		STOP		N 56
120		FORMAT (1H1,20A4)		N 58
130		FORMAT (1H0,T6,'I',T15,'GAMMAS')		N 59
140		FORMAT (1H0,T15,4HPART,I3)		N 60
150		FORMAT (16,6X,1P10E12.4/(12X10E12.4))		N 61
160		FORMAT (16H0SINGULAR MATRIX)		N 62
170		FORMAT (1H0,T6,'I',T15,'ETAS')		N 63
180		FORMAT (1HA)		N 64
		END		N 65-

G LEVEL	20	LSYSEQ	DATE = 73018	12/02/34
		SUBROUTINE LSYSEQ (T,A,B,L)		0 1
		DIMENSION T(1), A(1), B(1,1), L(1), S(1)		0 2
		COMMON /CMNA/ IOET,JRUB,IRES,NR		0 3
		INTEGER NS/1/,NO/10/		
		NC=NR+NS		0 4
		CALL DAFIL (10,NR,NC,'U',KL)		0 5
		IF (IRES.LT.2) GO TO 10		0 6
		READ (22) JLOW,(L(K),K=1,JLOW)		0 7
		WRITE (6,170) JLOW		0 8
		KK=22		0 9
		GO TO 20		0 10
10		JLOW=1		0 11
		KK=11		0 12
20		DO 30 J=1,NR		0 13
		READ (KK) (T(K),K=1,NC)		0 14
30		WRITE (NO'J) (T(K),K=1,NC)		0 15
		REWIND KK		0 16
		NST=NR+1-JLOW		0 17
		READ (NO'NST) (T(K),K=1,NC)		0 18
		DO 90 J=JLOW,NR		0 19
		IF (JRUB.NE.1) GO TO 50		0 20
		WRITE (12) J,(L(K),K=1,J)		0 21
		DO 40 KK=1,NR		0 22
		READ (NO'KK) (T(K),K=1,NC)		0 23
40		WRITE (12) (T(K),K=1,NC)		0 24
		END FILE 12		0 25
		REWIND 12		0 26
		WRITE (6,160) J,NR		0 27
		STOP		0 28
50		CONTINUE		0 29
		F(NO (NO'KL-1)		
		SUP=0.0		0 30
		L(J)=0		0 31
		DO 60 K=1,NR		0 32
		TLT=ABS(T(K))		0 33
		IF (SUP.GE.TLT) GO TO 60		0 34
		SUP=TLT		0 35
		L(J)=K		0 36
60		CONTINUE		0 37
		IF (L(J).EQ.0) GO TO 150		0 38
		LT=L(J)		0 39
		DO 70 K=1,NC		0 40
70		A(K)=T(K)/T(LT)		0 41
		A(LT)=1.0		0 42
		WRITE (NO'KL) (A(K),K=1,NC)		0 43
		IF (J.EQ.NR) GO TO 100		0 44
		FINO (NO'1)		
		JT=NR-J		0 45
		DO 90 JR=1,JT		0 46
		READ (NO'KL) (T(K),K=1,NC)		0 47
		FINO (NO'KL-1)		
		TLT=T(LT)		0 48
		DO 80 K=1,NC		0 49
80		T(K)=T(K)-TLT*A(K)		0 50
		T(LT)=0.0		0 51
90		WRITE (NO'KL) (T(K),K=1,NC)		0 52

G LEVEL	20	LSYSEQ	DATE = 73018	12/02/34
100	DO 110 K=1,NS			0 53
	KS=NR+K			0 54
	LS=L(NR)			0 55
110	B(K,LS)=A(KS)			0 56
	DO 130 J=2,NR			0 57
	J1=J-1			0 58
	JJ=NR-J+1			0 59
	LS=LIJJ			0 60
	READ (ND,KL) (A(K),K=1,NC)			0 61
	DO 130 K=1,NS			0 62
	KS=NR+K			0 63
	S(K)=A(KS)			0 64
	DO 120 KK=1,J1			0 65
	KKK=NR-KK+1			0 66
	LT=L(KKK)			0 67
120	S(K)=S(K)-A(LT)*B(K,LT)			0 68
130	B(K,LS)=S(K)			0 69
	FIND (ND,1)			
	DO 140 K=1,NS			0 70
140	WRITE (12) (B(K,KK),KK=1,NR)			0 71
	END FILE 12			0 72
	REWIND 12			0 73
	IDET=1			0 74
	RETURN			0 75
150	IDET=0			0 76
	RETURN			0 77
160	FORMAT (1H0,I5,3H OF,I5,10H IN LSYSEQ)			0 79
170	FORMAT (26H0STARTING IN LSYSEQ ON ROW,I5)			0 80
	END			0 81-

G LEVEL	20	USERV	DATE = 73018	12/02/34	
		SUBROUTINE USERV (M,N,ITR,AX,AY,AZ,X,Y,Z,G,H)			P 1
		DIMENSION M(1), N(1), ITR(1), AX(1), AY(1), AZ(1), XI(1), Y(1), Z(1), G(1), H(1)			P 2
		COMMON /CMMN8/ RER,TITLE(20)			P 3
		REAL SGN /-1./			P 4
		IU=13			P 5
		READ (5,50) NV			P 6
		IF (NV.EQ.0) GO TO 30			P 7
		IPAGE=0			P 8
		ILINE=62			P 9
		DO 20 J=1,NV			P 10
		READ (5,60) XV,YV,ZV			P 11
		CALL VELOCITY (M,N,ITR,AX,AY,AZ,X,Y,Z,G,H,XV,YV,ZV,U,V,W)			P 12
		IF (ILINE.LT.62) GO TO 10			P 13
		IPAGE=IPAGE+1			P 14
		ILINE=9			P 15
		WRITE (6,70) TITLE,IPAGE			P 16
		CALL VELLAB			P 17
10		ILINE=ILINE+1			P 18
20		CALL VELOUT (XV,YV,ZV,U,V,W,IU)			P 19
		WRITE (6,80)			P 20
30		IF (IU.EQ.0) GO TO 40			P 21
		WRITE (IU) (SGN,J=1,12)			P 22
		END FILE IU			P 23
		REWIND IU			P 24
40		RETURN			P 25
50		FORMAT (24I3)			P 27
60		FORMAT (6E12.0)			P 28
70		FORMAT (1H1,20A4,5X,'VELOCITIES',5X,'PAGE',I3)			P 29
80		FORMAT (1HA)			P 30
		END			P 31-

G LEVEL	20	USERS	DATE = 73018	12/02/34	
		SUBROUTINE USERS (M,N,ITR,AX,AY,AZ,X,Y,Z,G,H)			Q 1
		DIMENSION M(1), N(1), ITR(1), AX(1), AY(1), AZ(1), X(1), Y(1), Z(1), G(1), H(1)			Q 2
		REAL SGN /-1./			Q 3
		IU=14			Q 4
		READ (5,40) NS			Q 5
		IF (NS.EQ.0) GO TO 20			Q 6
		DO 10 J=1,NS			Q 7
		READ (5,50) XO,YO,ZO,DSO,AN,AM,NX,XN,XX,YN,YX,ZN,ZX			Q 8
		CALL STREAM (M,N,ITR,AX,AY,AZ,X,Y,Z,G,H,XO,YO,ZO,DSO,AN,AM,NX,XN,XX,YN,YX,ZN,ZX,IU)			Q 9
		IF (IU.EQ.0) GO TO 10			Q 10
		WRITE (IU) (SGN,K=1,12)			Q 11
10		CONTINUE			Q 12
20		IF (IU.EQ.0) GO TO 30			Q 13
		END FILE IU			Q 14
		REWIND IU			Q 15
30		RETURN			Q 16
40		FORMAT (24I3)			Q 17
50		FORMAT (6E12.0,I8/6E12.0)			Q 19
		END			Q 20
					Q 21-

G LEVEL	20	VELOCITY	OATE = 73018	12/02/34		
		SUBROUTINE VELOCY (M,N,ITR,AX,AY,AZ,X,Y,Z,G,H,XB,YO,ZO,TU,TV,TW)			R	1
		DIMENSION M(1), N(1), ITR(1), AX(1), AY(1), AZ(1)			R	2
		DIMENSION X(IV,KV,1), Y(IV,KV,1), Z(IV,KV,1), G(JV,KV,1), H(JV,KV,			R	3
		11)			R	4
		COMMON /CMMNA/ KL,JRUB,IREST,MNSUM,NWCDOE,LXY,LXZ			R	5
		COMMON /CMMNB/ RER,TITLE(20),FS,AM,AGAM,AMS,F1,F2			R	6
		COMMON /CMMNC/ IV,JV,KV,KXY,KXZ			R	7
		XO=F1*XB			R	8
		TU=FS			R	9
		TV=0.			R	10
		TW=0.			R	11
		JXY=1			R	12
		JXZ=1			R	13
		GO TO 30			R	14
10		CALL YEMY (JXZ,M,N,ITR,AX,AY,AZ,X,Y,Z)			R	15
		GO TO 30			R	16
20		CALL ZEMZ (JXY,M,N,ITR,AX,AY,AZ,X,Y,Z)			R	17
30		JPM=KXY*KXZ			R	18
		DO 80 L=1,NWCDOE			R	19
		N1=N(L)-1			R	20
		N2=N(L)			R	21
		M1=M(L)-1			R	22
		M2=M(L)+ITR(L)-1			R	23
		DO 40 K1=1,N1			R	24
		K2=K1+1			R	25
		DO 40 J1=1,M1			R	26
		GAM=JPM*G(J1,K1,L)			R	27
		CALL SEGM (GAM,X(J1,K1,L),Y(J1,K1,L),Z(J1,K1,L),X(J1,K2,L),Y(J1,K2			R	28
		1,L),Z(J1,K2,L),XO,YO,ZO,U,V,W)			R	29
		TU=TU+U			R	30
		TV=TV+V			R	31
40		TW=TW+W			R	32
		DO 70 K1=1,N2			R	33
		DO 60 J1=1,M2			R	34
		J2=J1+1			R	35
		IF (J1.GT.M1) GO TO 50			R	36
		GAM=JPM*H(J1,K1,L)			R	37
50		CALL SEGM (GAM,X(J1,K1,L),Y(J1,K1,L),Z(J1,K1,L),X(J2,K1,L),Y(J2,K1			R	38
		1,L),Z(J2,K1,L),XO,YO,ZO,U,V,W)			R	39
		TU=TU+U			R	40
		TV=TV+V			R	41
60		TW=TW+W			R	42
		CALL RAY (GAM,X(J2,K1,L),Y(J2,K1,L),Z(J2,K1,L),AX(L),AY(L),AZ(L),X			R	43
		10,YO,ZO,U,V,W)			R	44
		TU=TU+U			R	45
		TV=TV+V			R	46
70		TW=TW+W			R	47
80		CONTINUE			R	48
		IF (JXY.LT.0) GO TO 100			R	49
		IF (JXZ.LT.0) GO TO 90			R	50
		IF (LXZ.GT.0) GO TO 10			R	51
		IF (LXY.GT.0) GO TO 20			R	52
		GO TO 110			R	53
90		IF (LXY.GT.0) GO TO 20			R	54
		GO TO 110			R	55
100		IF (JXZ.LT.0) GO TO 10			R	56
110		TU=1.+F2*(TU-1.)			R	57
		TV=F1*TV			R	58
		TW=F1*TW			R	59
		RETURN			R	60
		END			R	61-

G LEVEL	20	VELOUT	DATE = 73018	12/02/34
		SUBROUTINE VELDUT (XD,YD,ZD,U,V,W,IU)		S 1
		COMMON /CMMN8/ RER,TITLE(20),FS,AM,AGIH,AMS		S 2
		REAL DPR/57.29578/		
		TUS=U*U+V*V+W*W		S 3
		TU=SQRT(TUS)		S 4
		ACH=1.+AGIH*AMS*(1.-TUS)		S 5
		IF (ACH.LE.0.) GO TO 10		S 6
		ACH=AM*TU/SQRT(ACH)		S 7
10		CONTINUE		S 8
		TV=DPR*ATAN2(V,U)		S 9
		TW=DPR*ATAN2(W,U)		S 10
		PC=1.-TUS		S 11
		D=ACH-AM		S 12
		IF (IU.EQ.0) GO TO 20		S 13
		WRITE (IU) XD,YD,ZD,U,V,W,TU,ACH,TV,TW,PC,D		S 14
20		WRITE (6,40) XD,YD,ZD,U,V,W,TU,ACH,TV,TW,PC,D		S 15
		RETURN		S 16
		ENTRY VELLAB		S 17
		WRITE (6,30)		S 18
		RETURN		S 19
30		FORMAT (1H0,T4,'X',T16,'Y',T28,'Z',T41,'U',T51,'V',T61,'W',T70,' V		S 21
		1 ',T81,'M',T88,'ATN(V/U)',T97,'ATN(W/U)',T108,'CP',T120,'M-MI')		S 22
40		FORMAT (1P3E12.4,0P5F10.5,F8.2,F9.2,1PE12.3,E11.3)		S 23
		END		S 24-

G	LEVFL	20	STREAM	DATE = 73018	12/02/34		
			SUBROUTINE STREAM (M1,M2,M3,A1,A2,A3,A4,A5,A6,A7,A8,X0,Y0,Z0,DS0,A			T	1
			IN,AX,NX,XN,XX,YN,YX,ZN,ZX,IU)			T	2
			DIMENSION M1(1), M2(1), M3(1), A1(1), A2(1), A3(1), A4(1), A5(1),			T	3
			A6(1), A7(1), A8(1)			T	4
			COMMON /CMMN8/ RER,TITLE(20)			T	5
			REAL RPD/.01745329/				
C			DC TODD 8/11/71			T	6
			REAL CODE(8)/'N>NX','X<XN','X>XX','Y<YN','Y>YX','Z<ZN','Z>ZX','D<D			T	7
			IN'/			T	8
			L=1			T	9
			IPAGE=0			T	10
			ILINE=62			T	11
			DSX=A8S(DS0)			T	12
			DSN=.001*OSX			T	13
			CX=COS(RPD*AN)			T	14
			CN=COS(RPD*AX)			T	15
			DS=DS0			T	16
			N=0			T	17
			X=X0			T	18
			Y=Y0			T	19
			Z=Z0			T	20
10			CALL VELOCITY (M1,M2,M3,A1,A2,A3,A4,A5,A6,A7,A8,X,Y,Z,U,V,W)			T	21
			IF (ILINE.LT.62) GO TO 30			T	22
			IPAGE=IPAGE+1			T	23
			ILINE=9			T	24
			WRITE (6,140) TITLE,IPAGE			T	25
			IF (IPAGE.GT.1) GO TO 20			T	26
			WRITE (6,150) DSX,AN,AX			T	27
			ILINE=ILINE+2			T	28
20			CALL VELLAB			T	29
30			CALL VELOUT (X,Y,Z,U,V,W,IU)			T	30
			ILINE=ILINE+1			T	31
			IF (N.GE.NX) GO TO 130			T	32
			IF (X.LE.XN) GO TO 120			T	33
			IF (X.GE.XX) GO TO 110			T	34
			IF (Y.LE.YN) GO TO 100			T	35
			IF (Y.GE.YX) GO TO 90			T	36
			IF (Z.LE.ZN) GO TO 80			T	37
			IF (Z.GE.ZX) GO TO 70			T	38
			T=SQRT(U*U+V*V+W*W)			T	39
40			F=DS/T			T	40
			X1=X+F*U			T	41
			Y1=Y+F*V			T	42
			Z1=Z+F*W			T	43
			CALL VELOCITY (M1,M2,M3,A1,A2,A3,A4,A5,A6,A7,A8,X1,Y1,Z1,U1,V1,W1)			T	44
			T1=SQRT(U1*U1+V1*V1+W1*W1)			T	45
			C=(U*U1+V*V1+W*W1)/(T*T1)			T	46
			IF (C.GE.CN) GO TO 50			T	47
			DS=.75*DS			T	48
			IF (A8S(DS).LE.DSN) GO TO 60			T	49
			GO TO 40			T	50
50			F=.5*DS			T	51
			X=X+F*(U/T+U1/T1)			T	52
			Y=Y+F*(V/T+V1/T1)			T	53
			Z=Z+F*(W/T+W1/T1)			T	54
			N=N+1			T	55

G LEVEL	20	STREAM	DATE = 73018	12/02/34
		IF (C.GT.CX) DS=SIGN(AMIN1(DSX,1.5*ABS(DS)),DS)		T 56
		GO TO 10		T 57
60		L=L+1		T 58
70		L=L+1		T 59
80		L=L+1		T 60
90		L=L+1		T 61
100		L=L+1		T 62
110		L=L+1		T 63
120		L=L+1		T 64
130		WRITE (6,160) CODE(L)		T 65
		RETURN		T 66
140		FORMAT (1H1,20A4,5X,'STREAMLINE',5X,'PAGE',I3)		T 68
150		FORMAT (1H0,1PE12.4,14H MAX STEP SIZE,OPF20.3,21H DEG MIN ANGLE CH		T 69
		ANGE,F20.3,21H DEG MAX ANGLE CHANGE)		T 70
160		FORMAT (8H0 ***** ,A4,6H *****)		T 71
		END		T 72-

SV1

NWCOOE 2		LXY 1		LXZ 0		L900 0		MINGU 8		IREST 0		MNSUM 72		LTOT 1365	
FREE STRM 1.0000E 00		RER 0.0		M1 9.0000E-01		K 1.4000E 00									
PART 1	M 13	N 4	ITR 0			AX 19.00	AY 109.00	AZ 90.00							
1	X	Y	Z			X	Y	Z			X	Y	Z		
1	1.3000E 01	2.0000E 00	-3.0000E 00			1.3000E 01	2.0000E 00	-2.0000E 00			1.3000E 01	2.0000E 00	-1.0000E 00		
	1.3000E 01	2.0000E 00	0.0												
2	1.3500E 01	2.0000E 00	-3.0000E 00			1.3500E 01	2.0000E 00	-2.0000E 00			1.3500E 01	2.0000E 00	-1.0000E 00		
	1.3500E 01	2.0000E 00	0.0												
3	1.4000E 01	1.9800E 00	-3.0000E 00			1.4000E 01	1.9800E 00	-2.0000E 00			1.4000E 01	1.9800E 00	-1.0000E 00		
	1.4000E 01	1.9800E 00	0.0												
4	1.4500E 01	1.9550E 00	-3.0000E 00			1.4500E 01	1.9550E 00	-2.0000E 00			1.4500E 01	1.9550E 00	-1.0000E 00		
	1.4500E 01	1.9550E 00	0.0												
5	1.5000E 01	1.9300E 00	-3.0000E 00			1.5000E 01	1.9300E 00	-2.0000E 00			1.5000E 01	1.9300E 00	-1.0000E 00		
	1.5000E 01	1.9300E 00	0.0												
6	1.5500E 01	1.8900E 00	-3.0000E 00			1.5500E 01	1.8900E 00	-2.0000E 00			1.5500E 01	1.8900E 00	-1.0000E 00		
	1.5500E 01	1.8900E 00	0.0												
7	1.6000E 01	1.8350E 00	-3.0000E 00			1.6000E 01	1.8350E 00	-2.0000E 00			1.6000E 01	1.8350E 00	-1.0000E 00		
	1.6000E 01	1.8350E 00	0.0												
8	1.6500E 01	1.7650E 00	-3.0000E 00			1.6500E 01	1.7650E 00	-2.0000E 00			1.6500E 01	1.7650E 00	-1.0000E 00		
	1.6500E 01	1.7650E 00	0.0												
9	1.7000E 01	1.6800E 00	-3.0000E 00			1.7000E 01	1.6800E 00	-2.0000E 00			1.7000E 01	1.6800E 00	-1.0000E 00		
	1.7000E 01	1.6800E 00	0.0												
10	1.7500E 01	1.5700E 00	-3.0000E 00			1.7500E 01	1.5700E 00	-2.0000E 00			1.7500E 01	1.5700E 00	-1.0000E 00		
	1.7500E 01	1.5700E 00	0.0												
11	1.8000E 01	1.4450E 00	-3.0000E 00			1.8000E 01	1.4450E 00	-2.0000E 00			1.8000E 01	1.4450E 00	-1.0000E 00		
	1.8000E 01	1.4450E 00	0.0												
12	1.8500E 01	1.2950E 00	-3.0000E 00			1.8500E 01	1.2950E 00	-2.0000E 00			1.8500E 01	1.2950E 00	-1.0000E 00		
	1.8500E 01	1.2950E 00	0.0												
13	1.9000E 01	1.1150E 00	-3.0000E 00			1.9000E 01	1.1150E 00	-2.0000E 00			1.9000E 01	1.1150E 00	-1.0000E 00		
	1.9000E 01	1.1150E 00	0.0												
PART 2	M 13	N 4	ITR 0			AX 19.00	AY 109.00	AZ 90.00							
1	X	Y	Z			X	Y	Z			X	Y	Z		
1	1.3000E 01	-2.0000E 00	-3.0000E 00			1.3000E 01	-2.0000E 00	-2.0000E 00			1.3000E 01	-2.0000E 00	-1.0000E 00		
	1.3000E 01	-2.0000E 00	0.0												
2	1.3500E 01	-2.0000E 00	-3.0000E 00			1.3500E 01	-2.0000E 00	-2.0000E 00			1.3500E 01	-2.0000E 00	-1.0000E 00		
	1.3500E 01	-2.0000E 00	0.0												
3	1.4000E 01	-2.0200E 00	-3.0000E 00			1.4000E 01	-2.0200E 00	-2.0000E 00			1.4000E 01	-2.0200E 00	-1.0000E 00		
	1.4000E 01	-2.0200E 00	0.0												
4	1.4500E 01	-2.0450E 00	-3.0000E 00			1.4500E 01	-2.0450E 00	-2.0000E 00			1.4500E 01	-2.0450E 00	-1.0000E 00		
	1.4500E 01	-2.0450E 00	0.0												
5	1.5000E 01	-2.0700E 00	-3.0000E 00			1.5000E 01	-2.0700E 00	-2.0000E 00			1.5000E 01	-2.0700E 00	-1.0000E 00		
	1.5000E 01	-2.0700E 00	0.0												
6	1.5500E 01	-2.1100E 00	-3.0000E 00			1.5500E 01	-2.1100E 00	-2.0000E 00			1.5500E 01	-2.1100E 00	-1.0000E 00		
	1.5500E 01	-2.1100E 00	0.0												
7	1.6000E 01	-2.1650E 00	-3.0000E 00			1.6000E 01	-2.1650E 00	-2.0000E 00			1.6000E 01	-2.1650E 00	-1.0000E 00		
	1.6000E 01	-2.1650E 00	0.0												
8	1.6500E 01	-2.2350E 00	-3.0000E 00			1.6500E 01	-2.2350E 00	-2.0000E 00			1.6500E 01	-2.2350E 00	-1.0000E 00		
	1.6500E 01	-2.2350E 00	0.0												
9	1.7000E 01	-2.3200E 00	-3.0000E 00			1.7000E 01	-2.3200E 00	-2.0000E 00			1.7000E 01	-2.3200E 00	-1.0000E 00		

10	1.7000E 01 -2.3200E 00 0.0	1.7500E 01 -2.4300E 00 -2.0000E 00	1.7500E 01 -2.4300E 00 -1.0000E 00
	1.7500E 01 -2.4300E 00 -3.0000E 00		
11	1.7500E 01 -2.4300E 00 0.0	1.8000E 01 -2.5550E 00 -2.0000E 00	1.8000E 01 -2.5550E 00 -1.0000E 00
	1.8000E 01 -2.5550E 00 -3.0000E 00		
	1.8000E 01 -2.5550E 00 0.0		
12	1.8500E 01 -2.7050E 00 -3.0000E 00	1.8500E 01 -2.7050E 00 -2.0000E 00	1.8500E 01 -2.7050E 00 -1.0000E 00
	1.8500E 01 -2.7050E 00 0.0		
13	1.9000E 01 -2.8850E 00 -3.0000E 00	1.9000E 01 -2.8850E 00 -2.0000E 00	1.9000E 01 -2.8850E 00 -1.0000E 00
	1.9000E 01 -2.8850E 00 0.0		

AEDC-TR-73-9

SV1

I	J	K	L	XI	ETA	ZETA	8X	8Y	8Z	V OUT N
1	1	1	1	3.0398E 01	2.0000E 00	-2.5000E 00	0.0	1.0000E 00	0.0	0.0
2	1	1	2	3.1545E 01	1.9900E 00	-2.5000E 00	1.7433E-02	9.9985E-01	0.0	0.0
3	1	1	3	3.2692E 01	1.9675E 00	-2.5000E 00	2.1789E-02	9.9976E-01	0.0	0.0
4	1	1	4	3.3839E 01	1.9425E 00	-2.5000E 00	2.1790E-02	9.9976E-01	0.0	0.0
5	1	1	5	3.4986E 01	1.9100E 00	-2.5000E 00	3.4850E-02	9.9939E-01	0.0	0.0
6	1	1	6	3.6133E 01	1.8625E 00	-2.5000E 00	4.7893E-02	9.9885E-01	0.0	0.0
7	1	1	7	3.7280E 01	1.8000E 00	-2.5000E 00	6.0912E-02	9.9814E-01	0.0	0.0
8	1	1	8	3.8427E 01	1.7225E 00	-2.5000E 00	7.3899E-02	9.9727E-01	0.0	0.0
9	1	1	9	3.9574E 01	1.6250E 00	-2.5000E 00	9.5458E-02	9.9543E-01	0.0	0.0
10	1	1	10	4.0721E 01	1.5075E 00	-2.5000E 00	1.0833E-01	9.9412E-01	0.0	0.0
11	1	1	11	4.1868E 01	1.3700E 00	-2.5000E 00	1.2966E-01	9.9156E-01	0.0	0.0
12	1	1	12	4.3015E 01	1.2050E 00	-2.5000E 00	1.5502E-01	9.8791E-01	0.0	0.0
1	2	1	13	3.0398E 01	2.0000E 00	-1.5000E 00	0.0	1.0000E 00	0.0	0.0
2	2	1	14	3.1545E 01	1.9900E 00	-1.5000E 00	1.7433E-02	9.9985E-01	0.0	0.0
3	2	1	15	3.2692E 01	1.9675E 00	-1.5000E 00	2.1789E-02	9.9976E-01	0.0	0.0
4	2	1	16	3.3839E 01	1.9425E 00	-1.5000E 00	2.1790E-02	9.9976E-01	0.0	0.0
5	2	1	17	3.4986E 01	1.9100E 00	-1.5000E 00	3.4850E-02	9.9939E-01	0.0	0.0
6	2	1	18	3.6133E 01	1.8625E 00	-1.5000E 00	4.7893E-02	9.9885E-01	0.0	0.0
7	2	1	19	3.7280E 01	1.8000E 00	-1.5000E 00	6.0912E-02	9.9814E-01	0.0	0.0
8	2	1	20	3.8427E 01	1.7225E 00	-1.5000E 00	7.3899E-02	9.9727E-01	0.0	0.0
9	2	1	21	3.9574E 01	1.6250E 00	-1.5000E 00	9.5458E-02	9.9543E-01	0.0	0.0
10	2	1	22	4.0721E 01	1.5075E 00	-1.5000E 00	1.0833E-01	9.9412E-01	0.0	0.0
11	2	1	23	4.1868E 01	1.3700E 00	-1.5000E 00	1.2966E-01	9.9156E-01	0.0	0.0
12	2	1	24	4.3015E 01	1.2050E 00	-1.5000E 00	1.5502E-01	9.8791E-01	0.0	0.0
1	3	1	25	3.0398E 01	2.0000E 00	-5.0000E-01	0.0	1.0000E 00	0.0	0.0
2	3	1	26	3.1545E 01	1.9900E 00	-5.0000E-01	1.7433E-02	9.9985E-01	0.0	0.0
3	3	1	27	3.2692E 01	1.9675E 00	-5.0000E-01	2.1789E-02	9.9976E-01	0.0	0.0
4	3	1	28	3.3839E 01	1.9425E 00	-5.0000E-01	2.1790E-02	9.9976E-01	0.0	0.0
5	3	1	29	3.4986E 01	1.9100E 00	-5.0000E-01	3.4850E-02	9.9939E-01	0.0	0.0
6	3	1	30	3.6133E 01	1.8625E 00	-5.0000E-01	4.7893E-02	9.9885E-01	0.0	0.0
7	3	1	31	3.7280E 01	1.8000E 00	-5.0000E-01	6.0912E-02	9.9814E-01	0.0	0.0
8	3	1	32	3.8427E 01	1.7225E 00	-5.0000E-01	7.3899E-02	9.9727E-01	0.0	0.0
9	3	1	33	3.9574E 01	1.6250E 00	-5.0000E-01	9.5458E-02	9.9543E-01	0.0	0.0
10	3	1	34	4.0721E 01	1.5075E 00	-5.0000E-01	1.0833E-01	9.9412E-01	0.0	0.0
11	3	1	35	4.1868E 01	1.3700E 00	-5.0000E-01	1.2966E-01	9.9156E-01	0.0	0.0
12	3	1	36	4.3015E 01	1.2050E 00	-5.0000E-01	1.5502E-01	9.8791E-01	0.0	0.0
1	1	2	37	3.0398E 01	-2.0000E 00	-2.5000E 00	0.0	1.0000E 00	0.0	0.0
2	1	2	38	3.1545E 01	-2.0100E 00	-2.5000E 00	1.7432E-02	9.9985E-01	0.0	0.0
3	1	2	39	3.2692E 01	-2.0325E 00	-2.5000E 00	2.1789E-02	9.9976E-01	0.0	0.0
4	1	2	40	3.3839E 01	-2.0575E 00	-2.5000E 00	2.1790E-02	9.9976E-01	0.0	0.0
5	1	2	41	3.4986E 01	-2.0900E 00	-2.5000E 00	3.4850E-02	9.9939E-01	0.0	0.0
6	1	2	42	3.6133E 01	-2.1375E 00	-2.5000E 00	4.7893E-02	9.9885E-01	0.0	0.0
7	1	2	43	3.7280E 01	-2.2000E 00	-2.5000E 00	6.0912E-02	9.9814E-01	0.0	0.0
8	1	2	44	3.8427E 01	-2.2775E 00	-2.5000E 00	7.3899E-02	9.9727E-01	0.0	0.0
9	1	2	45	3.9574E 01	-2.3750E 00	-2.5000E 00	9.5458E-02	9.9543E-01	0.0	0.0
10	1	2	46	4.0721E 01	-2.4925E 00	-2.5000E 00	1.0833E-01	9.9412E-01	0.0	0.0
11	1	2	47	4.1868E 01	-2.6300E 00	-2.5000E 00	1.2966E-01	9.9156E-01	0.0	0.0
12	1	2	48	4.3015E 01	-2.7950E 00	-2.5000E 00	1.5502E-01	9.8791E-01	0.0	0.0
1	2	2	49	3.0398E 01	-2.0000E 00	-1.5000E 00	0.0	1.0000E 00	0.0	0.0
2	2	2	50	3.1545E 01	-2.0100E 00	-1.5000E 00	1.7432E-02	9.9985E-01	0.0	0.0
3	2	2	51	3.2692E 01	-2.0325E 00	-1.5000E 00	2.1789E-02	9.9976E-01	0.0	0.0
4	2	2	52	3.3839E 01	-2.0575E 00	-1.5000E 00	2.1790E-02	9.9976E-01	0.0	0.0
5	2	2	53	3.4986E 01	-2.0900E 00	-1.5000E 00	3.4850E-02	9.9939E-01	0.0	0.0
6	2	2	54	3.6133E 01	-2.1375E 00	-1.5000E 00	4.7893E-02	9.9885E-01	0.0	0.0
7	2	2	55	3.7280E 01	-2.2000E 00	-1.5000E 00	6.0912E-02	9.9814E-01	0.0	0.0
8	2	2	56	3.8427E 01	-2.2775E 00	-1.5000E 00	7.3899E-02	9.9727E-01	0.0	0.0
9	2	2	57	3.9574E 01	-2.3750E 00	-1.5000E 00	9.5458E-02	9.9543E-01	0.0	0.0

10	2	2	58	4.0721E 01	-2.4925E 00	-1.5000E 00	1.0833E-01	9.9412E-01	0.0	0.0
11	2	2	59	4.1868E 01	-2.6300E 00	-1.5000E 00	1.2966E-01	9.9156E-01	0.0	0.0
12	2	2	60	4.3015E 01	-2.7950E 00	-1.5000E 00	1.5502E-01	9.8791E-01	0.0	0.0
1	3	2	61	3.0398E 01	-2.0000E 00	-5.0000E-01	0.0	1.0000E 00	0.0	0.0
2	3	2	62	3.1545E 01	-2.0100E 00	-5.0000E-01	1.7432E-02	9.9985E-01	0.0	0.0
3	3	2	63	3.2692E 01	-2.0325E 00	-5.0000E-01	2.1789E-02	9.9976E-01	0.0	0.0
4	3	2	64	3.3839E 01	-2.0575E 00	-5.0000E-01	2.1790E-02	9.9976E-01	0.0	0.0
5	3	2	65	3.4986E 01	-2.0900E 00	-5.0000E-01	3.4850E-02	9.9939E-01	0.0	0.0
6	3	2	66	3.6133E 01	-2.1375E 00	-5.0000E-01	4.7893E-02	9.9885E-01	0.0	0.0
7	3	2	67	3.7280E 01	-2.2000E 00	-5.0000E-01	6.0912E-02	9.9814E-01	0.0	0.0
8	3	2	68	3.8427E 01	-2.2775E 00	-5.0000E-01	7.3899E-02	9.9727E-01	0.0	0.0
9	3	2	69	3.9574E 01	-2.3750E 00	-5.0000E-01	9.5458E-02	9.9543E-01	0.0	0.0
10	3	2	70	4.0721E 01	-2.4925E 00	-5.0000E-01	1.0833E-01	9.9412E-01	0.0	0.0
11	3	2	71	4.1868E 01	-2.6300E 00	-5.0000E-01	1.2966E-01	9.9156E-01	0.0	0.0
12	3	2	72	4.3015E 01	-2.7950E 00	-5.0000E-01	1.5502E-01	9.8791E-01	0.0	0.0

SV1

I	GAMMAS		
	PART 1		
1	-2.6910E-02	-3.7687E-02	-4.2204E-02
2	-3.9423E-02	-5.0148E-02	-5.4085E-02
3	-2.3481E-02	-3.2517E-02	-3.6239E-02
4	-1.8803E-02	-2.7657E-02	-3.1518E-02
5	-3.8027E-02	-4.9782E-02	-5.4653E-02
6	-4.2671E-02	-5.6683E-02	-6.2129E-02
7	-4.5117E-02	-6.0405E-02	-6.6425E-02
8	-4.7960E-02	-6.4546E-02	-7.1061E-02
9	-5.9279E-02	-7.7402E-02	-8.4270E-02
10	-4.9699E-02	-6.7039E-02	-7.3738E-02
11	-5.7512E-02	-7.4463E-02	-8.0564E-02
12	-5.3067E-02	-6.5876E-02	-7.0085E-02
	PART 2		
1	-2.6272E-02	-3.6702E-02	-4.1042E-02
2	-3.8728E-02	-4.9117E-02	-5.2886E-02
3	-2.2823E-02	-3.1513E-02	-3.5059E-02
4	-1.8058E-02	-2.6494E-02	-3.0141E-02
5	-3.6915E-02	-4.8299E-02	-5.2680E-02
6	-4.1370E-02	-5.4715E-02	-5.9822E-02
7	-4.3721E-02	-5.8288E-02	-6.3940E-02
8	-4.6579E-02	-6.2441E-02	-6.8588E-02
9	-5.7993E-02	-7.5479E-02	-8.2026E-02
10	-4.9023E-02	-6.6002E-02	-7.2520E-02
11	-5.7390E-02	-7.4297E-02	-8.0382E-02
12	-5.3556E-02	-6.6661E-02	-7.1031E-02
I	ETAS		
	PART 1		
1	2.6910E-02	1.0777E-02	4.5167E-03
2	6.6334E-02	2.1501E-02	8.4537E-03
3	8.9814E-02	3.0537E-02	1.2176E-02
4	1.0862E-01	3.9391E-02	1.6037E-02
5	1.4664E-01	5.1346E-02	2.0708E-02
6	1.8931E-01	6.5354E-02	2.6154E-02
7	2.3443E-01	8.0648E-02	3.2172E-02
8	2.8239E-01	9.7234E-02	3.8687E-02
9	3.4167E-01	1.1536E-01	4.5555E-02
10	3.9137E-01	1.3270E-01	5.2254E-02
11	4.4888E-01	1.4965E-01	5.8356E-02
12	5.0195E-01	1.6246E-01	6.2565E-02
	PART 2		
1	2.6272E-02	1.0437E-02	4.3395E-03
2	6.5000E-02	2.0819E-02	8.1084E-03
3	8.7823E-02	2.9509E-02	1.1655E-02
4	1.0588E-01	3.7945E-02	1.5302E-02
5	1.4280E-01	4.9329E-02	1.9682E-02
6	1.9417E-01	6.2674E-02	2.4784E-02
7	2.2789E-01	7.7241E-02	3.0442E-02
8	2.7447E-01	9.3103E-02	3.6589E-02
9	3.3246E-01	1.1059E-01	4.3137E-02
10	3.8148E-01	1.2757E-01	4.9655E-02
11	4.3887E-01	1.4447E-01	5.5740E-02
12	4.9243E-01	1.5758E-01	6.0110E-02

SVI

VELOCITIES PAGE 1

X	Y	Z	U	V	W	V	M	ATN(V/U)	ATN(W/U)	CP	M-MI
1.9000E 01	-2.5000E 00	2.0000E 00	0.90933	-0.26413	-0.17142	0.96231	0.86094	-16.20	-10.68	7.396E-02	-3.906E-02
1.9000E 01	-2.0000E 00	2.0000E 00	0.93893	-0.21809	-0.10026	0.96825	0.86705	-13.09	-6.10	6.249E-02	-3.295E-02
1.9000E 01	-1.5000E 00	2.0000E 00	0.95128	-0.18660	-0.05226	0.97082	0.86970	-11.10	-3.14	5.751E-02	-3.030E-02
1.9000E 01	-1.0000E 00	2.0000E 00	0.95370	-0.17431	-0.00564	0.96952	0.86836	-10.36	-0.34	6.003E-02	-3.164E-02
1.9000E 01	-0.5000E 00	2.0000E 00	0.94954	-0.17796	0.04053	0.96692	0.86568	-10.62	2.44	6.507E-02	-3.432E-02
1.9000E 01	0.0	2.0000E 00	0.94093	-0.19901	0.08792	0.96576	0.86448	-11.94	5.34	6.731E-02	-3.552E-02
1.9000E 01	5.0000E -01	2.0000E 00	0.92890	-0.24102	0.13898	0.96967	0.86851	-14.55	8.51	5.973E-02	-3.149E-02
1.9000E 01	1.0000E 00	2.0000E 00	0.92765	-0.28072	0.51055	1.09544	1.00227	-16.84	28.83	-2.000E-01	1.023E-01
1.9000E 01	-2.5000E 00	1.5000E 00	0.89792	-0.30121	-0.06486	0.94931	0.84763	-18.54	-4.13	9.880E-02	-5.237E-02
1.9000E 01	-2.0000E 00	1.5000E 00	0.92852	-0.25405	-0.06287	0.96470	0.86340	-15.30	-3.87	6.935E-02	-3.660E-02
1.9000E 01	-1.5000E 00	1.5000E 00	0.94072	-0.22536	-0.03501	0.96797	0.86676	-13.47	-2.13	6.304E-02	-3.324E-02
1.9000E 01	-1.0000E 00	1.5000E 00	0.94229	-0.21335	-0.00342	0.96615	0.86488	-12.76	-0.21	6.656E-02	-3.512E-02
1.9000E 01	-0.5000E 00	1.5000E 00	0.93726	-0.21696	0.02856	0.96246	0.86109	-13.03	1.75	7.367E-02	-3.891E-02
1.9000E 01	0.0	1.5000E 00	0.92840	-0.23667	0.05882	0.95989	0.85846	-14.30	3.62	7.860E-02	-4.154E-02
1.9000E 01	5.0000E -01	1.5000E 00	0.91753	-0.27536	0.07911	0.96122	0.85982	-16.70	4.93	7.605E-02	-4.018E-02
1.9000E 01	1.0000E 00	1.5000E 00	0.91268	-0.32908	0.01761	0.97036	0.86922	-19.83	1.11	5.841E-02	-3.078E-02
1.9000E 01	-2.5000E 00	1.0000E 00	0.90012	-0.29780	-0.06112	0.95007	0.84840	-18.31	-3.88	9.736E-02	-5.160E-02
1.9000E 01	-2.0000E 00	1.0000E 00	0.92419	-0.27209	-0.03766	0.96415	0.86283	-16.41	-2.33	7.042E-02	-3.717E-02
1.9000E 01	-1.5000E 00	1.0000E 00	0.93434	-0.24944	-0.02087	0.96729	0.86606	-14.95	-1.28	6.435E-02	-3.394E-02
1.9000E 01	-1.0000E 00	1.0000E 00	0.93491	-0.23903	-0.00178	0.96498	0.86368	-14.34	-0.11	6.881E-02	-3.632E-02
1.9000E 01	-0.5000E 00	1.0000E 00	0.92961	-0.24206	0.01775	0.96077	0.85935	-14.59	1.09	7.693E-02	-4.065E-02
1.9000E 01	0.0	1.0000E 00	0.92143	-0.25830	0.03572	0.95761	0.85612	-15.66	2.22	8.298E-02	-4.388E-02
1.9000E 01	5.0000E -01	1.0000E 00	0.91479	-0.28502	0.05205	0.95957	0.85813	-17.31	3.26	7.922E-02	-4.187E-02
1.9000E 01	1.0000E 00	1.0000E 00	0.92262	-0.30520	0.19185	0.99054	0.89013	-18.30	11.75	1.882E-02	-9.866E-03
1.9000E 01	-2.5000E 00	5.0000E -01	0.89536	-0.31254	-0.01642	0.94848	0.84677	-19.24	-1.05	1.004E-01	-5.323E-02
1.9000E 01	-2.0000E 00	5.0000E -01	0.92146	-0.28301	-0.01685	0.96409	0.86276	-17.07	-1.05	7.054E-02	-3.724E-02
1.9000E 01	-1.5000E 00	5.0000E -01	0.93093	-0.26260	-0.00962	0.96731	0.86607	-15.75	-0.59	6.432E-02	-3.393E-02
1.9000E 01	-1.0000E 00	5.0000E -01	0.93084	-0.25331	-0.00072	0.96469	0.86339	-15.22	-0.04	6.937E-02	-3.661E-02
1.9000E 01	-0.5000E 00	5.0000E -01	0.92546	-0.25590	0.00843	0.96022	0.85879	-15.46	0.52	7.797E-02	-4.121E-02
1.9000E 01	0.0	5.0000E -01	0.91767	-0.27019	0.01662	0.95676	0.85525	-16.41	1.04	8.460E-02	-4.475E-02
1.9000E 01	5.0000E -01	5.0000E -01	0.91135	-0.29614	0.02139	0.95849	0.85702	-18.00	1.34	8.129E-02	-4.298E-02
1.9000E 01	1.0000E 00	5.0000E -01	0.91512	-0.32920	0.00321	0.97254	0.87147	-19.79	0.20	5.417E-02	-2.853E-02
1.9000E 01	-2.5000E 00	0.0	0.89860	-0.30489	0.00001	0.94891	0.84722	-18.74	0.00	9.956E-02	-5.278E-02
1.9000E 01	-2.0000E 00	0.0	0.92104	-0.28521	0.00001	0.96419	0.86286	-17.21	-0.00	7.035E-02	-3.714E-02
1.9000E 01	-1.5000E 00	0.0	0.92987	-0.26668	0.00000	0.96736	0.86613	-16.00	0.00	6.422E-02	-3.387E-02
1.9000E 01	-1.0000E 00	0.0	0.92957	-0.25787	0.00000	0.96467	0.86337	-15.50	-0.00	6.941E-02	-3.663E-02
1.9000E 01	-0.5000E 00	0.0	0.92415	-0.26028	0.00000	0.96010	0.85867	-15.73	-0.00	7.821E-02	-4.133E-02
1.9000E 01	0.0	0.0	0.91664	-0.27356	0.00001	0.95659	0.85507	-16.62	0.00	8.494E-02	-4.493E-02
1.9000E 01	5.0000E -01	0.0	0.91224	-0.29486	0.00001	0.95871	0.85724	-17.91	-0.00	8.088E-02	-4.276E-02
1.9000E 01	1.0000E 00	0.0	0.92219	-0.31001	0.00011	0.97291	0.87185	-18.58	0.01	5.345E-02	-2.815E-02

SV1

STREAMLINE PAGE 1

2.5000E-01 MAX STEP SIZE

1.000 DEG MIN ANGLE CHANGE

3.000 DEG MAX ANGLE CHANGE

X	Y	Z	U	V	W	V	M	ATN(V/U)	ATN(W/U)	CP	M-MI
1.9000E 01	-8.8500E-01	0.0	0.92866	-0.25743	-0.00000	0.96368	0.86235	-15.49	-0.00	7.131E-02	-3.765E-02
1.9241E 01	-9.5203E-01	4.3769E-12	0.92448	-0.25833	0.0	0.95989	0.85846	-15.61	0.0	7.860E-02	-4.154E-02
1.9482E 01	-1.0193E 00	1.1210E-09	0.92143	-0.25760	-0.00000	0.95676	0.85524	-15.62	-0.00	8.461E-02	-4.476E-02
1.9722E 01	-1.0865E 00	3.3622E-09	0.91942	-0.25626	-0.00000	0.95446	0.85289	-15.57	-0.00	8.900E-02	-4.711E-02
1.9963E 01	-1.1535E 00	5.6121E-09	0.91814	-0.25485	-0.00000	0.95285	0.85124	-15.51	-0.00	9.207E-02	-4.876E-02
2.0204E 01	-1.2203E 00	5.6200E-09	0.91733	-0.25355	-0.00000	0.95173	0.85009	-15.45	-0.00	9.421E-02	-4.991E-02
2.0445E 01	-1.2868E 00	5.6248E-09	0.91681	-0.25243	-0.00000	0.95093	0.84927	-15.39	-0.00	9.574E-02	-5.073E-02
2.0686E 01	-1.3530E 00	5.6289E-09	0.91647	-0.25149	-0.00000	0.95035	0.84868	-15.34	-0.00	9.684E-02	-5.132E-02
2.0927E 01	-1.4191E 00	3.3822E-09	0.91622	-0.25071	-0.00000	0.94990	0.84823	-15.30	-0.00	9.768E-02	-5.177E-02
2.1168E 01	-1.4850E 00	5.6339E-09	0.91605	-0.25008	-0.00000	0.94957	0.84788	-15.27	-0.00	9.832E-02	-5.212E-02
2.1410E 01	-1.5508E 00	6.9781E-08	0.91591	-0.24956	-0.00000	0.94930	0.84761	-15.24	-0.00	9.883E-02	-5.239E-02
2.1651E 01	-1.6164E 00	1.0695E-07	0.91581	-0.24914	-0.00000	0.94910	0.84740	-15.22	-0.00	9.922E-02	-5.260E-02
2.1892E 01	-1.6820E 00	7.9951E-08	0.91572	-0.24881	-0.00000	0.94892	0.84722	-15.20	-0.00	9.956E-02	-5.278E-02
2.2133E 01	-1.7476E 00	8.1094E-08	0.91564	-0.24855	-0.00000	0.94878	0.84708	-15.19	-0.00	9.983E-02	-5.292E-02
2.2375E 01	-1.8130E 00	1.0588E-07	0.91557	-0.24836	-0.00000	0.94866	0.84696	-15.18	-0.00	1.000E-01	-5.304E-02
2.2616E 01	-1.8785E 00	2.5343E-07	0.91550	-0.24822	-0.00000	0.94855	0.84665	-15.17	-0.00	1.002E-01	-5.315E-02
2.2857E 01	-1.9439E 00	2.2641E-07	0.91544	-0.24813	-0.00000	0.94847	0.84676	-15.17	-0.00	1.004E-01	-5.324E-02
2.3098E 01	-2.0093E 00	2.3882E-07	0.91537	-0.24808	-0.00000	0.94839	0.84668	-15.16	-0.00	1.006E-01	-5.332E-02
2.3340E 01	-2.0747E 00	2.1068E-07	0.91529	-0.24807	-0.00000	0.94831	0.84660	-15.16	-0.00	1.007E-01	-5.340E-02
2.3581E 01	-2.1401E 00	2.9969E-07	0.91522	-0.24809	-0.00000	0.94825	0.84654	-15.17	-0.00	1.008E-01	-5.346E-02
2.3822E 01	-2.2055E 00	2.6928E-07	0.91515	-0.24814	-0.00000	0.94819	0.84648	-15.17	-0.00	1.009E-01	-5.352E-02
2.4064E 01	-2.2709E 00	2.6592E-07	0.91507	-0.24822	-0.00000	0.94814	0.84643	-15.18	-0.00	1.010E-01	-5.357E-02
2.4305E 01	-2.3364E 00	3.9776E-07	0.91499	-0.24832	-0.00000	0.94809	0.84637	-15.18	-0.00	1.011E-01	-5.363E-02
2.4546E 01	-2.4019E 00	3.5496E-07	0.91490	-0.24845	-0.00000	0.94804	0.84632	-15.19	-0.00	1.012E-01	-5.368E-02
2.4787E 01	-2.4674E 00	2.7947E-07	0.91482	-0.24860	-0.00000	0.94800	0.84628	-15.20	-0.00	1.013E-01	-5.372E-02
2.5029E 01	-2.5330E 00	3.6062E-07	0.91473	-0.24877	-0.00000	0.94795	0.84624	-15.21	-0.00	1.014E-01	-5.376E-02

***** X>XX *****

SVI

STREAMLINE PAGE 1

2.5000E-01 MAX STEP SIZE

1.000 DEG MIN ANGLE CHANGE

3.000 DEG MAX ANGLE CHANGE

X	Y	Z	U	V	W	V	M	ATN(V/U)	ATN(W/U)	CP	M-MI
1.9000E 01	-8.8500E-01	0.0	0.92866	-0.25743	0.00000	0.96368	0.86235	-15.49	0.00	7.131E-02	-3.765E-02
1.8759E 01	-8.1886E-01	-3.9391E-12	0.93336	-0.25337	0.0	0.96714	0.86590	-15.19	0.0	6.464E-02	-3.410E-02
1.8517E 01	-7.5449E-01	1.0984E-09	0.93766	-0.24521	0.0	0.96919	0.86802	-14.66	0.0	6.067E-02	-3.198E-02
1.8275E 01	-6.9278E-01	1.0984E-09	0.94184	-0.23351	0.0	0.97036	0.86922	-13.92	0.0	5.841E-02	-3.078E-02
1.8032E 01	-6.3443E-01	1.0984E-09	0.94639	-0.21963	0.0	0.97154	0.87044	-13.07	0.0	5.611E-02	-2.956E-02
1.7788E 01	-5.7986E-01	4.4453E-13	0.95134	-0.20480	-0.00000	0.97313	0.87208	-12.15	-0.00	5.302E-02	-2.792E-02
1.7543E 01	-5.2923E-01	5.5052E-10	0.95672	-0.18975	-0.00000	0.97536	0.87438	-11.22	-0.00	4.868E-02	-2.562E-02
1.7298E 01	-4.8258E-01	-6.1020E-10	0.96216	-0.17463	-0.00000	0.97788	0.87699	-10.29	-0.00	4.374E-02	-2.301E-02
1.7051E 01	-4.3993E-01	-1.0855E-09	0.96731	-0.15943	-0.00000	0.98036	0.87956	-9.36	-0.00	3.890E-02	-2.044E-02
1.6804E 01	-4.0122E-01	-1.0147E-09	0.97185	-0.14445	-0.00000	0.98253	0.88180	-8.45	-0.00	3.464E-02	-1.820E-02
1.6557E 01	-3.6632E-01	3.4650E-10	0.97603	-0.13016	-0.00000	0.98467	0.88403	-7.60	-0.00	3.042E-02	-1.597E-02
1.6309E 01	-3.3502E-01	1.0938E-09	0.97988	-0.11665	-0.00000	0.98679	0.88623	-6.79	-0.00	2.624E-02	-1.377E-02
1.6060E 01	-3.0711E-01	-7.2677E-10	0.98341	-0.10387	-0.00000	0.98888	0.88841	-6.03	-0.00	2.211E-02	-1.159E-02
1.5811E 01	-2.8241E-01	-1.1273E-09	0.98651	-0.09168	-0.00000	0.99076	0.89036	-5.31	-0.00	1.839E-02	-9.637E-03
1.5562E 01	-2.6075E-01	-2.4691E-09	0.98918	-0.08011	-0.00000	0.99242	0.89208	-4.63	-0.00	1.511E-02	-7.918E-03
1.5313E 01	-2.4195E-01	-1.1173E-09	0.99128	-0.06923	-0.00000	0.99370	0.89342	-4.00	-0.00	1.257E-02	-6.581E-03
1.5064E 01	-2.2579E-01	-1.0469E-09	0.99288	-0.05933	-0.00000	0.99465	0.89442	-3.42	-0.00	1.067E-02	-5.585E-03
1.4814E 01	-2.1197E-01	-3.0576E-09	0.99399	-0.05067	-0.00000	0.99528	0.89507	-2.92	-0.00	9.419E-03	-4.932E-03
1.4564E 01	-2.0016E-01	-1.7123E-09	0.99498	-0.04339	-0.00000	0.99593	0.89575	-2.50	-0.00	8.126E-03	-4.254E-03
1.4314E 01	-1.9008E-01	-4.3882E-09	0.99625	-0.03694	-0.00000	0.99693	0.89679	-2.12	-0.00	6.129E-03	-3.207E-03
1.4065E 01	-1.8164E-01	-3.7575E-09	0.99779	-0.03044	-0.00000	0.99826	0.89818	-1.75	-0.00	3.481E-03	-1.821E-03
1.3815E 01	-1.7493E-01	-4.3131E-09	0.99937	-0.02318	-0.00000	0.99964	0.89963	-1.33	-0.00	7.126E-04	-3.732E-04
1.3565E 01	-1.7016E-01	4.7015E-09	1.00061	-0.01499	-0.00000	1.00072	0.90076	-0.86	-0.00	-1.449E-03	7.571E-04
1.3315E 01	-1.6748E-01	2.1094E-09	1.00111	-0.00647	-0.00000	1.00113	0.90119	-0.37	-0.00	-2.270E-03	1.186E-03
1.3065E 01	-1.6681E-01	8.3201E-09	1.00078	0.00117	-0.00000	1.00078	0.90081	0.07	-0.00	-1.555E-03	8.129E-04
1.2815E 01	-1.6781E-01	8.3825E-09	0.99979	0.00682	-0.00000	0.99982	0.89981	0.39	-0.00	3.675E-04	-1.920E-04
1.2565E 01	-1.6989E-01	8.4702E-09	0.99862	0.00981	-0.00000	0.99867	0.89861	0.56	-0.00	2.658E-03	-1.390E-03
1.2315E 01	-1.7245E-01	8.5580E-09	0.99785	0.01057	0.00000	0.99790	0.89781	0.61	0.00	4.190E-03	-2.191E-03
1.2065E 01	-1.7504E-01	8.5998E-09	0.99762	0.01012	0.00000	0.99767	0.89756	0.58	0.00	4.661E-03	-2.438E-03
1.1815E 01	-1.7746E-01	8.5789E-09	0.99769	0.00923	0.00000	0.99773	0.89763	0.53	0.00	4.539E-03	-2.375E-03
1.1565E 01	-1.7965E-01	8.6233E-09	0.99787	0.00825	0.00000	0.99790	0.89781	0.47	0.00	4.194E-03	-2.194E-03
1.1315E 01	-1.8160E-01	8.7213E-09	0.99807	0.00733	0.00000	0.99810	0.89802	0.42	0.00	3.794E-03	-1.985E-03
1.1065E 01	-1.8333E-01	8.8237E-09	0.99828	0.00651	0.00000	0.99830	0.89822	0.37	0.00	3.402E-03	-1.779E-03
1.0815E 01	-1.8488E-01	9.0796E-09	0.99845	0.00581	0.00000	0.99847	0.89840	0.33	0.00	3.063E-03	-1.602E-03
1.0565E 01	-1.8626E-01	8.6787E-09	0.99860	0.00521	-0.00000	0.99862	0.89855	0.30	-0.00	2.765E-03	-1.446E-03
1.0315E 01	-1.8750E-01	8.7413E-09	0.99873	0.00469	0.00000	0.99874	0.89869	0.27	0.00	2.514E-03	-1.314E-03
1.0065E 01	-1.8862E-01	8.7664E-09	0.99885	0.00425	0.00000	0.99886	0.89881	0.24	0.00	2.278E-03	-1.191E-03
9.8149E 00	-1.8963E-01	8.7163E-09	0.99894	0.00387	0.0	0.99895	0.89890	0.22	0.0	2.100E-03	-1.098E-03

***** X<XN *****

UNCLASSIFIED

Security Classification

DOCUMENT CONTROL DATA - R & D

(Security classification of title, body of abstract and indexing annotation must be entered when the overall report is classified)

1. ORIGINATING ACTIVITY (Corporate author) Arnold Engineering Development Center Arnold Air Force Station, Tennessee 37389		2a. REPORT SECURITY CLASSIFICATION UNCLASSIFIED	
		2b. GROUP N/A	
3. REPORT TITLE A METHOD TO INCREASE THE FULL-SCALE INLET/ENGINE SYSTEM TESTING CAPABILITY OF THE AEDC 16-FT TRANSONIC WIND TUNNEL			
4. DESCRIPTIVE NOTES (Type of report and inclusive dates) January 1971 to July 1972--Final Report			
5. AUTHOR(S) (First name, middle initial, last name) R. L. Palko, ARO, Inc.			
6. REPORT DATE June 1973		7a. TOTAL NO. OF PAGES 137	7b. NO. OF REFS 8
8a. CONTRACT OR GRANT NO.		9a. ORIGINATOR'S REPORT NUMBER(S) AEDC-TR-73-9	
b. PROJECT NO.			
c. Program Element 64719F		9b. OTHER REPORT NO(S) (Any other numbers that may be assigned this report) ARO-PWT-TR-72-121	
d.			
10. DISTRIBUTION STATEMENT Approved for public release; distribution unlimited.			
11. SUPPLEMENTARY NOTES Available in DDC		12. SPONSORING MILITARY ACTIVITY Arnold Engineering Development Center, Air Force Systems Command, Arnold AF Station, Tennessee 37389	
13. ABSTRACT A study was conducted of a new testing technique using flow shaping that together with some modifications of the AEDC 16-ft Transonic Propulsion Wind Tunnel will provide the capability to test full-scale inlet/engine configurations with forebody effects at high maneuvering angles at transonic velocities. The method used to obtain the flow simulation for high maneuvering angles utilized auxiliary flow shaping and geometric pitch. An analytical potential flow method was used to determine the configuration of devices necessary to produce the required flow fields; these devices were then checked experimentally to verify the results. The experimental results compare favorably with the predicted flow fields, and the use of flow shaping devices for simulation of the inlet flow field for certain inlet configurations is promising for angles of attack up to 20 deg with angles of yaw up to 5 deg.			

DD FORM 1 NOV 65 1473

UNCLASSIFIED

Security Classification

UNCLASSIFIED

Security Classification

14. KEY WORDS	LINK A		LINK B		LINK C	
	ROLE	WT	ROLE	WT	ROLE	WT
test facilities supersonic wind tunnels inlet/engine systems flow shaping devices flow field mathematical model vortex-lattice method analytical techniques jet engine inlets transonic flow						

APSC
Approved APS Team

UNCLASSIFIED

Security Classification